Cold-start effects on performance and efficiency for vehicle fuel cell systems

by
Stephen Daniel Gurski

Thesis submitted to the Faculty of
Virginia Polytechnic Institute and State University
in partial fulfillment of the requirements for the degree of
Master of Science in
Mechanical Engineering

Dr. Douglas J. Nelson

Dr. Michael W. Ellis

Dr. Michael R. von Spakovsky

December 19, 2002
Blacksburg, Virginia

Key Words:
Fuel Cell, Cold-start, Modeling, Hybrid Vehicles, Transient

Cold-start effects on performance and efficiency for vehicle fuel cell systems

Stephen Daniel Gurski

Abstract

In recent years government, academia and industry have been pursuing fuel cell technology as an alternative to current power generating technologies. The automotive industry has targeted fuel cell technology as a potential alternative to internal combustion engines. The goal of this research is to understand and quantify the impact and effects of low temperature operation has on the performance and efficiency of vehicle fuel cell systems through modeling. More specifically, this work addresses issues of the initial thermal transient known to the automotive community as "cold-start" effects. Cold-start effects play a significant role in power limitations in a fuel cell vehicle, and may require hybridization (batteries) to supplement available power. A fuel cell system model developed as part of this work allows users to define the basic thermal fluid relationships in a fuel cell system. The model can be used as a stand-alone version or as part of a complex fuel cell vehicle model.

Fuel cells are being considered for transportation primarily because they have the ability to increase vehicle energy efficiency and significantly reduce or eliminate tailpipe emissions. A proton exchange membrane fuel cell is an electrochemical device for which the operational characteristics depend heavily upon temperature. Thus, it is important to know how the thermal design of the system affects the performance of a fuel cell, which governs the efficiency and performance of the system.

This work revealed that the impact on efficiency of a cold-start yielded a 5 % increase in fuel use over a regulated drive cycle for the converted sport utility vehicle. The performance of the fuel cell vehicle also suffered due to operation at low temperatures. Operation of the fuel cell at 20 C yielded only 50% of the available power to the vehicle system.

Acknowledgements

The National Renewal Energy Laboratories under contract XCL-1-31116-01 sponsored this work. I would like to thank my colleagues at the CTTS system analysis team, especially Keith Wipke, Tony Markel, Kristina Haraldsson, and Bill Kramer for their support and direction. It made this work tangible and possible.

I owe a great deal of thanks to the past and present team members of Hybrid Electric Vehicle Team at Virginia Tech. I would especially like to thank Mike Ogburn and Andrew Pogany for taking the time and introducing me to the world of HEVT and FutureCar / FutureTruck. Without you, I would not have stumbled down this path in life.

I would also like to thank my faculty advisor, Dr. Doug Nelson for his support, patience, and friendship. And for taking the chance on me as well as challenging me in graduate school. I hope I did not disappoint you.

I also have to thank all the friends that I have met in my time here at Virginia Tech. You all have made my time at Virginia Tech the most memorable in my life. You donkeys know who you are.

Finally, I have to thank the most important people in my life, my parents. Their unrelenting encouragement and support has taught me everything I need to succeed in life and I would not be here without them. I am truly lucky.

TABLE OF CONTENTS

Nomenclature

$PPO_2@Inlet$	=	Partial pressure of oxygen at the inlet to the cathode (ATM)
P_{inlet}	=	Pressure @ inlet to cathode (ATM)
Rh	=	Relative humidity (%/100)
$Psat$	=	Saturation pressure of water @ operating temperature (ATM)
$PPO_2@Outlet$	=	Partial pressure oxygen @ the cathode outlet (ATM)
$Poutlet$	=	Pressure @ outlet of cathode (ATM)
Sr	=	Stoichiometric ratio of air
h_{elec}	=	Electrical efficiency of air compressor motor drive
$h_{adiabatic}$	=	Adiabatic efficiency of compressor
k	=	Specific heat ratio for air
T_{amb}	=	Temperature of the ambient air (K)
Cp_{air}	=	Specific heat air (j /kg –k)
$\overset{*}{m}$	=	Mass flow rate (kg/s)
Pr	=	Pressure ratio through the air compressor
$Qgen$	=	Heat generated in the fuel cell stack (W)
ΔT	=	Temperature rise across stack (K or C)
$\overset{*}{m}_{coolant}$	=	Mass flow rate of coolant through coolant pump (kg/s)
$Cp_{coolant}$	=	Specific heat of coolant (J/ kG-K)
h_{rad}	=	Heat transfer coefficient of the radiator (kW/m^2-K)
Fr_{area}	=	Frontal Area of a heat transfer device (m^2)
T_{ai}	=	Temperature of the air into the device (K)
$Qcondenser$	=	Heat rejection of the condenser (W)
$Qvap\_cond$	=	Heat of vaporization (or condensation) in the condenser (W)
$\dot{m}_{wv\_in}$	=	Mass flow rate of water into device (kg/s)
h_{fg}	=	Heat of vaporization of water (kj./kg)

LIST OF FIGURES

List of Tables

1 Introduction

Fuel cells are being considered for transportation because they have the ability to increase vehicle energy efficiency and significantly reduce or eliminate tailpipe emissions. A proton exchange membrane fuel cell is an electrochemical device for which the operational characteristics depend heavily upon temperature. Thus, it is important to know how the thermal design of the system affects the performance of a fuel cell, which governs the efficiency and performance of the system. More specifically, this work addresses issues of the initial thermal transient known to the automotive community as "cold-start" effects. Cold-start effects play a significant role in power limitations in a fuel cell vehicle, and may require hybridization (batteries) to supplement available power. The results include a comparison of cold-start and hot-start fuel cell power, efficiency, and fuel economy for a hybrid fuel cell vehicle.

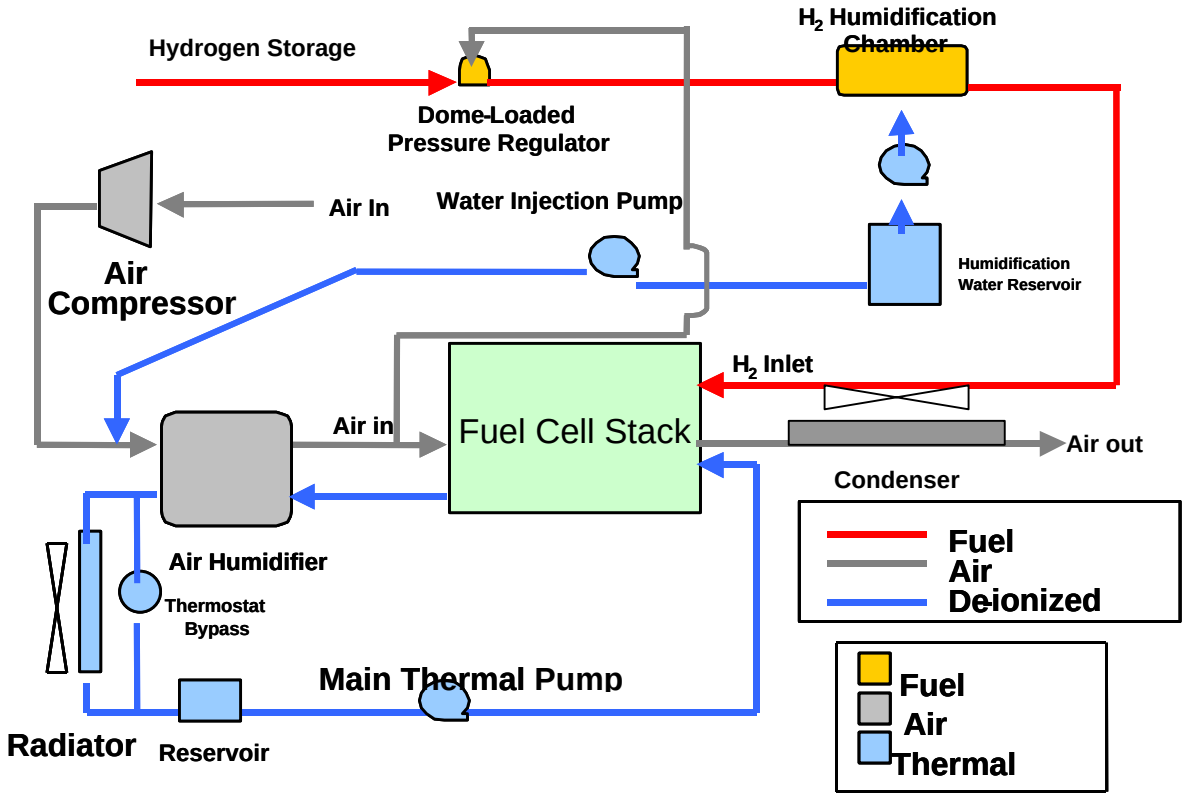

Figure 1. System diagram for model.

This work presents a model based upon a fuel cell vehicle developed at Virginia Tech. Figure 1 above is the diagram of a simplified fuel cell system that has been modeled for analysis. Specific to this model is a transient finite difference thermal model that captures cold-start effects. This transient thermal model of a fuel cell system has been developed and integrated into vehicle simulation software called ADVISOR™ that allows users to simulate a variety of vehicles. The model allows users to define the basic thermal fluid relationships that exist in a fuel cell system.

Magellan, a fuel cell vehicle developed at Virginia Tech is the vehicle design for the examples used in this paper. Magellan is a hybrid fuel cell vehicle based on a Ford Explorer™ platform that has a 50 kW net fuel cell system, a 83 kW traction drive and a 3 kWh lead acid battery pack.

The objective of this work is to develop a net power request model of a vehicle fuel cell system. This model will also be able to quantify the impact that cold-start has on the performance and efficiency of a fuel cell vehicle. Specifically this model will pay particular attention to the thermal system and the role that it plays on the initial thermal transient known as cold-start. Current models for vehicle simulations in ADVISOR™ do not account for the impact of the thermal fluid systems on the overall efficiency and performance of a fuel cell system. Quantifying the impact on efficiency will show the increase in energy use over a vehicle drive cycle. Using drive cycles with higher speeds and aggressive acceleration will show the overall performance loss due to operation at low temperatures.

1.1 Overview of the Model

Two types of analysis have been performed using the fuel cell system model. The first type presented in this work is steady state and transient tests used to *characterize the response of the system*. Some of the tests include steady state operation at varying temperature to characterize efficiency and a step request of system power to characterize power and the thermal response of the system. The second type of analysis performed

uses the model *in a dynamic vehicle environment*. For this test, ADVISOR™[1] is used to couple the fuel cell model to a vehicle model and evaluate the system over a drive cycle. Production vehicles are tested for emissions and fuel economy on drive cycles that manufacturers and government utilize for approval and ratings. The combined vehicle / fuel cell model is evaluated for one of these drive cycle to yield results for fuel economy and emissions.

One of the vehicle drive cycles used to determine vehicle emissions and fuel economy is a state of charge corrected FTP-75 (Federal Test Procedure) cycle. This drive cycle is used by the EPA for testing fuel economy of production vehicles. This analysis will use the FTP-75 drive cycle to compare the hot and cold-start operation and fuel economy of the Explorer. Using the model developed for this work the following results were generated. Table 1 is the fuel economy and fuel use for the hot and cold cycle comparisons.

Table 1. Fuel economy and fuel use comparison of the FTP-75 drive cycle.

FTP –75 Cycle	System Start Temperature (C)	Fuel Economy (mpgge)	Fuel Use (kJ)
HOT	80	36.36	38689
COLD	20	34.29	40924
	Decrease	5.46%	

From the results in Table 1, the model predicts that a cold-start will increase the fuel use by 5.46 %. The increase in energy use is a result of the reduced efficiency of fuel cell operation at low temperatures that is a result of heating thermal masses in the fuel cell system. Figure 2 shows the temperature time history for the fuel cell stack.

[1] ADVISOR™ -**ADV**anced **V**eh**I**cle **S**imulat**OR**

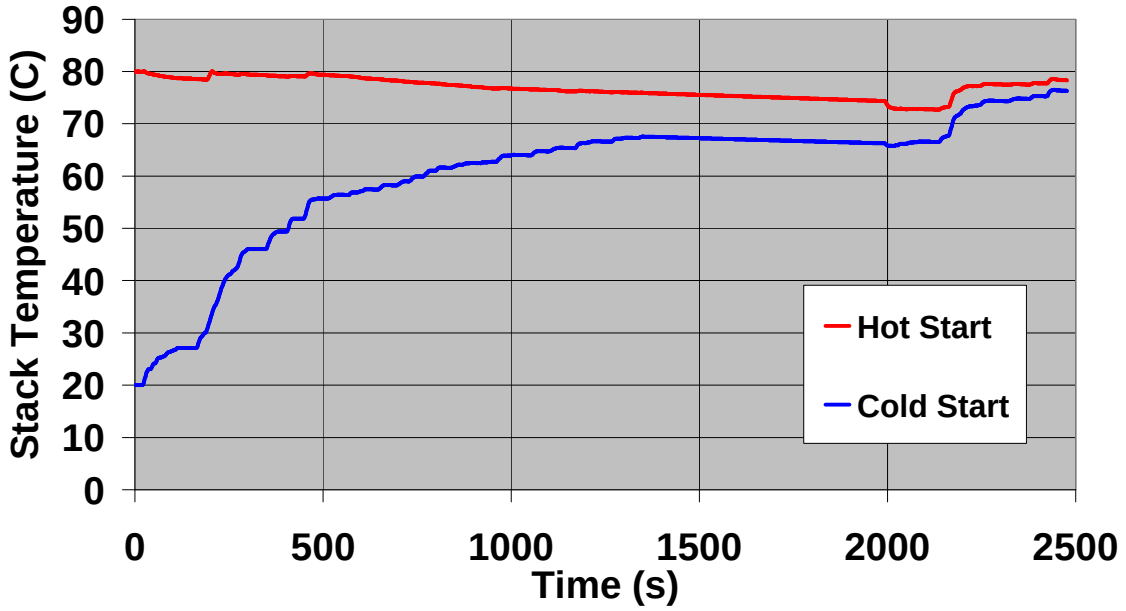

Figure 2. Comparison of fuel cell stack temperature during FTP-75 drive cycle.

Note that to raise the temperature of the fuel cell system requires a significant amount of time during the drive cycle. The fuel cell model has an internal thermal model that uses a transient finite difference method to keep track of the fuel cell stack and reservoir temperatures. Users specify characteristics and operating conditions of the fuel cell system that are used by the fuel cell system model to evaluate the performance and efficiency.

The vehicle model has the ability to look at the fuel cell system efficiency and losses within the fuel cell system. Analyses of the losses in the system are able to quantify the fuel economy difference shown in Table 1. Looking at how the fuel cell system operates during the drive cycle may explain why the cold-start system experienced a decrease in fuel economy. Each of the points in Figure 3 and Figure 4, represent an efficiency that the fuel cell system achieved at that time during the drive cycle.

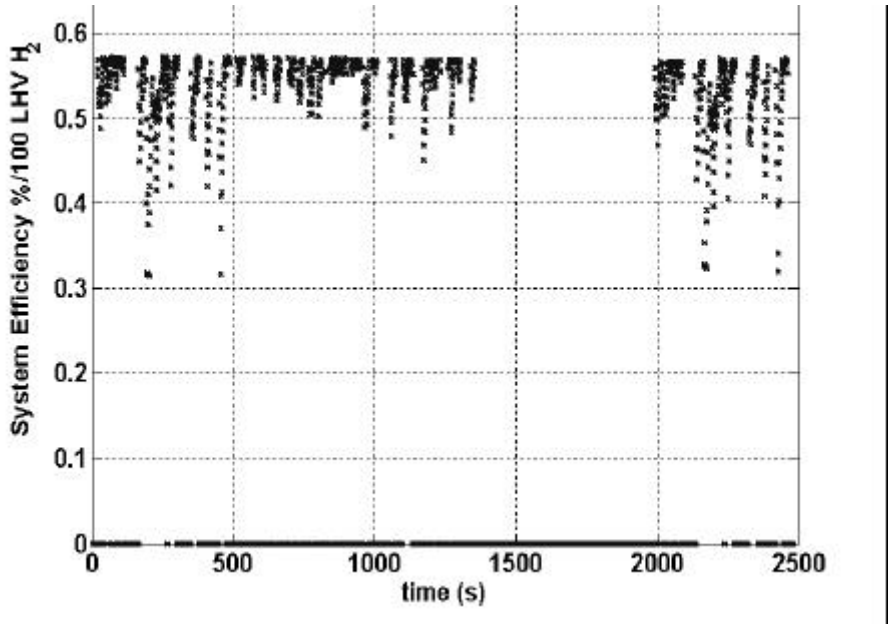

Figure 3. Fuel cell efficiency during hot-start FTP-75.

Figure 3 is the hot FTP case that began the cycle at the desired fuel cell operating temperature, which is 80° C; therefore, the maximum efficiency is possible during the entire drive cycle.

However, illustrated in Figure 4, the cold-start case for the FTP-75 run did not yield the same result.

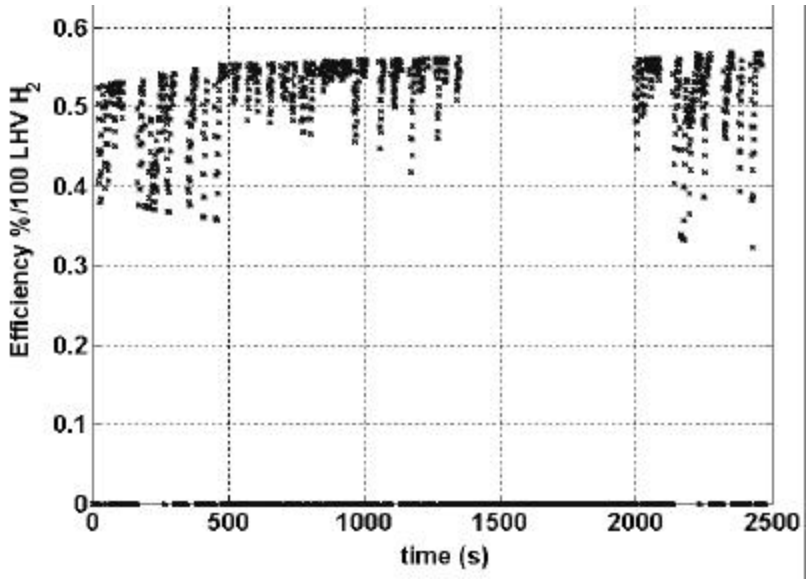

Figure 4. Fuel cell efficiency during cold-start FTP-75,

The cold-start case begins with a fuel cell system temperature at 20° C. A general increase in the maximum efficiency occurs during the first 1000 s of the FTP-75 drive cycle. This is because the system temperature is increasing which also increases system efficiency.

Temperature not only affects the overall system efficiency, but also the power that the system is able to generate. Temperature is not the only factor that limits power; other factors such as system operating pressure, losses internal to the fuel cell stack and control strategies can also contribute.

Power limiting behavior captured in the model is the result of imposing a minimum cell voltage criterion under which the fuel cell system will not operate. For example, if a power request to the system requires the cell voltage to be below the cell voltage criterion (i.e. 0.6 V/cell), then the model limits the power and provides the corresponding power available at the minimum cell voltage limit criterion.

Figure 5 below displays the relationship between the efficiency and power of the fuel cell system for the cold FTP drive cycle. In this figure, it is possible to see two of the power limiting factors that occur during the drive cycle.

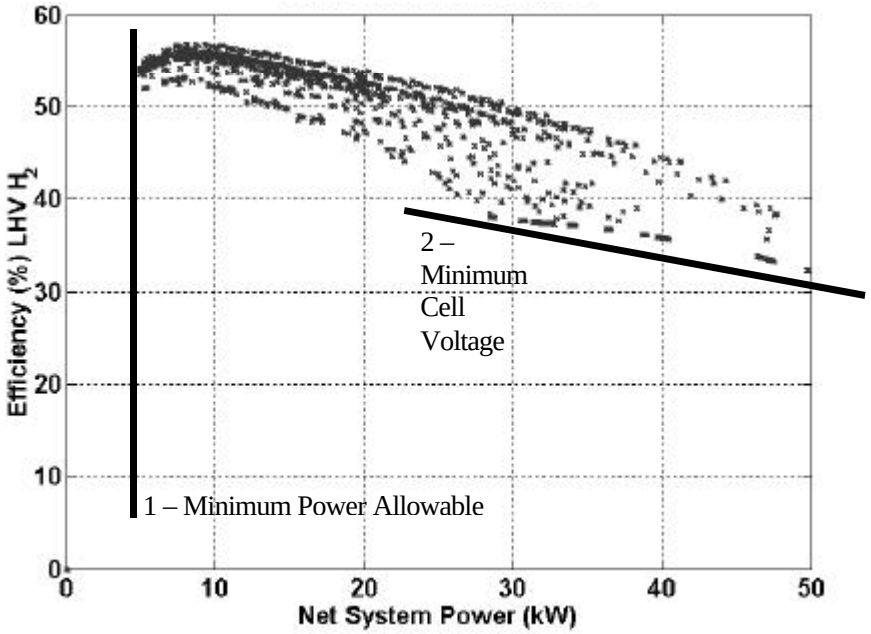

Figure 5. Fuel cell power vs. efficiency during cold-start FTP-75 drive cycle.

Labeled one in Figure 5 is a minimum power that the fuel cell system will not operate below that is imposed by the energy management control strategy. Since the vehicle is a hybrid, the power not able to be produced from the fuel cell to run the vehicle will be available from the battery storage. However, batteries also have limitation due to temperature and state of charge. It is the responsibility of the design of the vehicle and the control strategy to maintain the maximum performance. Due to research on air compression systems by Kulp (2001), a minimum power point was chosen to 5 kW because of the impact that the air supply system on overall system efficiency. The second limitation that can be seen is the minimum cell voltage limitation on power, seen in Figure 5, labeled two. Low cell voltages occur when the temperature or pressure is too low for the requested power, or the requested current density is too high.

Discussed in detail in the following chapters is the development of the net power model, specifically the electrochemistry and thermal models that define fuel cell operation. The operating conditions and operating control strategy of the fuel cell system will be discussed in detail. Finally, the system is characterized using steady state and dynamic examples that will quantify the performance and efficiency of the system as part of a vehicle system.

2 Literature Review

2.1 Overview

A plethora of research and development is currently focused on in fuel cells for transportation applications. The motivation for the research in fuel cells is due to scientific findings that energy use has a discernable impact on the environment and the world has a finite amount of fossil fuels available. Operation of PEM fuel cells offer zero regulated emissions as well as an increase in the overall energy efficiency to convert fuels other than oil to useful electrical energy.

Since the topic of the current work deals with proton exchange membrane (PEM) fuel cell system modeling it is of interest to compare and contrast this work against published materials. Since the work is of some practical importance, comparing the modeling work of this system to demonstration vehicles has been performed.

2.2 Fuel Cell System Models

Boettner, et al. (2001) have developed a fuel cell system model for an automotive application. The model takes into account auxiliary systems such as the air compressor and cooling system. Many of these auxiliary components utilize constant efficiencies and thermodynamic relationships to calculate power. Boettner states that significant improvements in system efficiency can be made with the control of the air compressor operating line. It is unclear from the literature as to the details associated with cold-start performance and thermal transients, but Boettner states that the system is capable of performing cold-starts. Using an in-house vehicle simulator called VP-SIM, the fuel cell model has been integrated and tested for a variety of vehicle simulations. It also appears that Boettner has taken into account all of the major components for a fuel cell system

model. More information would be required from the authors to directly compare and contrast with this work.

Candusso, et al. (2001) have also developed a model for a fuel cell hybrid power source for a small electric vehicle. Their approach to developing a fuel cell model was to determine a single system operating line. The model is static, constraining system temperature and operating conditions as constants. However, a dynamic aspect has been given to the model by allowing the fuel cell power to be changed at prescribed rates. This model does not take into account thermal masses and cathode operating conditions (water balance, humidity, etc.) This model is the fuel cell model currently used in ADVISOR™, which is the National Renewable Energy Laboratory's advanced vehicle simulator.

Ceraolo, et al. (2001) have presented a dynamic model of a proton exchange membrane fuel cell. A simple model that describes the complex chemical kinetics in a PEM fuel cell has been developed. Their goal was to develop a simplified dynamic model of a PEM fuel cell that is based on the chemical-physical description of the phenomena occurring inside the fuel cell stack. The model itself is 1-D, isothermal, and isobaric. Included in the model are the cathode kinetics and gas diffusion through the cathode as well as the model neglects kinetics at the anode. Using Matlab™ / Simulink, the model has the ability to predict current density and voltage in the fuel cell. The model has also been compared to single cell empirical data.

Barbir, et al. (1999) have performed an optimization study of an automotive fuel cell system. The model uses empirical pressure, temperature, and polarization data that allows the optimization study to be performed. Their results call for a high-pressure system, operating at relatively low-temperature (~60^{o} C). Use of an expander to recapture energy at the cathode outlet is a requirement for the high-pressure operating condition. The low temperature operation allows for a minimal amount of heat rejection equipment to be used. This system model and optimization analysis also includes a hydrocarbon fuel processor, which is assumed to generate a stream of 40 % hydrogen, 40

% nitrogen, and 20 % carbon dioxide. Fuel not consumed in the fuel cell system is reused in a tail gas burner integrated into the fuel reformer. The model uses fixed efficiencies for pumps, compressors, and expanders.

Fronk, et al. (2000) examined the interaction of the thermal fluid systems on board a fuel cell vehicle. This work looks at thermal management issues that drive the design of heat rejection components in fuel cell systems. The authors state that operating conditions of the stack, specifically the operating pressure of the fuel cell stack, significantly effect the heat rejection requirements of the liquid cooling system. However, decreasing pressure shifts the heat rejected from the liquid coolant to the cathode outlet. Shifting the heat rejection to the cathode makes maintaining water balance difficult. To maintain the water balance in the system, a condenser is required in the system to capture the condensate water from the system. The authors conclude that a significant engineering challenge arises when developing a system that operates above 50 kWe because of the low operational temperature difference between the system and the ambient. They also conclude that high-pressure operation can help with the thermal engineering challenge. However, an increase in parasitic power will reduce system efficiency. Finally Fronk, et al. suggest that development of membranes requiring less water and subsequently higher temperature, and use of better dielectric coolants could provide the necessary solution for the thermal engineering challenges.

Ngy-Srun, et al. (2001) have also looked at thermal design issues in fuel cell vehicle systems. Specifically, the authors have looked at the performance of automotive heat transfer systems and the effects that vehicle velocity and system design have on cooling capacity. The paper presents information about the size, power, and performance of the electric radiator fan; fan shroud, and vehicle parameters that influence heat transfer in the system. Few details are offered about the fuel cell system, but the paper offers some results about design geometry for a 50 kWe system. 0.46 m^2 of heat transfer surface is required, a 400 W electric water pump, and two 250 W electric fans. With this pure fuel cell vehicle design, the vehicle can travel at 140 km/h on a flat road or 90 km/h on a 5% grade.

Doss, et al. (1998) have developed a fuel cell model that describes the performance of advanced power generation. The model is used to study has been used to study the performance of PEM fuel cell systems during steady state and transient operating conditions. Also studied is the performance of a system under cold-start conditions, where the initial temperature is 300 K. Finally, the paper looks at a fuel cells and their use in a Ford AIV (Aluminum Intensive Vehicle) Sable. The fuel cell model addresses radiator fan, air compressor, expander, and radiator. However, not taken into account are the water management issues (humidifier, condenser) in fuel cell systems.

2.3 Vehicle Demonstrations

Ijaz, et al. (2001) have presented a paper on a vehicle-level review of Mazda's Premacy fuel cell electric vehicle. This vehicle utilizes a liquid methanol reformer system coupled with a Ballard-XcellSis/ Ecostar fuel cell drive system. The fuel cell used is a Ballard Mark 901 stack. Contained in Table 2 are the vehicle specifications for the Mazda Premacy fuel cell vehicle.

Table 2. Mazda Premacy Vehicle specifications.

Attribute	Value
Frontal Area	2.7 m^2
Vehicle Weight	1816 kg
Power Train	65 kW peak
Acceleration 0-100 kph	28.5 s
Fuel Economy[2]	~40 mpgge (8.5 km/L CH_30H)

This vehicle does not utilize battery storage as a supplement to traction power. Batteries and DC-DC converters are utilized to provide high voltage power for vehicle startup and some regenerative energy storage.

[2] Unknown driving cycle for fuel economy

Adams, et al. (1999) have developed a fuel cell vehicle dubbed the P2000 that boasts the full performance of a comparable passenger vehicle. The paper describes the design choices behind choosing a fuel cell electric vehicle. In Table 3 are the characteristics and specifications for Ford's P2000 fuel cell vehicle.

Table 3. Ford P2000 Vehicle specifications.

Attribute	Value
Frontal Area	2.2 m^2 (estimated)
Vehicle Weight	1514 kg
Power Train	65 kW peak
Acceleration 0-96 kph	12.3 s
Fuel Economy (FUDS / HWFET / Combined)	56/79/56 mpgge (24/34/28 km/l)

The fuel cell system utilizes three Ballard Mark 700 fuel cell stacks capable of 75 kWe gross or 67 kWe net total. The system operating temperature was between 60^o C and 70^o C, and 207 kPa air pressure at the cathode inlet.

Yamanashi, et al. (2001) have presented their development work with Nissan Motor Corporation. The vehicle is based upon the Nissan 2000 Xterra platform. The authors have developed a series fuel cell hybrid vehicle utilizing fuel cell and battery technology. Nissan's past work with fuel cell vehicles utilized a methanol reformate fuel cell system. However, development of the thermal fluid systems on board the vehicle and moving towards a direct hydrogen fuel cell system could yield further improvement in efficiency and performance. A very limited amount of information has been given about the vehicle, or about vehicle performance. The fuel cell system is based upon a Ballard Mark 901 fuel cell stack with 75 kWe peak output. A fuel cell system efficiency of 45 % has been targeted.

3 Model Overview and Operation

The purpose of this work is to develop a computational model that has the ability to evaluate the performance of fuel cell systems in general and thermal fluid interactions within the fuel cell system. A part of this work of modeling fuel cell systems is to make the model so that it can be used with vehicle simulation software.

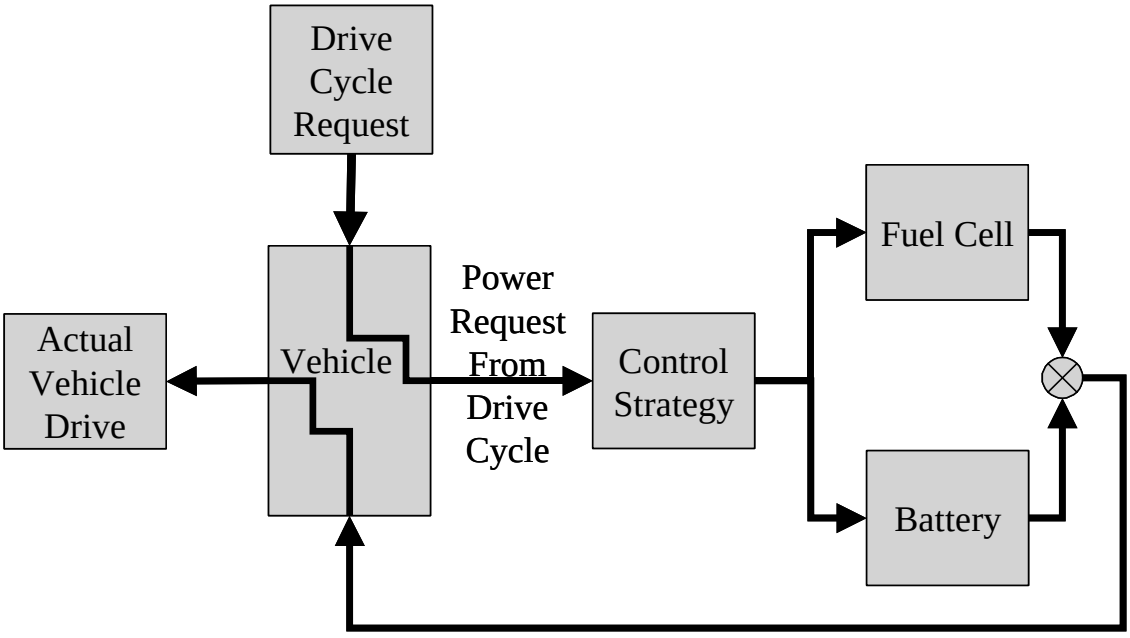

Figure 6. Block diagram a of vehicle model.

Figure 6 is a simple block diagram of the vehicle model. At each time step during a drive cycle the drive cycle makes a request to the vehicle and the vehicle control strategy. The control strategy determines how much power to request from the fuel cell and battery models. Then the models supply the power requested to the vehicle that may or may not meet the drive cycle request because of power limiting effects in the system.

The control strategy in ADVISOR™ provides a net power request to the fuel cell system. To meet the requirement of a net power request, the fuel cell model developed for this work is broken into two major parts: the electrochemistry model and the thermal model.

Figure 7 shows a basic block diagram for the fuel cell system model developed for this work.

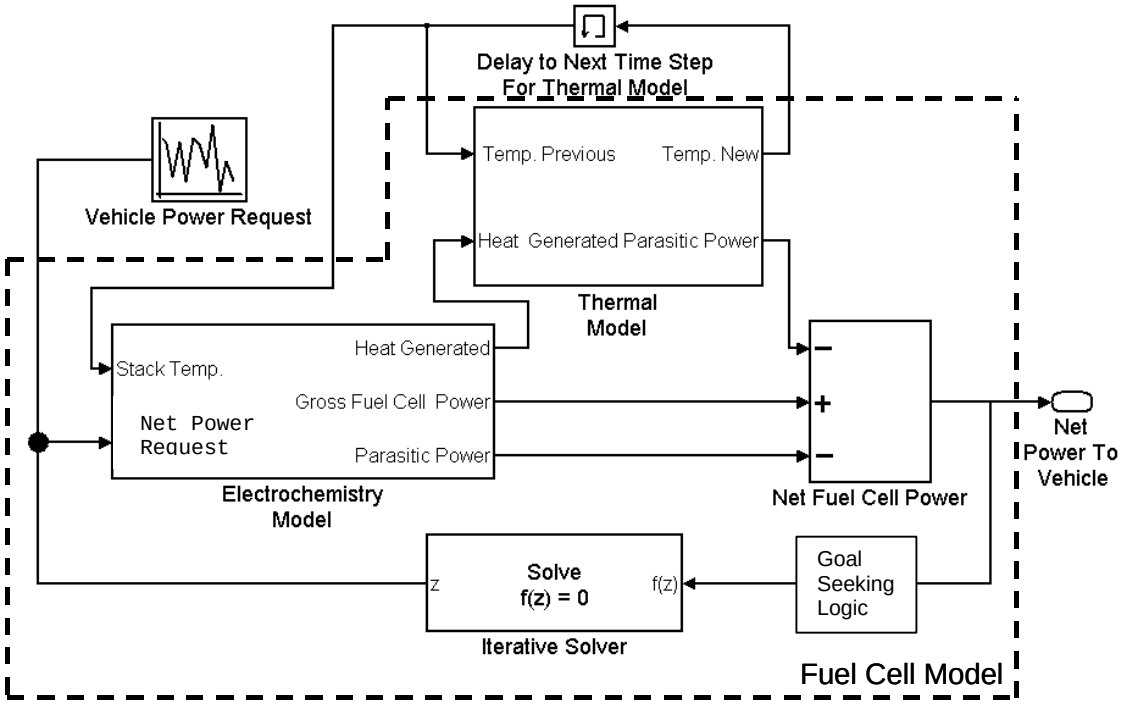

Figure 7. Block diagram of the fuel cell model.

The electrochemistry model relates the operating conditions (temperature, pressure, humidity, etc.) to a fuel cell stack voltage and current. At this point, the vehicle power request makes a net power request to the fuel cell system. To start the solution, the iterative solver uses an initial condition that relates the net power request to a gross power request. The basic inputs to the electrochemistry model are the gross power request and the fuel cell stack temperature. With these inputs to the electrochemistry model three basic pieces of information are developed:

1. Thermal energy generated inside the fuel cell stack;
2. Gross fuel cell power at the present operating conditions;
3. Parasitic power required to run the fuel cell system at the present gross power operating point.

The thermal model uses the results of the electrochemistry model to determine the operating temperatures in the fuel cell system. The temperatures of the fuel cell stack as well as the reservoir and water balance are also input from a delayed feedback loop. At each time step, the results of the previous time step (or initial conditions) are used in the thermal model. With the water balance and temperature information from the previous time step, as well as the characteristics of the thermal system, the thermal model is able to perform energy and mass balances on components in the fuel cell system. Here information such as water balance, parasitic power, cathode operating conditions; humidification, condensation, and heat rejection requirements are generated.

Using the information about the gross power point and the parasitic power required from the electrochemistry and thermal model, a net power operating point is established. During each time step, the iterative solver repeats the thermal and electrochemistry calculations to refine the gross power input to meet the requested net power output. Internal to the iterative solver are logic steps that refine the solution to different goals in order to meet different operating scenarios.

3.1 Block diagrams

The model developed for this work is built in Matlab's™ Simulink™ modeling tool, and the detailed block diagrams are available in Appendix A. These block diagrams define the mathematical relationships and logic required for the model. Building the model required four main levels of programming.

The first or top level is the interface to the model that accepts the requests to the model and provides results. The second level is responsible for imposing the limits or goal as previously discussed in the text. At the second level, the model is selecting the appropriate paths to calculate the operation of the fuel cell system. The logic contained in the second level, chooses one of the three goals that is contained in the third level of the model. At this point, the electrochemistry and thermal model are evaluated at the current operating conditions, meeting a net power request, either cell voltage, or no

power generation. The fourth level uses simple functions or subroutines that calculate fluid properties or relationships.

3.2 Net power generation scenarios and goal seeking

The fuel cell model has the ability to converge to three different goals when given a net power request. These are listed in Table 4.

Table 4. Goal scenarios of the fuel cell model.

Goal #1	Generate the net power requested
Goal #2	Generate a power that has been limited due to operating conditions
Goal #3	Generate zero gross power

Trial and error in programming yielded the order in computation given below to provide a stable and fast approach to calculating a net power operating point.

The first step is to determine if the current net power request to the system fulfills the requirements of goal #3. As part of the fuel cell control strategy of increasing system efficiency, a minimum power point is used. If the net power requested is less than the minimum allowed system power, then the model generates zero gross system power. Goal #3 continues to calculate through the thermal model in the system where components cool down due to ambient losses.

In the next step, if goal #3 is not chosen, the model logic sets the goal of the iterative solver to find the maximum power that the fuel cell can generate at the current operating conditions by forcing the cell voltage of the stack to the minimum cell voltage allowed which is goal #2.

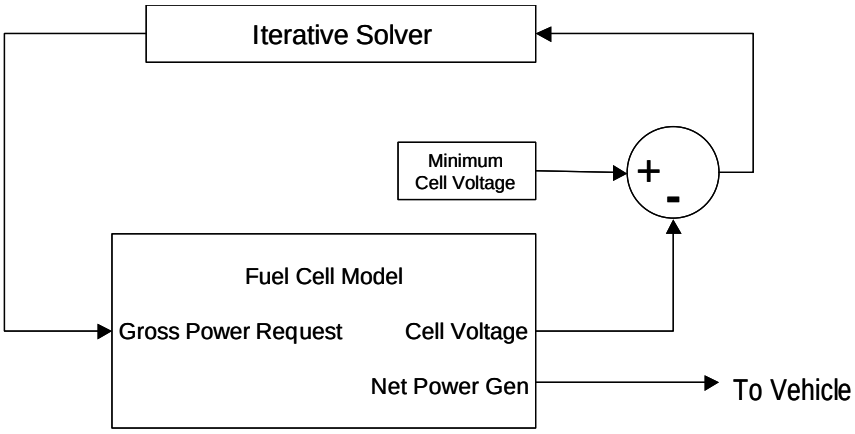

Figure 8. Block diagram of the iterative methods to impose a cell voltage.

Figure 8 above shows the block diagram of the iterative solver used to impose the minimum cell voltage criteria. The iterative solver built into Simulink™ is placed in a feedback loop that drives the input of the solver towards zero. Because the goal of this iterative model is to converge the solution towards a minimum cell voltage, the input of the iterative solver is the minimum cell voltage subtracted from that output by the fuel cell model. When the input to the iterative solver is zero then the minimum cell voltage criteria and the operating cell voltage are equal.

After this operating point is established, logic that decides which goal scenario has been chosen determines if the net power generated at the minimum cell voltage operating point is greater than the present net power requested to the fuel cell system. If the net power at the present operating point is less than the current net power request to the system, then the current operating conditions will not allow the fuel cell to generate the requested power. If the present operating point is greater than the requested net power, then the model recalculates the operating point towards a net power request operating point (Goal #1) that is shown below in Figure 9.

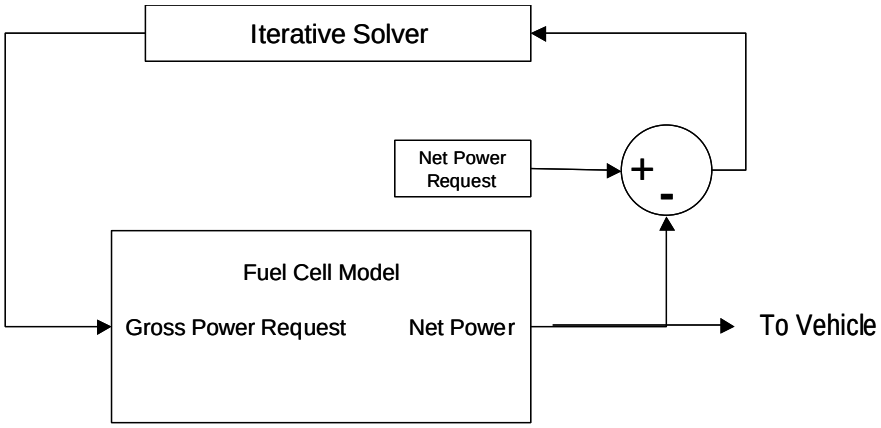

Figure 9. Block diagram of the iterative method to meet the net power request.

Goal # 1 is achieved using an iterative method that is similar to those used in goal #2. Instead of imposing a cell voltage criterion on the system, a net power criteria is the goal of the iterative solver. Again, the iterative solver drives its input to zero, so it is necessary to subtract the present net power request from the net power that is generated at the current operating conditions. When the input to the solver is zero, then the net power presently generated by the fuel cell model equals the net power requested from the vehicle.

4 Electrochemistry and Parasitics Model

At each time step, the fuel cell model determines the operating point of the fuel cell based upon a request made to the system. The electrochemistry model needs an operating condition for the current density, temperature, and pressure. Also apart of the electrochemistry model is calculation of the parasitics associated with the fuel cell model. To calculate parasitics, mass flow and the heat generated by the reaction need to be used to determine parasitics and couple the electrochemistry model to the thermal model.

4.1 Evaluation of the Polarization Curve

To evaluate the polarization curve, three pieces of information are required; current density, temperature, and pressure. The net power has a functional relationship with current density that is further refined using the iterative methods discussed in section 3.2. Use of the thermal model that will be discussed in chapter 5, determines the temperature operating point of the fuel cell. Finally, the operating pressure is related to the present current density of the fuel cell that is discussed further in chapter 6.

4.1.1 Current Density Approximation

From the goal seeking functions of Matlab™, a gross power request is made to the fuel cell operating point and thermal model. The gross power request is then related to a current density using an equation that was developed from the fuel cell stack polarization curve approximation. The following polarization equation only needs current, temperature, and the partial pressure of oxygen to approximate an operating point and fuel cell power.

$$cell\_voltage = (voc - tafel * Log10(1e3 * current) - (ohmic - temp * Tcell)) * current + concentration * Log10(PO_2) + ((Tcell) - ref\_temp) * temperature * Log10(1e3 * current))\ \ Volts \quad (1)$$

Equation 1. General Polarization Equation

Evaluating Equation 1 at 60 C and an O_2 partial pressure of 0.2 atm over a range of 0.001 A/cm^2->1 A/cm^2, and plotting power vs. current, results of the polarization cure are given in Figure 10.

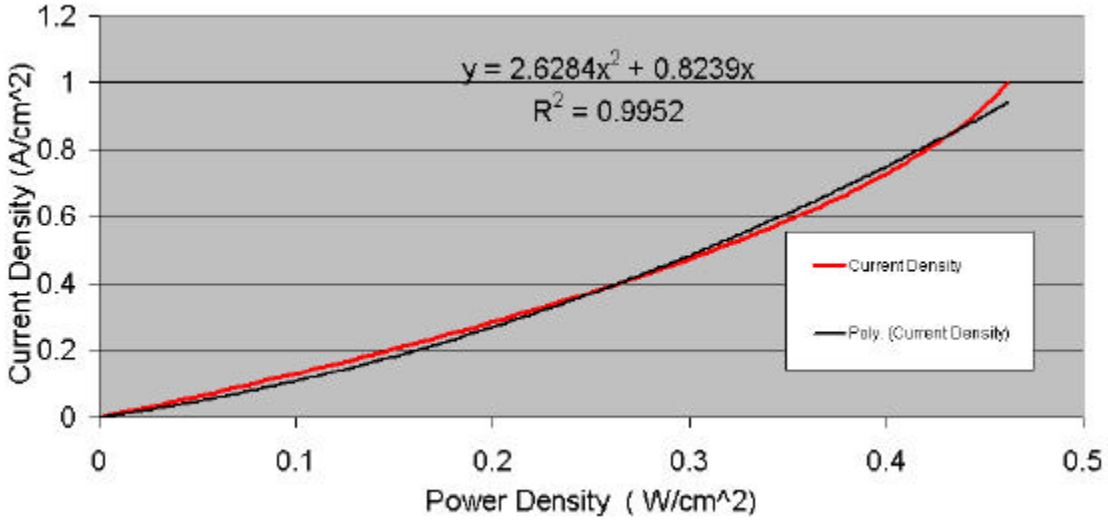

Figure 10. Current density vs. power density approximation.

A regression analysis of the curve in Figure 10. results in a second order polynomial. For a different fuel cell stack, a different curve would result to account for the differences in geometry. The second order polynomial fit of the polarization curve given above is written as:

$$current\_density = 2.6284 * power\_request^2 + 0.8239 * power\_request \quad \frac{A}{cm^2} \qquad (2)$$

Equation 2. Current density approximation function to relate current density to gross power request

A requirement for Equation 2 is it passes through the zero point. This will increase the stability of the solution at low or zero power.

4.1.2 Fuel Cell Operating Temperature and Pressure

To evaluate the polarization curve given by equation 1, the operational values for the average fuel cell temperature, pressure, and relative humidity must be known. The

average fuel cell stack temperature is obtained from the transient thermal model that is covered in chapter 5. Relative humidity is obtained from operating conditions that are defined by the user in the input to the system model covered in section 6.4.

Finally, the average partial pressure of oxygen is the last piece of information needed to evaluate the polarization curve. The average partial pressure of oxygen is calculated by averaging the inlet partial pressure and the outlet partial pressure. The inlet partial pressure of oxygen is calculated through the following relationship:

$$PPO_2@Inlet = (P_{inlet} - (Rh \times Psat)) \times 0.2095 \qquad atm \quad (3)$$

Equation 3. Partial pressure oxygen at the cathode inlet

The stack inlet pressure is obtained from the system control strategy given in chapter 5. And is dependent on current and temperature. Note that each of the equations uses the appropriate unit conversions to yield the partial pressures in units of atm.
To account for the oxygen used during the reaction, the outlet relationship for partial pressure of oxygen has to be modified using the stoichometric ratio of air for the cathode, namely,

$$PPO_2@Outlet = ((Poutlet - (Rh \times Psat)) \times 0.2095) \times (1 - \frac{(Sr-1)}{Sr}) \qquad atm \quad (4)$$

Equation 4. Partial pressure of oxygen at the cathode outlet

4.1.3 Stack Gross Power

With the three operating conditions previously discussed, temperature, pressure, and current density, it is possible to calculate the stack gross power using equations 2 to 4 and the following relationship:

$$Gross\ Power = Cell\ Voltage * Current\ Density * Total\_Cell\_Area \quad W \quad (5)$$

Equation 5. Gross power

4.2 Calculating System Parasitics

A fuel cell system requires the use of components such as pumps and fans that require energy input. As a result, the parasitic energy consumed by these devices must be subtracted from the overall gross power generated by the fuel cell stack to determine the net operating point of the system. Four devices contribute to the parasitic power required for operation of the fuel cell system. They include the air compressor, thermal coolant pump, radiator fan, and condenser fan.

4.2.1 Air Compressor System

Air mass flow and air pressure are required to calculate the impact that the air compressor has on the parasitics power use. The amount of air used is obtained from a simple relationship Laramie and Dicks, 2000 given by:

$$Air\ usage = \frac{3.57E^{-7} \times Sr * Gross\ Power}{Cell\_Voltage} \quad kg/s \quad (6)$$

Equation 6. Oxygen / air usage relationship

The model has a minimum cathode flow rate of 1 gm/s (1% total mass flow at 50kWe net) to provide stability for the calculation of the air compressor power required. Very

small mass flow rates lead to very large powers because of limited data for the air compressor.

At this point empirical data measured from air compressors is used to lookup volumetric efficiency, adiabatic efficiency, and temperature rise. The temperature rise across the compressor is used for the inlet temperature of the humidifier and the thermal model. Each of these attributes are retrieved using mass flow and pressure. The power is ten calculated utilizing the following:

$$Power = \frac{1}{h_{elec} h_{adiabatic}} (\dot{m} Cp_{air} T_{amb} \Pr^{((\frac{k-1}{k})-1)}) \qquad W \qquad (7)$$

Equation 7. Compressable work for air compressor

4.2.2 Coolant Pump

The coolant pump circulates coolant through the system to move energy through the stack, humidifier, and radiator. The coolant mass flow is the first operating condition for the coolant to determine. One of the operating requirements of a fuel cell stack is to limit the temperature rise across the fuel cell for practical reasons.

If we assume that all the internal energy generated is transferred to the coolant, then we can use the following relationship:

$$Qgen = Qcoolant \qquad (8a)$$

$$\dot{m}_{coolant} = \frac{Qgen}{Cp_{coolant} \times \Delta T} \quad kg/s \qquad (8b)$$

Equation 8. Mass flow rate for coolant relationship

We then need to know how much thermal energy, Qgen is generated in the stack. The following equation Laramie and Dicks, 2000 Qgen is used:

$$Qgen = Stack\ gross\ power - \frac{Stack\ gross\ power * 1.05E^{-8} * LHV\ H_2}{CellVoltage} \quad W \qquad (9)$$

Equation 9. Internal heat generation for fuel cell

Stack gross power and cell voltage are obtained from the polarization curve of the fuel cell. To determine the power needed to pump the fluid, the pressure drop in the system is required. For this specific model, the pressure drop and power were measured on the vehicle, and an operating line was determined. A 1-D lookup table was generated to interpolate between operating points and make a continuous operating line as a function of mass flow rate alone. The function in the lookup table is depicted in Figure 11 and relates head, efficiency, and power to the flow rate.

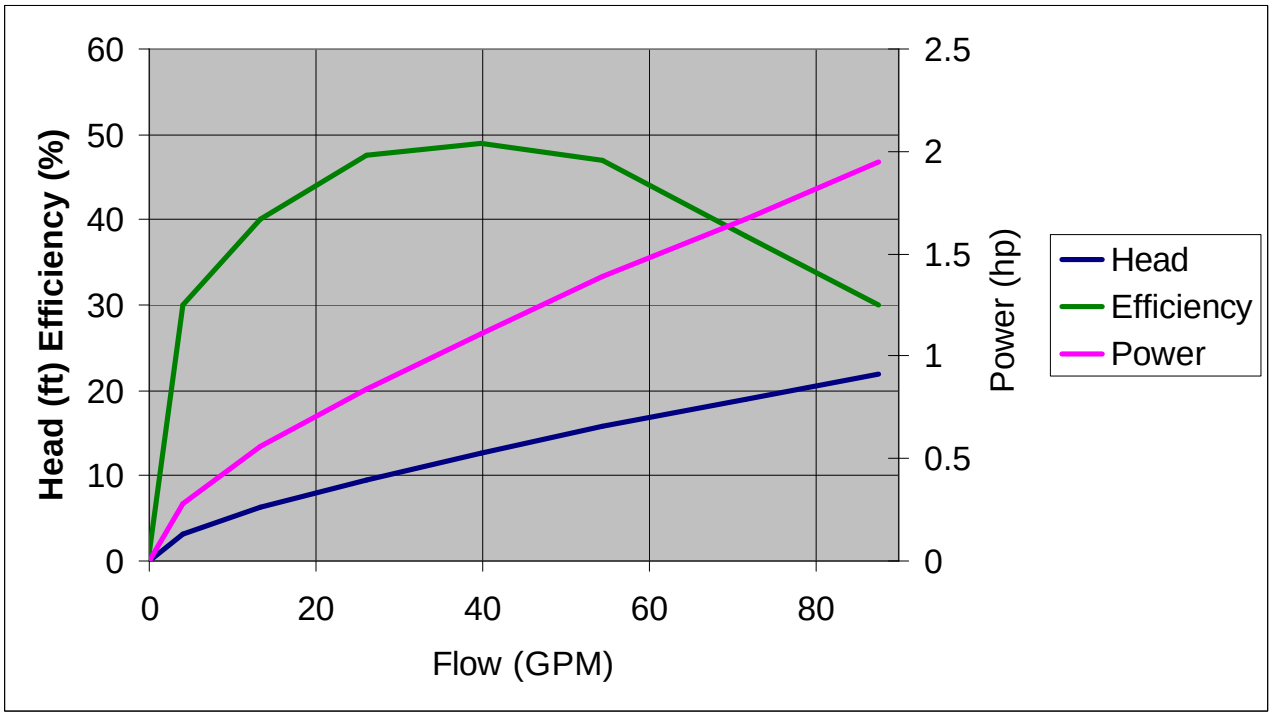

Figure 11. Coolant pump operating line.

4.2.3 Radiator Fan and Condenser Fan

The final two components that contribute to the parasitic power are the radiator and condenser fans. The model needs pressure and mass flow through the fan to calculate the power required. During model simulation, the fans are turned on and off, depending

upon temperatures through the radiator or condenser that are determined by the control strategy. The mass flow is a user-defined input to the model, and the pressure drop is obtained from (Kroger, 1984), i.e. a relationship based upon empirical data that has been fitted with a curve:

$$\mathrm{Pr}essure\_Drop = (326.12 * Mass\_Flow - 75.396) + 101.325 \qquad kPa \qquad (10)$$

Equation 10. Pressure drop through radiator relationship

The following thermodynamic relationship is used to calculate the fan power:

$$Power = \frac{1}{h_{elec} h_{fan}} (\dot{m} Cp_{air} T_{amb} \mathrm{Pr}^{((\frac{k-1}{k})-1)}) \qquad W \qquad (11)$$

Equation 11. Power for radiator fan

Since temperatures in the thermal system determine if the fans need to be operating, it is necessary to solve the thermal model to complete the net power operating point. The fan is determined to be on or off by the thermal model that will be covered in the next chapter.

5 Thermal Model

The thermal model consists of four major components that are modeled using energy and mass balances to calculate outlet temperatures of the devices. A lumped capacity finite difference thermal model has been used for the fuel cell stack and the thermal reservoir. Specifically an explicit finite difference method is used to evaluate the transient nature of the model. The goal of the research is to understand the impact that these thermal masses have on the overall efficiency and power of the fuel cell system. Two thermal masses are accounted for in the fuel cell model; fuel cell stack, and coolant reservoir. In the model, the reservoir accounts for the thermal mass of the coolant; plumbing and components as well as the heat transfer from the plumbing to ambient in the system. Highlighted in red Figure 12 are the components that are a part of the thermal model.

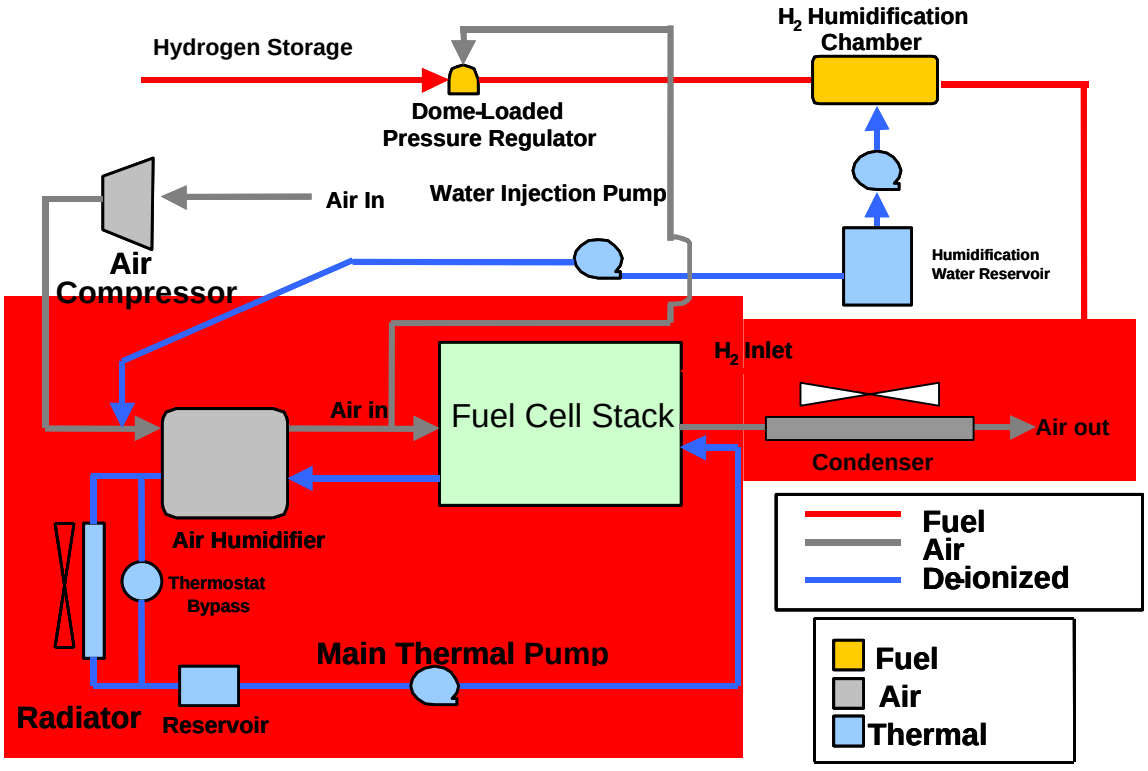

Figure 12. Fuel cell system model diagram.

5.1 Fuel cell stack

The fuel cell model uses a black box approach that accounts for the energy and mass entering and leaving the stack. Below in Figure 13 is the black box diagram of what is included in the energy and mass balance of the fuel cell stack.

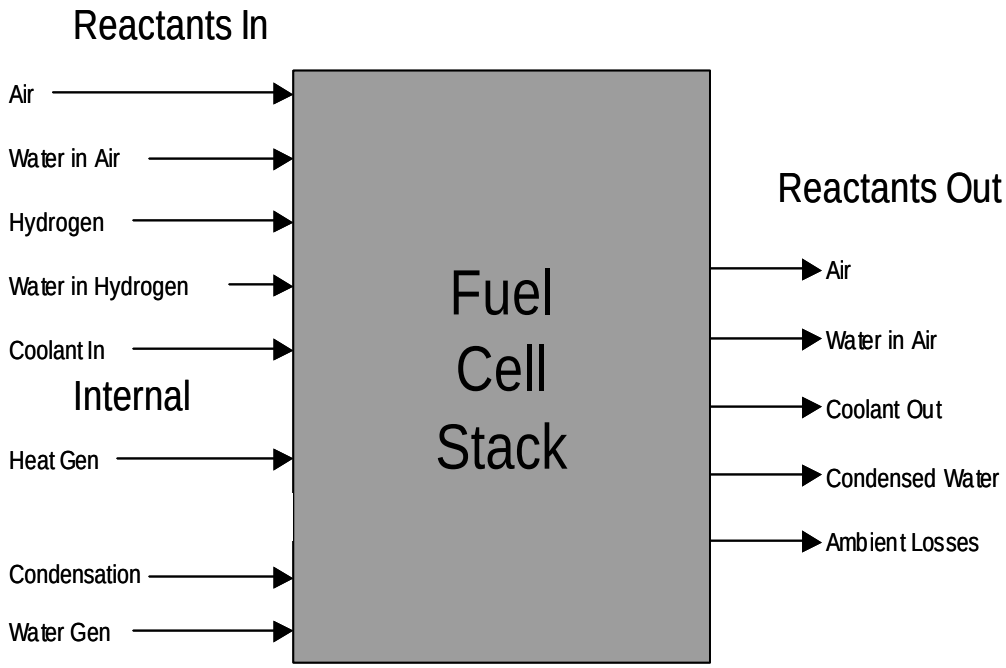

Figure 13. Fuel cell black box model.

The reactant streams entering the stack include the air, coolant and hydrogen as well as the water in both air and hydrogen entering the stack. Water vapor entering the stack in the air and hydrogen streams have been separated for simplicity in the model. Internal to the stack is heat generation, water generation, and condensation of excess water.

Taking a closer look at the cathode (air) side of the fuel cell stack, air enters the stack from the humidifier with some water vapor. Inside the stack, water is generated as the byproduct of power generation. Since the lower heating value of hydrogen has been used, all the water produced due to energy conversion is assumed to be in the form of vapor. Depending on the operating conditions of the fuel cell, specifically the temperature and relative humidity of the air entering the cathode, the excess water vapor generated in the stack will go towards saturating the cathode outlet air stream. If the sum of the water entering the stack and the water generated inside the stack exceeds the water

vapor capacity of the air at the outlet temperature of the cathode, then the excess water is condensed and additional heat is released inside the fuel cell stack.

The reactants leaving the stack are air, water in air, coolant, condensed water, and energy losses to the ambient. An assumption is made that all the water entering the stack from the anode (hydrogen) stream is diffused through the proton exchange membrane and leaves thru the cathode. The diffused water is then included towards saturating the water vapor content of the cathode. Condensed water leaves the stack because of the saturation of the cathode air stream. A part of the model assumption is that hydrogen does not carry a significant amount of energy in or out of the stack, so it has been neglected thermally. Thus all of the water in the air and hydrogen entering the stack leave via the cathode. Ambient losses include convection heat transfer from the exterior of the fuel cell stack to the ambient.

The fuel cell stack also has a lumped thermal capacitance as part of the finite difference model. The energy and mass balance with the finite difference method applied is

$$Tstack = Tprevious + \frac{TimeStep}{LumpedCapacatnce}(HeatGen - Qcoolant - Qambient - Qair \quad (12a)$$
$$- Qwater\_vapor + Qcondensng) \qquad K$$

More specifically, each of the energy and mass contributors are calculated using the following equation:

$$Tstack = T_{sp} + \frac{\Delta t}{M_{stack} Cp_{stack}}(q_{gen} - \dot{m}_c C_{pw}(T_{c\_in} - T_{sp}) - UA(T_{sp} - T_{amb}) - \dot{m}_{air} Cp_a(T_{air\_in} - T_{sp})$$
$$- \dot{m}_{wv\_out} * Cp_{wv}(T_{sp}) + \dot{m}_{wv\_in} * Cp_{wv}(T_{wv\_in}) + \dot{m}_{h_2 0\_condensed} h_{fg}) \qquad K \quad (12b)$$

Equation 12. Fuel cell stack energy balance equation

Each of the components below is pertinent to the fuel cell stack model.

Table 5. Fuel cell stack energy balance equation components.

Variable	Description	Units
Tstack	Temperature of stack at current time step	Kelvin
T_{sp}	Previous stack temperature or initial condition	Kelvin
Δt	Time Step	Seconds
M_{stack}	Mass Stack	Kg
Cp_{stack}	Specific Heat Stack	kJ/kg-k
q_{gen}	Heat gen internal to stack	Watts
$\dot{m}_c$	Coolant flow rate	kg/s
Cp_w	Specific heat water	J/kg-k
T_{c_in}	Temperature of the coolant entering the stack	Kelvin
UA	Overall heat transfer from fuel cell stack	kj/K
T_{sp}	Temperature of the fuel cell stack in the previous time step	Kelvin
$\dot{m}_{air}$	Mass flow rate air	Kg/s
Cp_a	Specific heat air	j-kg/k
$\dot{m}_{wv\_out}$	Mass flow water vapor out of stack in air	kg/s
Cp_{wv}	Specific heat water vapor	J/kg-K
T_{wv_in}	Temperature of water vapor in cathode	Kelvin
$\dot{m}_{wv\_in}$	Mass flow water into stack cathode	kg/s
h_{fg}	Heat of vaporization of water	J/kg
$\dot{m}_{h_2o\_condensed}$	Mass flow rate of condensed water	Kg/s

Specific to the fuel cell stack are the following operating conditions in Table 6. These operating conditions are set by a configuration file for the model,

Table 6. Fuel cell stack operating conditions.

Location	Temp	Pressure	Humidity
Cathode Inlet	Previous Stack Temperature	Based upon present stack current density	60% RH
Anode Inlet	Previous Stack Temperature	Based upon present stack current density	80% RH
Coolant Input	Previous Time Step Outlet Reservoir	N.A	N.A
Cathode Output	Calculated temperature current time step	Pressure drop across stack	Calculated 100% RH Max
Coolant Output	Calculated temperature current time step	N/A	N/A

5.2 Humidifier

The humidifier conditions the air entering the fuel cell stack from the air compressor to the appropriate temperature and humidity. This device uses the waste heat from the fuel cell stack coolant as energy to vaporize the water added to the air stream. The goal of the humidifier is to humidify the air from the compressor to the humidity required by the control strategy. Since humidity is based upon temperature and pressure, the present operating pressure is used and the temperature of the fuel cell stack cathode inlet temperature is used. It has been assumed that the humidifier can always condition the air entering the cathode to the inlet coolant temperature of the fuel cell stack. This is possible because the coolant used in the humidifier for vaporization energy is the outlet coolant and the hottest coolant in the system. Taking a black box approach to the problem, an energy and mass balance on the system has been preformed to determine the temperature drop of the coolant across the humidifier.

Figure 14. Humidifier black box diagram.

An energy balance has been preformed between the coolant and the remaining fluids into the system:

$$Qcoolant = Qair - Qvaporization\_humidification + Qsensible\_humidity\_water + Qvapor\_out \quad (13a)$$

The specific equation used in the model is the following:

$$Thumidifer\_coolant\_out = Tci + \frac{1}{\dot{m}_{h20} Cp_{h_2 0}} (\dot{m}_{air} Cp_{air} (T_{air\_out} - T_{air\_in}) - \dot{m}_{wv\_in} Cp_{wv} T_{air\_in} - \dot{m}_{hw} Cp_{h_2 0} T_{hw} + \dot{m}_{wv\_out} Cp_{wv} T_{air\_out} - \dot{m}_{hw} h_{fg}) \quad K \quad (13b)$$

Equation 13. Humidifier energy balance equation

Each of the variables in equation 13 are described in Table 7 below.

Table 7. Humidifier equation components.

Variable	**Description**	Units
Thumidifer _coolant _out	Temperature of coolant water out of humidifier	Kelvin
Tci	Temperature of coolant water into humidifier	Kelvin
$\dot{m}_{h20}$	Mass flow rate of coolant water (liquid)	kg/s
$Cp_{h_2 0}$	Specific heat water	j/kg-K
$\dot{m}_{air}$	Mass flow rate of air	kg/s
Cp_{air}	Specific heat air	j/kg-K
$\dot{m}_{wv\_in}$	Mass flow water vapor in (Ambient Water Vapor)	kg/s
Cp_{wv}	Specific Heat Water Vapor	J/kg-K
T_{air_in}	Temperature air in	Kelvin
$\dot{m}_{hw}$	Mass flow rate humidity water (liquid)	Kg/s
T_{hw}	Temperature Humidity Water (liquid)	Kelvin
$\dot{m}_{wv\_out}$	Mass flow rate water vapor in air out	Kg/s
T_{air_out}	Temperature of air leaving humidifier	Kelvin
h_{fg}	Heat of vaporization of water	j/kg

Located below in Table 8 are the operating conditions for the humidifier.

Table 8. Humidifier operating conditions

	Temp	Pressure	Humidity
Air In	Temperature rise across air compressor	Specified by pressure / stack current relationship	Calculate from ambient contribution
Humidification Water in	Current time step fuel cell stack temperature	N/A	N/A
Coolant In	Current time step fuel cell coolant outlet temperature	N/A	N/A
Air Out	Current time step fuel cell inlet temperature	Specified by pressure / stack current relationship	Specified by parameter: 60% RH

5.3 Radiator

The purpose of the radiator in the fuel cell system is to maintain the operating temperature of the fuel cell stack by rejecting excess heat to the ambient. Any of the energy not required for humidification or raising the temperature of the thermal masses of the fuel cell stack and reservoir must be rejected to the ambient. Current conventional vehicles utilize a thermostat bypass to decrease the cold-start transient and increase the operating efficiency. Typically, in a conventional vehicle system the thermostat is connected to the outlet of the internal combustion engine and diverts flow to the radiator or around the radiator. The thermostat also can blend the two outlets so as not to send large slugs of cold water through the engine. The location of the thermostat is shown in Figure 12. Fuel cell system model diagram. In this model the thermostat is located between the humidifier and the radiator where the bypass around the radiator to the coolant reservoir.

One of the key elements of the radiator is modeling the heat transfer capabilities. So as not to require a complicated iterative model, D.G. Kroger (SAE 1994) has developed relationships that model heat transfer and pressure drop based upon a typical vehicle radiator. For a standard 33-tube single pass vehicle radiator that is 0.5 m^2 of frontal area the following equations apply:

$$\Pr essure\_Drop = (326.12x - 75.396) + 101.325 \qquad kPa \tag{14}$$

Equation 14. Pressure drop relationship for a radiator

$$h_{rad} = -1.4495x^2 + 5.9045x - 0.1157 \qquad \frac{kW}{m^2 C^o} \tag{15}$$

Equation 15. Heat transfer relationship for a radiator

Where x is the air mass flow through the radiator (kg/s). An energy balance is performed on the radiator:

$$Qcoolant = Qradiator$$

$$Tradiator\_coolant\_out = T_{ci} - 0.5 * \frac{Fr_{Area}(T_{ci} - T_{amb})h_{rad}}{\dot{m}_{coolant} Cp_{coolant}} \qquad K \qquad (16a,b)$$

Equation 16. Energy balance for radiator

Equation 16b has been generated to allow for any size radiator. The work done by Kroger was performed on a 0.5 m^2 radiator. The 0.5 constant located in Equation 16b was inserted to allow definition of any size radiator for the model.

Table 9. Radiator energy balance equation components.

Variable	Description	Units
$Tradiator\_coolant\_out$	Coolant Temperature out of Radiator	Kelvin
T_{ci}	Coolant Temperature into Radiator	Kelvin
Fr_{Area}	Frontal Area Radiator	m^2
T_{amb}	Ambient Temperature	Kelvin
h_{rad}	Heat transfer coefficient radiator	kW/m^2-C
$\dot{m}_{coolant}$	Mass flow rate through coolant	Kg/s
$Cp_{coolant}$	Specific heat coolant	Kj/kg-K

Table 10. Radiator operating conditions.

	Temperature
$Tradiator\_coolant\_out$	Goal to meet minimum fuel cell inlet temperature
T_{ci}	From outlet of humidifier coolant

The thermostat logic operates based upon the fuel cell temperature and is the following:

If
Stack inlet temperature > Fuel cell operating temperature set point
Then
Radiator outlet temperature = Calculated using heat transfer relations
Fan Power = Calculated using pressure drop relationship
Else
Radiator outlet temperature = Radiator inlet temperature
Fan Power = 0

To calculate fan power we need pressure drop and mass flow to figure out the power required. During the model simulation, the fans are turned on and off depending upon

the thermostat logic previously described. The mass flow is a user-defined input, and the pressure drop is obtained from equation 14.

Using a thermodynamic relationship for the fan power:

$$Power = \frac{1}{h_{elec} h_{fan}} (\overset{*}{m} Cp_{air} T_{amb} \Pr^{((\frac{k-1}{k})-1)}) \qquad W \tag{17}$$

Equation 17. Fan power thermodynamic relationship

We now have a model for the thermal performance of the radiator in the system and the parasitic power to run the system.

5.4 Reservoir

The final device in the thermal subsystem of the fuel cell system is the reservoir. In the thermal system, the reservoir is responsible for providing a source that the coolant pump can draw from and allow for the thermal expansion of the water in the system. In the model, the reservoir accounts for the thermal mass of the coolant; plumbing and components as well as the heat transfer from the plumbing to ambient in the system. A backward looking finite difference method was used to perform an energy balance on the system:

$$Treservoir = T\,\mathrm{Re}servoir\_previous - \frac{TimeStep}{LumpedCapaci\tan ce}(Qcoolant - Qambient)$$
$$Treservoir = T_r^p - \frac{\Delta t}{M_{res} Cp_{res}}(\dot{m}^c Cp^c (T_r^p - T_{ri}) + UA(T_{ri} - T_{amb}) \qquad K \tag{18}$$

Equation 18. Energy balance equation for reservoir

Table 11. Reservoir energy balance equation components.

Variable	Description	Units
Treservoir	Temperature of Reservoir end of Time Step	Kelvin
T_r^p	Temperature of Reservoir Previous Time Step	Kelvin
Δt	Time step	Seconds
M_{res}	Equivalent mass coolant water in system	Kg
Cp_{res}	Specific heat of coolant	J/kg-k
$\dot{m}_c$	Mass flow rate of coolant into reservoir	Kg/s
Cp_c	Specific Heat Coolant	J/kg-k
T_{ri}	Temperature of Coolant into Reservoir	Kelvin
UA	Heat transfer of Plumbing to ambient	J/K
T_{amb}	Temperature of Ambient	Kelvin

5.5 Condenser

Water balance is of interest for a vehicle fuel cell system because of its logistical and practical implications when the water balance is negative. Water balance is defined as the net amount of water needed to run a fuel cell system. Water is required to humidify the inlet cathode and anode reactant streams for proper fuel cell operation. Inside the fuel cell, water is generated as a byproduct of the energy conversion. A simple performance model of the condenser has been implemented to quantify how much water could be recovered from the outlet of the cathode. The condenser uses the same heat transfer and pressure drop relationships as the radiator model to approximate the performance, see:

Equation 14. Pressure drop relationship for a radiator
Equation 15. Heat transfer relationship for a radiator

The model performs an energy balance between the capacity of the condenser and the amount of energy that must be removed to condense the water in the cathode air stream.

First using the heat transfer relationship in Equation 15, the heat capacity of the condenser is formulated as:

$$Qcondenser = h_{rad}\, Fr_{area} \times 0.5 \times (T_{ai} - T_{amb}) \tag{19}$$

Equation 19. Heat capacity of airside of condenser

Next, the heat needed to condense all of the water in the condenser is formulated as:

$$Qvap\_cond = m_{wv\_in}\, h_{fg} \tag{20}$$

Equation 20. Energy required to condense water in cathode air stream

Modeling of the condenser is an energy balance between what energy would be required to condense all the water vapor out of the cathode air stream and the amount of energy the condenser is able to reject to ambient. Air and water vapor enters the condenser and is then cooled from heat transfer to the ambient. The amount of water that is condensed is proportional to the amount of energy the condenser can reject to the ambient. An energy balance has been used between the air and water vapor entering, and the energy needed to condense all the water vapor in the air. Setting equations 19,20 equal and rearranging, the water recovered is formulated as:

$$Water\_recovered = \frac{Qcondenser}{Qvap\_cond} MassFlow\_Water\_Vapor$$

$$Water\_recovered = \frac{h_{rad} \times C_a \times Fr_{area}(T_{ai} - T_{amb})}{\dot{m}_{wv\_in} h_{fg}} \dot{m}_{wv\_in} \tag{21 a,b}$$

Equation 21. Water recovered from condenser

The water balance for the system is calculated as follows:

$$Total\_Water\_recovered = Previous Water\ Balance + Condenser Water\ Recovered - anode\_water - cathode\_water \tag{22}$$

Contained in Table 12 are the variables and descriptions associated with the condenser energy balance equations 21 a,b.

Table 12. Condenser energy balance equation components.

Variable	Description	Units
h_{rad}	Heat transfer coefficient condenser	kW/m^2-C
Fr_{area}	Frontal area condenser	m^2
T_{ai}	Temperature of Air and water entering condenser	Kelvin
T_{amb}	Temperature of Ambient	Kelvin
$\dot{m}_{wv\_in}$	Mass flow rate water vapor into condenser	kg/s
h_{fg}	Heat of vaporization of water	kj/kg
C_a	Constant = 0.5	Dimensionless

6 Fuel Cell System Control and Operating Conditions

The operating conditions of a fuel cell are closely linked to the performance of the fuel cell system. It is important to accurately describe the operating conditions of the fuel cell system such as the fuel cell stack characteristics, thermal fluid operating conditions, and the vehicle control strategy

6.1 Fuel cell stack characteristics

This section describes the characteristics of the fuel cell system taken into account about the geometric and physical configuration of the fuel cell stack(s). See Appendix B for the computer model specifics associated with these characteristics.

Cell Area: Fuel cell stack active area. If the fuel cells are multiple stacks that are electrically connected in parallel, add the individual cell areas of the stack connected in parallel.

For example: If you have 3 individual stacks, each has an active cell area of 200 cm^2 and these stacks are wired in parallel then the appropriate cell area would be 600cm^2.

Number of Cells: Total number of cells that are electrically connected in series.

For example: If you have three individual stack, each has 125 cells, and the stacks are electrically connected in series, the appropriate number of cells would be 375.

Lumped capacitance: The lumped heat capacitance of the fuel cell stacks. The value was developed assuming the majority of the fuel cell stack with thermal influence consists of graphite. Graphite has a specific heat of 709 J/kg –K, so the lumped heat capacitance would be the specific heat multiplied by the mass of graphite in the stack in kg.

Convection heat transfer coefficient: The heat transfer coefficient associated with the natural convection of the fuel cell stack. The number was calculated using Nussult

correlations from Incopera, et al. (1996), specifically the correlations associated with vertical and horizontal plates. A heat transfer coefficient for one vertical side and multiplied by four was used to account for the sides of the fuel cell stack. Then a heat transfer coefficient was developed for the horizontal (top) surface of the fuel cell and added to the vertical heat transfer coefficient. The bottom surface has been neglected because of the assumption that the surface is well insulated to convection due to securing the device when used in an application. Conduction of heat through the base has also been neglected.

Cathode pressure drop percentage: Since the fuel cell stack has a pressure drop across the fuel cell, a relationship provided by Nelson, et.al. (2001) figures that 15% of the total pressure on the stack is the pressure drop across the cathode inlet to outlet. This is consistent with the goals set forth by the Department of Energy's fuel cell and air management goals.

6.2 Polarization Equation

The polarization equation is used to relate the electrochemistry of the fuel cell to physical properties that can be evaluated quickly. For this particular model, an equation developed by Nelson (2001) that takes into account electrochemistry effects and additionally temperature dependent properties.

$$cell\_voltage = (voc - tafel * Log10(1e3 * current) - (ohmic - temp * Tcell)) * current + concentration * Log10(PO_2) + ((Tcell) - ref\_temp) * temperature * Log10(1e3 * current))$$

Equation 22. General cell polarization equation.

Where:

Voc:	Open circuit voltage of an individual cell
tafel:	Constant associated with activation losses
ohmic:	Constant to account for resistance or ohmic losses in the fuel cell
temp:	Constant to account for temperature effects associated with ohmic

losses Nelson (2001)

concentration: Constant associated with concentration of mass transfer losses in the fuel cell.

Ref_temp: Temperature at which the temperature effects (ohmic & temp) are referenced

Temperature: Constant at which that effects the overall open circuit voltage, Nelson (2001)

6.3 Thermal system characteristics

The design of the fuel cell system utilizes devices that define the thermal performance of the fuel cell stack. These characteristics account for the geometry and physical configuration of the components in the fuel cell system, excluding the fuel cell stack.

System coolant capacity: Total volume in gallons of coolant that is contained in the fuel cell system

Plumbing heat transfer coefficient: Heat transfer coefficient of the plumbing in the fuel cell system. The number was measured by placing a external heater on the fuel cell system and determining the steady state power to maintain temperature

Radiator frontal area: Frontal area in square meters of the main radiator in the system

Radiator fan flow rate: The mass flow rate in CFM that the fans associated with the radiator are capable of producing at the radiator pressure drop when operating

Condenser fan flow rate: The mass flow rate in CFM that the fans associated with the condenser are capable of producing at the radiator pressure drop when operating

Condenser frontal area: Frontal area in square meters of the condenser in

	the system
Coolant Pump max flow rate:	The maximum flow rate of the coolant pump allowed in the system in gallons per minute
Coolant pump minimum flow rate:	The minimum pump flow rate allowed in the fuel cell system
Coolant pump minimum power:	The minimum power that the coolant pump at the pump's minimum flow. Note: This in not the power at the minimum coolant pump flow rate
Coolant pump maximum power:	Maximum power required for the coolant pump in horsepower. Note: This is the power required at the coolant pump maximum flow rate.

6.4 Thermal Fluid Operating Conditions

The fuel cell system as stated before is heavily dependent upon the operating conditions in the fuel cell system. The following operating conditions or constraints are for components where variations of fuel cell system operating conditions exist.

Minimum cell voltage:	The minimum individual cell voltage that the fuel cell stack will not operate below
Stoichiometric rate of air	The ratio of actual air flow rate to Stoichiometric air flow needed for reaction. This value is held constant for all loads
Minimum current density:	Minimum current density at which an individual cell will operate.
Cathode humidity:	The relative humidity at the inlet of the cathode that the system will provide is constant for all loads and operating conditions except zero power
Mass flow rate of air minimum:	The minimum flow rate of air that the system will use.

Anode inlet humidity:	The relative humidity at the inlet to the anode of the fuel cell.
Minimum temperature for heat rejection:	The minimum temperature the fuel cell will reject heat to the ambient. If the radiator is properly sized and the operating conditions are not at extremes, then it is generally the fuel cell operating temperature.
Stack allowable temperature rise:	The maximum allowable temperature rise in the stack from the coolant inlet to the outlet.
Maximum cathode inlet pressure:	The maximum amount of pressure allowed at the cathode inlet
Minimum cathode inlet pressure:	The minimum pressure at the cathode inlet, 1 atm

6.5 Vehicle and fuel cell system control conditions

From the vehicle model, a net power request is made to the fuel cell system. Likewise, the fuel cell system must command the air compressor and coolant pump to supply the necessary reactants to the fuel cell stack. On board the development vehicle Magellan, the air compressor and the coolant pump speeds are based upon the fuel cell stack current. Three different characteristics of the system are available to the control strategy; fuel cell current, temperature, and system power request.

The fuel cell cathode operating pressure is dependent upon the fuel cell stack current. Kulp, et. al. determined that the parasitic power required for an air compressor at low fuel cell power dominates the efficiency of the system. Constant pressure in operation of the fuel cell stack is not desirable due to the poor system efficiency at low stack pressure. Particular to this work is a simple linear relationship chosen between fuel cell stack current and operating pressure that addresses the issue of low system efficiency at low power.

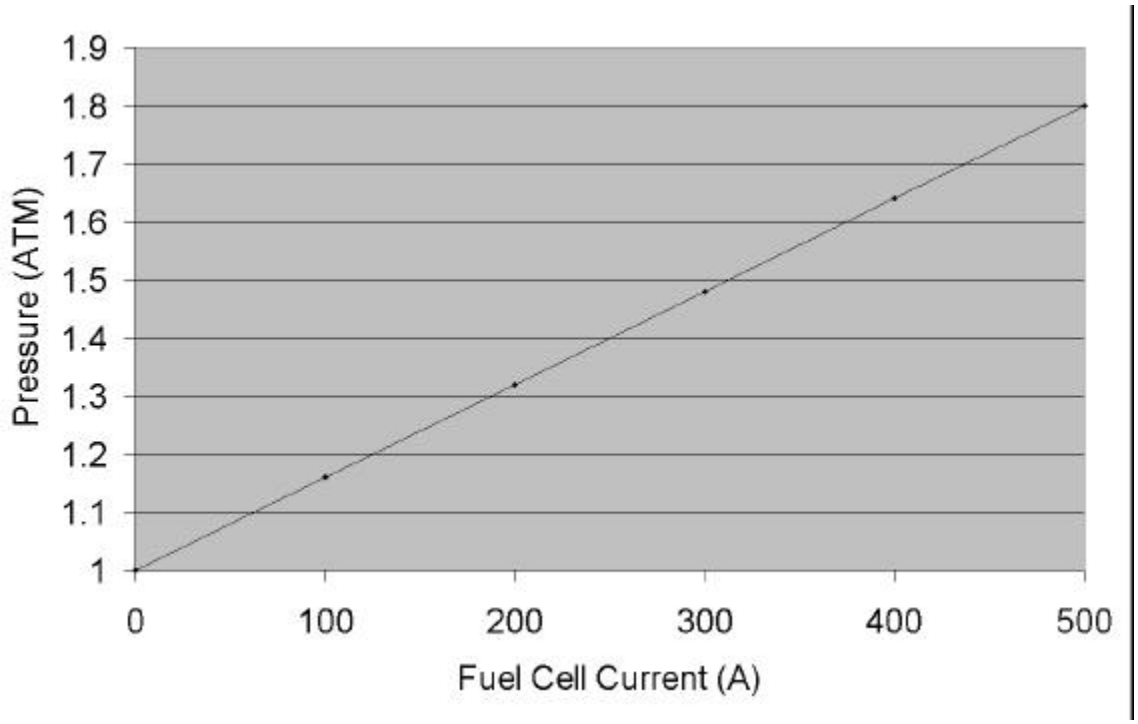

Figure 15. Operating pressure control strategy.

In Figure 15 above, is a simple linear relationship between the fuel cell current and the desired operating pressure. For this model, at zero Amps, the operating pressure is one atm, and at 500 A (full power) the operating pressure is 1.8 atm. In Simulink™ a simple 1-D linear interpolation routine is available. Simulink™ only requires the user to specify the range of input values and the range of output values. For this model, an input range of 0 to 500 A and an output of 1 to 1.8 atm have been chosen.

Also available to the system is the correction of operating pressure due to temperature. The correction factor is added as a constant depending upon temperature to the operating pressure control strategy previously described. A 1-D linear interpolation routine is used to apply the correction factor. Two operating ranges must be supplied for the input to the model, the temperature range, and the correction range. Typically the temperature range is 0 C to 100 C. The correction range is the added pressure (subtracted if the value is negative) to the base operating pressure range at the present fuel cell stack operating temperature. Figure 16 contains the results of applying a temperature correction factor to the baseline operating pressure control strategy.

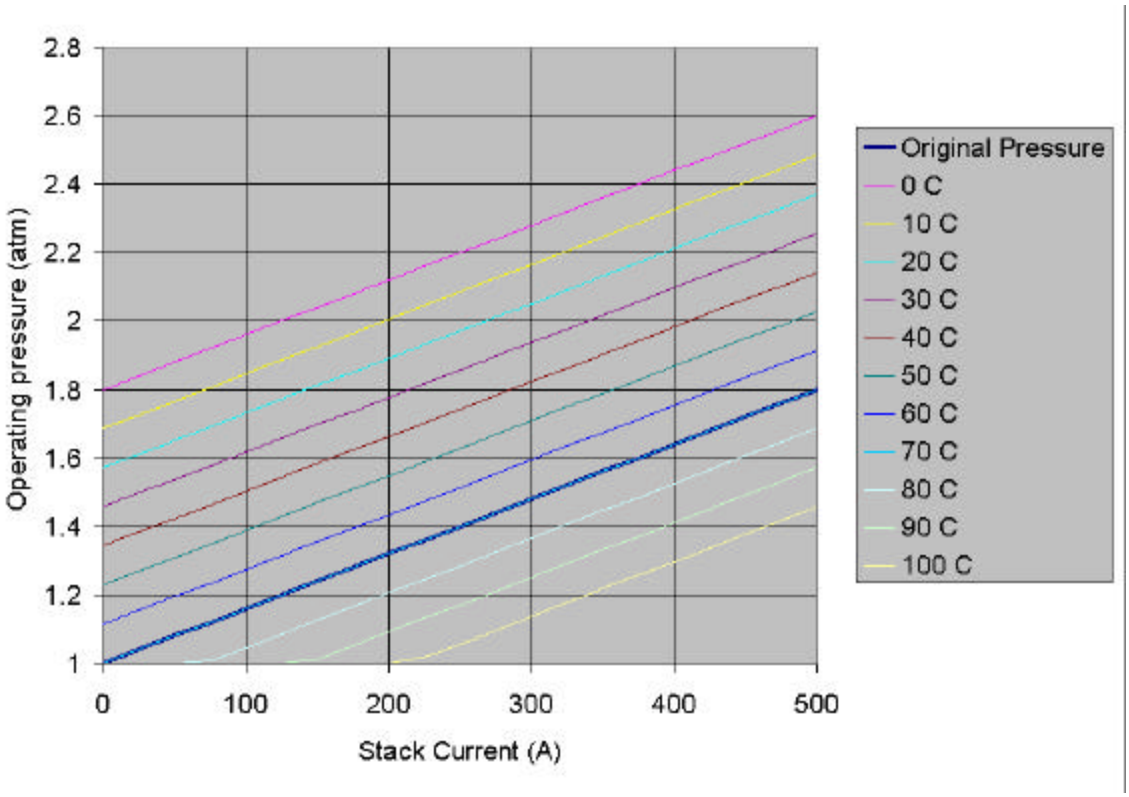

Figure 16. Operating pressure with temperature correction.

For this temperature correction, approximately 0.8 atm is added to the base operating pressure case at 0 C and 0.3 atm is subtracted at 100 C. Using this additional temperature control strategy will change the efficiency vs. power relationship.

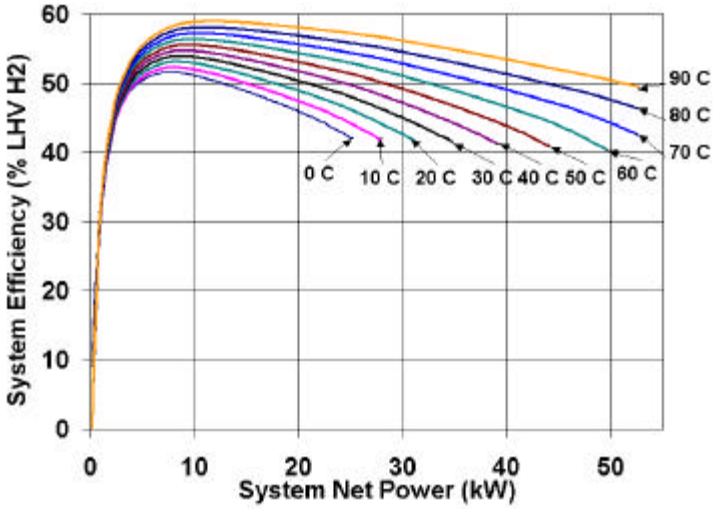

Figure 17. System Efficiency with varying temperature.

Figure 17 and Figure 18 present the steady state output of the model that describes the system efficiency versus power at varying operating temperatures. From the output of the figures below, the difference is a direct results of the temperature correction factor.

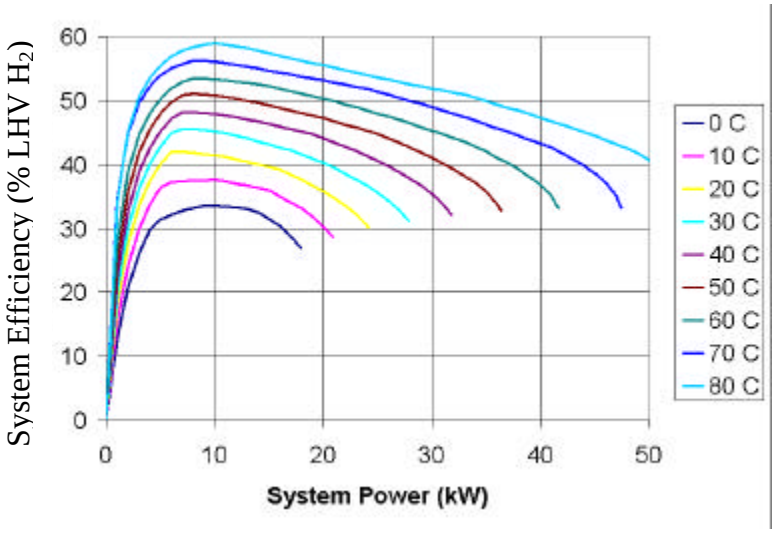

Figure 18. System efficiency with temperature / pressure correction.

Temperature correction of pressure was not used in the system or vehicle performance and efficiency analysis of this work.

7 Characterizing the System

Before exercising the model in a dynamic vehicle environment, simple tests have been performed that describe the system during steady state and simple transients. During these tests, it is possible to see the contributions that the parasitics and operating conditions have on the fuel cell system. Specifically the following section will discuss the steady state and step transient responses of the system.

7.1 Steady State System Characterization

The first test performed on the model fuel cell system is a steady state characterization of the system parasitic power used to run the fuel cell stack. In Figure 19 below, the parasitic power of the system was determined over the range of net system power up to 50 kWe.

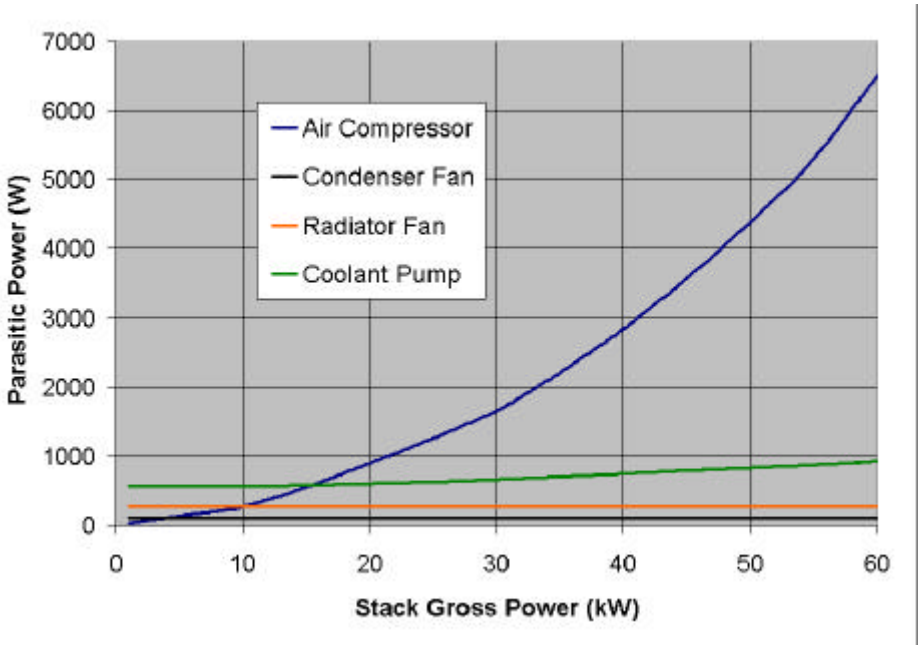

Figure 19. Fuel cell system parasitic power characteristics.

This test was performed at normal operating temperature of 80 C. The maximum cathode pressure is 1.8 atm, which corresponds to a stack gross power of 60 kWe, or 430 A. The

minimum stack pressure is 1.05 atm. From Figure 19 it is possible to see that the air compressor has the largest contribution towards parasitic power in the system.

7.2 System Efficiency Characterization at Fixed Temperatures

Further understanding of the temperature performance limitations for a fuel cell, Figure 20 was developed using a version of the model that could evaluate steady state, fixed conditions of the fuel cell system.

The system was run at a varying temperatures and along the pressure line in Figure 15 to evaluate the overall system performance. Each of the curves represents a different operating temperature, and the remaining operating conditions are the same at each power level. For example, each of the temperatures for the fuel cell that are operating at 20 kWe would have the same cathode pressure, mass flow, etc. As shown in Figure 20, the increase in temperature increases the overall system efficiency, and increases the net system power available. Temperatures range from 0 C to 80 C in 10-degree increments, increasing from the lower left to the upper right. Each of the efficiency lines end when a minimum cell voltage or maximum system power is encountered.

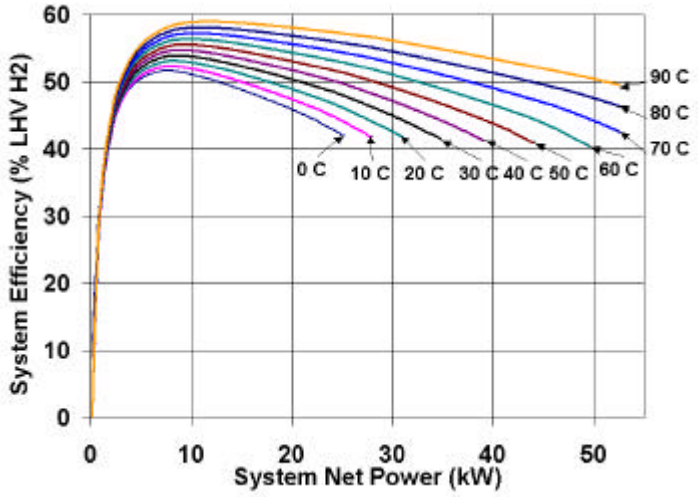

Figure 20. Fuel cell power and efficiency varied with temperature.

From this figure, the temperature effects are evident in decreasing the available system power and maximum fuel cell system efficiency. A 10% increase in system efficiency is seen as a result of increasing the temperature by 80 C. The dashed line represents the power as limited by a minimum cell voltage. Not seen in previous figures is the performance of the system at low system power on the left hand side of the figure. This is a result of parasitic loads associated with the fuel cell system dominating and imposed minimum flow rates. A key point for vehicle hybridization is that the fuel cell system power is influenced heavily by temperature. For these operating conditions shown in Figure 20, only 50% of the fuel cell system power capability is available at low temperatures.

In both Figure 19 and Figure 20, the air compressor speed and power were allowed to go to zero. In practice, this is difficult to achieve and still have acceptable dynamic response of the system. Figure 20 shows that a minimum power operating strategy can eliminate the low system efficiency region of operation at low loads, which also sets a minimum speed and flow for the air compressor. The benefits of a minimum power point are more evident and will be discussed in section 8.3.

7.3 Thermal Transient Response to Step Input

Since it is desirable to operate the system at its maximum available efficiency and power, characterizing the thermal transient or cold-start performance is necessary. This test is to understand the temperature and power response of the system to a step-power input. A step-power input to the system requesting the maximum system design power of 50 kWe net is shown in Figure 21.

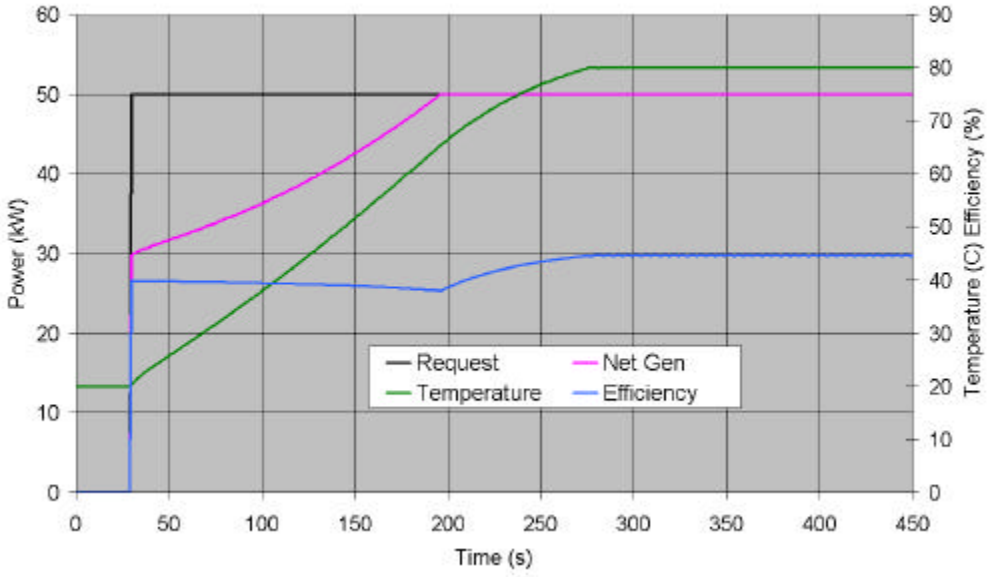

Figure 21. Fuel cell stack temperature response to a step input.

When requesting a 50 kWe load initially from the fuel cell system, there is a period where net system power is less than requested due to the low stack temperature. For this system, it takes 280 seconds for the fuel cell system to initially warm up to the steady state operating temperature. After 190 seconds, the system has the capability to produce the full rated net power. The fuel cell net system efficiency is defined as:

$$Efficiency = \frac{NetPower}{mass\ flowrate\, H_2 * LHV\, H_2} \times 100 \qquad (23)$$

Equation 23. Efficiency calculation for the fuel cell

Initially the system operates at a fixed cell voltage and increasing current density. Current density increases due to the temperature increases. However, efficiency is decreasing due to ohmic losses within the stack because of the increased current density. 200 s into the test, the system has the ability to generate the 50 kWe request made to the system. At this point, efficiency increases because cell voltage is rising and current density is decreasing because of continued heating of the fuel cell stack. Finally, the system achieves a steady state temperature, efficiency, cell voltage, and current density.

8 Vehicle Modeling and Energy Impact

The following section describes the work associated with the fuel cell vehicle model and how it is used to understand the fuel economy and efficiency impacts on vehicles during cold-start scenarios. In previous chapters, the fuel cell system was characterized during steady state and simple transient operations. Now the fuel cell system model will be used in a dynamic vehicle environment. The dynamic vehicle environment chosen is one of two standard drive cycle used for testing vehicle emissions and fuel economy. For this work, two different drive cycles have been chosen. A simple comparison between the US06 and FTP driving schedule used in the comparisons mentioned has been performed in Table 13 below.

Table 13. Drive cycle statistics.

Attribute	**US06**	**FTP-75**	Units
Time	600	2477	S
Distance	8.01	11.04	Mi
Max speed	80.3	56.7	Mph
Average speed	47.97	16.04	Mph
max accell	12.32	4.84	ft/s^2
max decel	-10.12	-4.84	ft/s^2
average accell	2.2	1.68	ft/s^2
average decel	-2.39	-1.89	ft/s^2
idle time	45	361	S
No of Stops	5	22	Dim

Notice that the majority of the statistical attributes of the drive cycle have increased for the US06 drive cycle over those for the FTP-74 drive cycle. In addition, as a comparison to current production vehicles, standard EPA vehicle tests for fuel economy have been performed. Detailed also is the impact that the minimum power control strategy point has on vehicle efficiency during the FTP-75 drive cycle.

8.1 Sport Utility Vehicle Model

The vehicle model is based upon a 2002 Ford Explorer that has been converted to a hybrid fuel cell vehicle at Virginia Tech.

Figure 22. Converted 2002 Ford Explorer XLT.

The Hybrid Electric Vehicle Team (HEVT) of Virginia Tech has been working with fuel cell vehicles for the past 5 years. Magellan is the most current vehicle that utilizes a 60 kWe gross fuel cell stack from Honeywell / GE. Magellan is part of the FutureTruck competition that challenges engineering students to design and build vehicles that meet three goals:

1. Increase the vehicle fuel economy by 25%
2. Decrease tailpipe emissions
3. Maintain performance and features available on the vehicle

Development of Magellan during the 2001–2002 school year at Virginia Tech involved developing and integrating a fuel cell and electric drive system on board the vehicle. The fuel cell system design was based upon work completed in the previous two years (1999-2001) on another vehicle called ZeBurban. Research and work done by Ogburn et al.

(2000) and Gurski et al. (2001), yielded significant design and development improvements during the building of the fuel cell vehicle.

Magellan is a fuel cell series hybrid vehicle that utilizes a 60 kWe gross fuel cell system, 83 kWe peak electric drive system, and a 3 kWh lead acid battery pack. The component sizes were based upon three factors:

1. Design of optimal component sizes through modeling;
2. Use of the most cost effective and available parts and materials;
3. Design for the weight, space and safety constraints imposed by FutureTruck

Table 14 lists the characteristics of the vehicle model used for the drive cycle simulations.

Table 14. Vehicle Model attributes.

Attribute	Value
Mass	2400 kg
Cd	.41
Fa	2.8 m^2
Drivetrain	83 kW GE EV2000
Batteries	16 Ahr 336 V Lead Acid
Fuel Cell	50 kW Net

Virtual performance tests have been performed in ADVISOR™ and Table 15 contains results of the vehicle tests. The tests were performed using a fuel cell system with an initial temperature of 80° C.

Table 15. Model vehicle performance.

Attribute	Model
0-97 kph	18 sec
1/8 mile	15 sec
Gradeability	4.8% @ 55mph

Based upon available data, Magellan is a vehicle that represents what is now currently produced as production demonstrations. The overall vehicle size is comparable to Yamanashi's fuel cell powered X-Terra (Yamanashi et al. 2001). For vehicles reviewed in the literature, each offers a similar power to weight ratio that for the vehicles found in the Adams, et al. (1999) and Ijaz, et al. (2001), namely 0.042, and 0.035, respectively. Magellan is 0.034.

All vehicles previously mentioned utilize a direct hydrogen fuel cell system of similar design and construction to that for Magellan. We can thus, conclude that Magellan is a viable candidate on which to basis to use for this modeling effort, of understanding vehicle impact of the fuel cell system. One should note that Magellan is a 2WD vehicle that requires an additional electric drive and batteries to achieve similar performance the stock vehicle. Atwood, et al. (2002) have performed a degree of hybridization study that addresses such issues.

8.2 Energy Impact on the FTP Driving Cycle

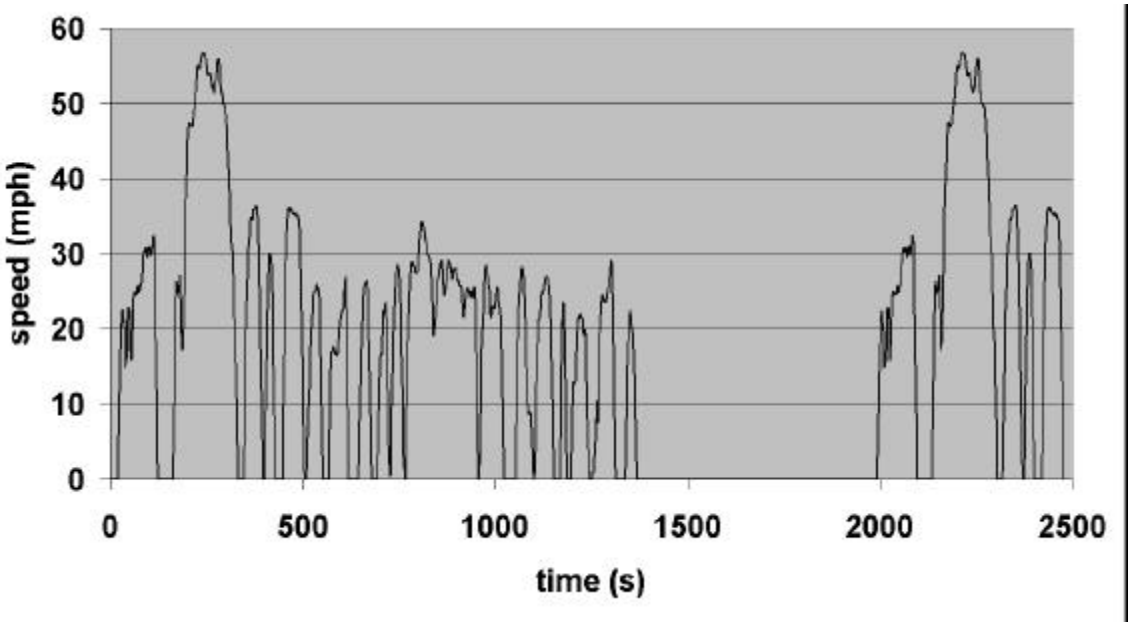

Figure 23. FTP-75 drive cycle speed request.

The first drive cycle used for a hot and cold-start comparison is a standard EPA FTP-75 cycle. The FTP-75 is the standard federal exhaust emissions drive cycle shown in Figure

23. This cycle has three separate phases: a cold-start (505- second) phase, a hot-transient (506 to1376 seconds) phase, and finally a hot-start repeat of the first 505 seconds. A 600 second cool-down phase exists between the second and third phases. A vehicle travels 11 miles during the 2457 s drive cycle. The maximum speed is 56 mph and the average speed is 21 mph.

Using vehicle simulation software called ADVISOR™, the fuel cell vehicle model is used to compare the energy impact for a hot-and cold-start on the FTP-75. Both runs use the same control strategy and have the same characteristics with the exception of the initial starting temperature. The initial temperature for the cold-start is 20 C and the hot-start temperature is 80 C. In addition, both of the runs are battery state of charge (SOC) corrected for each drive cycle within ½%. Correcting a simulation for battery SOC requires that the batteries used in the vehicle begin and end the simulation with the same amount of energy. By imposing this criteria, all energy used by the vehicle is fuel input to the system and a meaningful comparison of fuel economy can be performed.

Table 16. Energy use on FTP-75 drive cycle.

	Hot	Cold	% Difference
Fuel In	38689	40924	5.46

The results show that the cold driving cycle consumed 5.46% more fuel than the hot drive cycle. From Figure 24, the hot-start system is more efficient and the majority of the losses are incurred with the fuel cell system.

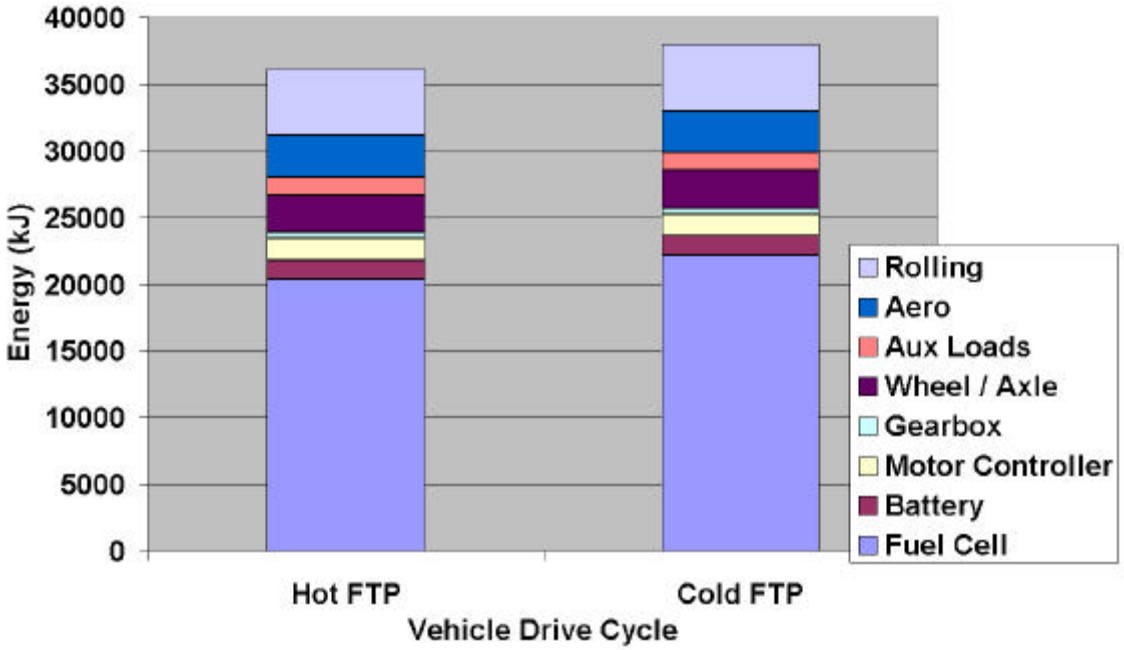

Figure 24. Hot-start and cold-start energy loss comparison on FTP-75.

Each of the items in Figure 24 represents a loss that occurred in the system during the ADVISOR simulation. These losses are the total inefficiencies over the drive cycle in each of the devices. The rolling and aero losses are the energy required to move the vehicle during the drive cycle. The wheel and axle account for losses due to friction in the bearings of the wheels, differentials, and other post transmission components. The gearbox or more commonly know, as transmissions are losses with the gear reduction set. Since this vehicle utilizes an electric motor, the motor controller accounts for the losses in the power electronics and the electric motor. Finally inefficiencies in the traction battery, used for hybridization and the fuel cell account for the final losses in the system.

What is difficult to see in Figure 24 is where the majority of the changes occurred in the vehicle and fuel cell system. Table 17 below details how many kJ of energy were lost in the system for the duration of the drive cycles. More clearly illustrated in Table 17 are the majority of the losses and the change in losses occurred due to fuel cell operation.

Table 17. Component Energy Loss Comparison.

Component Loss	Hot FTP	Cold FTP	Difference	% of Total Loss
Fuel Cell	20355.00	22145.00	1790.00	94.46
Battery	1455.00	1508.00	53.00	2.8
Motor Controller	1617.00	1598.00	19.00	1.00
Gearbox	432.00	426.00	6.00	0.32
Wheel / Axle	2835.00	2862.00	27.00	1.42
Aux Loads	1314.00	1314.00	0	0
Aero	3130.00	3130.00	0	0
Rolling	5020.00	5020.00	0	0
Total kJ Loss	36158.00	38003.00	1895.00	

In Table 17 losses between the hot and cold-start cycles have been subtracted from each other, labeled Difference. Here we can further see that the fuel cell had the largest change in losses in between the hot and cold cycle. In addition, in Table 17 is a column labeled as "% of Total Loss" which is simply the Difference *100 / Total Losses or the percentage of the total losses in the vehicle. The other losses are small compared to the fuel cell operation on a percentage basis.

Taking a closer look at the fuel cell systems losses, Figure 25 shows that the majority of the losses accounted for in inefficiencies associated with the fuel cell stack, specifically the energy conversion that generates electrical power.

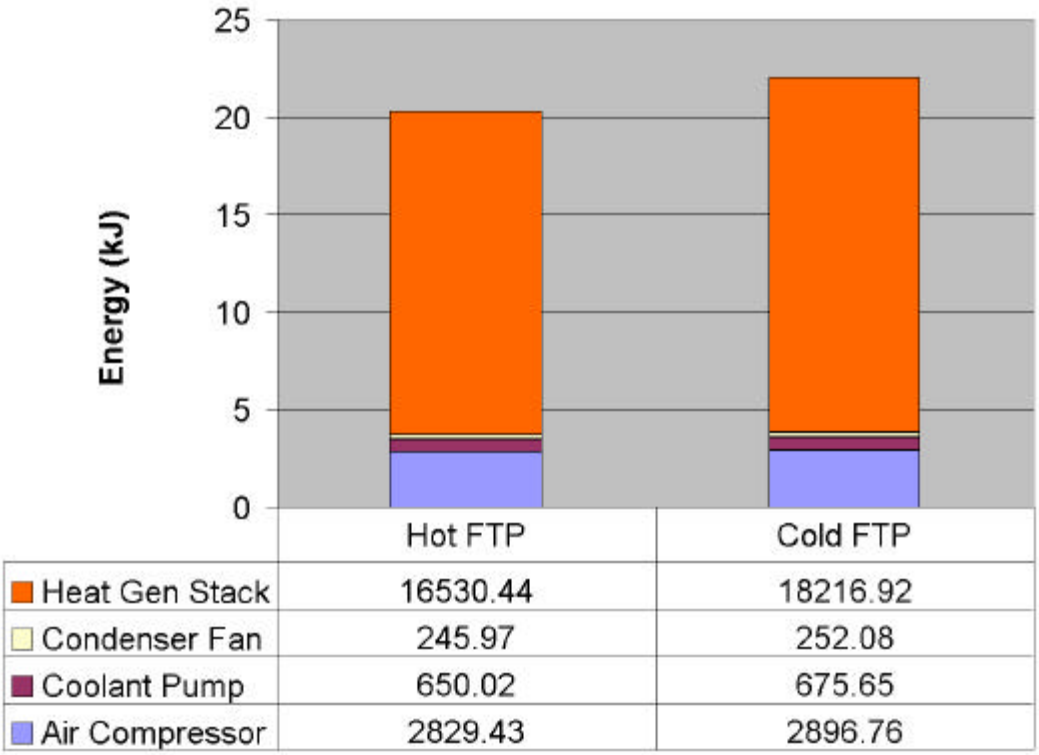

	Hot FTP	Cold FTP
Heat Gen Stack	16530.44	18216.92
Condenser Fan	245.97	252.08
Coolant Pump	650.02	675.65
Air Compressor	2829.43	2896.76

Figure 25. Fuel cell system loss comparison on FTP-75.

The fuel cell stack is responsible for the majority of the difference in losses for the hot and cold drive cycles. The losses in the stack are a result of heat generated in the stack; the more heat generated the larger the losses.

To better understand why the fuel cell system is generating more heat, Figure 26 compares the operating points of the fuel cell stack and the relative efficiencies. Each of the points in Figure 26 represents an operating point of the fuel cell. The efficiency is the fuel cell system efficiency % based on the lower heating value of the fuel. The hot FTP-75 case on the left has a much tighter cluster of points, nearest to the maximum efficiency at the temperature and power level. The cold-start FTP-75 on the right hand side shows a much broader area of operation. Temperature trends in efficiency and power account for the broader range of points located on the right hand figure.

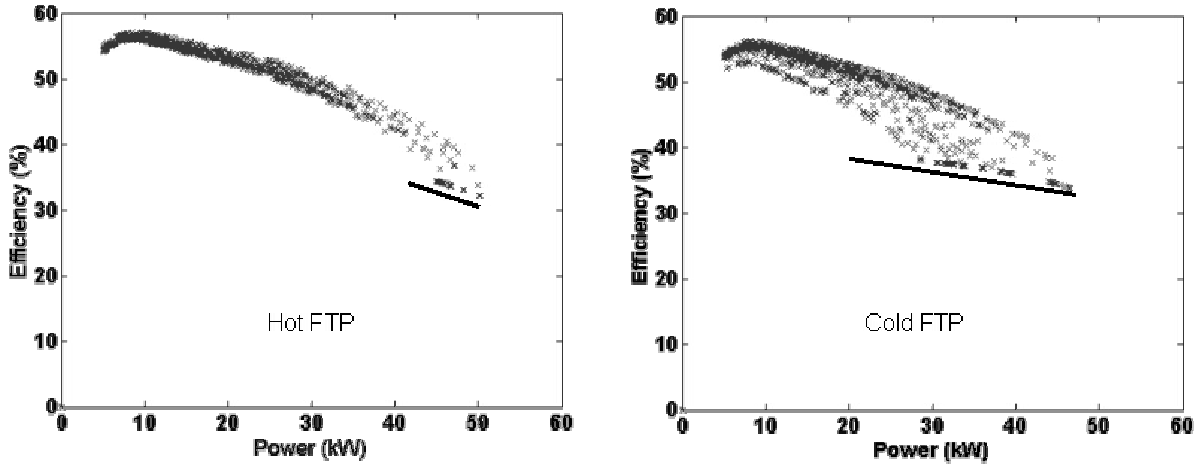

Figure 26. Comparison of hot and cold efficiency points on the FTP-75.

Operating points below the solid line in the figure are not possible because of the minimum cell voltage limitation imposed by the control strategy. This strategy also prevents operation of the stack at lower efficiencies, and so tends to make the cold-start energy penalty relatively small. However, by imposing this minimum power strategy, requests below 5 kW are fulfilled completely by the batteries that lead to an increase in battery losses. However for this case, the losses are very small, approximately 50 kJ of energy.

8.3 Impact on Efficiency for Minimum Power Control Strategy

The air compressor and coolant pump have minimum flow rates or speeds associated with normal operation. This is a key point for the argument for hybridizing fuel cell vehicles for the explicit reason that you can increase the overall vehicle efficiency by imposing a minimum power request to the fuel cell.

To illustrate this example, Table 18 depicts how the efficiency of the system would decrease with no minimum power limit in place. To compare the energy efficiency change between these cycles, a standard FTP test has been chosen using the Magellan vehicle model. Each fuel cell system started at 20 C ambient temperature and the analysis has been performed correcting for the state of charge of the battery pack.

Case 1 in Table 18 below has a system control strategy that does not allow power requests to the fuel cell system below 5 kW. System power requirements below 5 kW are fulfilled by the batteries on the vehicle. The control strategy for case 2 does not have a minimum power request, and net fuel cell system requests as low as 0 kW are possible. A 0 kW net power request amounts to a small gross power request, on the order of 0.3-0.4 kW.

Table 18. Effects of minimum power on vehicle fuel economy.

Cycle-FTP 75	Fuel Input – kJ	Fuel Economy MPGGE	Fuel Cell Losses – kJ	Vehicle Losses – kJ
Case 1 Cold-start, 5kW min pwr request	40924	34.3	21605	19319
Case 2 Cold-start, No Min Pwr request	42533	33.3	23228	19305
Percent Change	+3.78 %	-3.00%	+6.98%	-0.0007%

A significant change in the fuel cell system efficiency and vehicle efficiency can be seen in this comparison. Overall, the vehicle required 3.78% more fuel to allow net system requests below 5 kW and the overall fuel economy dropped by 3.00 %. In each of the situations the vehicle losses, not including the fuel cell are very close (0.0007% difference) and the change in vehicle efficiency and fuel economy is a result of the change in fuel cell system operating efficiency. Shown in Table 18, the fuel cell losses increased by 6.98% because of the change in minimum power request allowed in the vehicle control strategy. This strategy does increase the amount of energy that must be processed through the battery energy storage system, and may increase battery losses as well as sizing requirements.

8.4 Condenser Operation and Water Balance

One of the technical issues associated with fuel cell vehicles is the topic of water balance. A requirement for current fuel cell technology is the humidification of the fuel and air

entering the fuel cell stack. The constant addition of water for humidification without reclamation would lead to refilling of a water reservoir on board the vehicle. To consumers refilling a water tank would be an undesirable task to perform on a regular basis in addition to refueling the vehicle. The addition of a condenser in the system will allow the reclamation of water that is used for humidification as well as water generated as a byproduct of power generation of the fuel cell stack. As part of the fuel cell model a simple condenser model has been used to predict the amount of water reclaimed with its use. Figure 27 shows the water balance over the drive cycle and the fuel cell stack temperature.

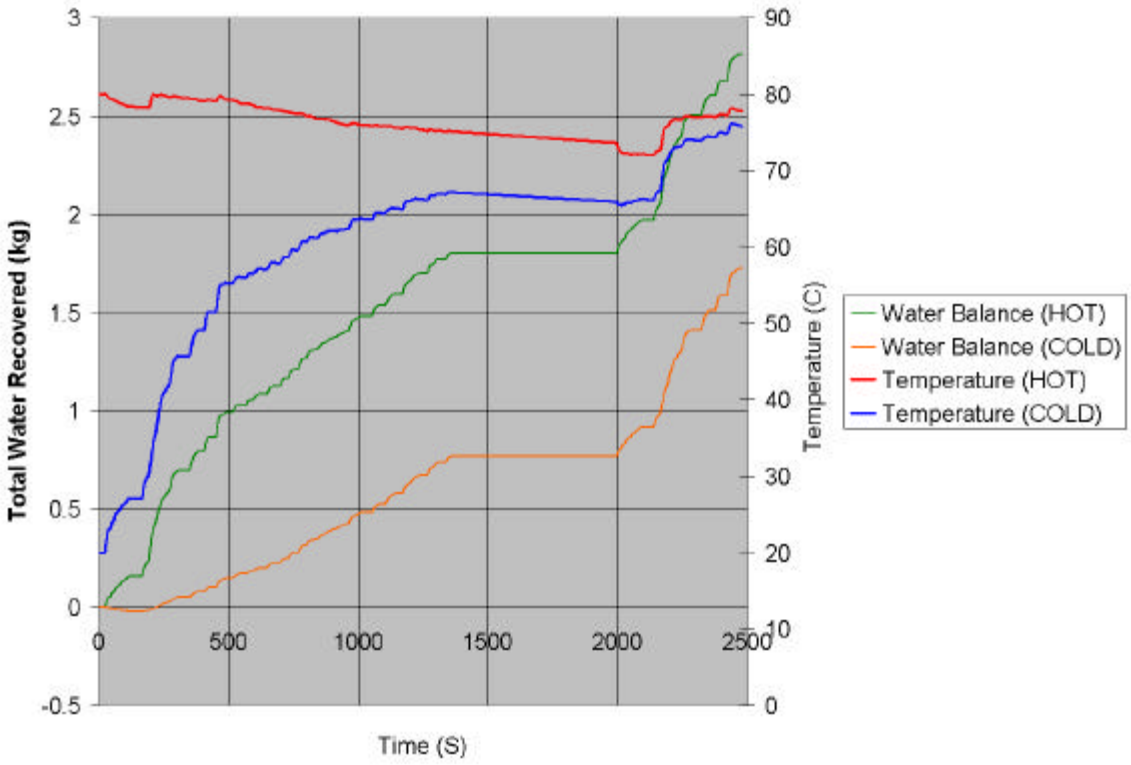

Figure 27. Water balance during FTP 75 drive cycle.

The condenser size is more than adequate to maintain the water balance in the system over the entire drive cycle. However, during the cold-start cycle, the first 220 seconds had a negative water balance in the system. This is a result of the low temperature difference between the cathode air stream and the ambient.

To obtain the water balance performance of the system as shown in Figure 27, the condenser must be able to reject a large amount of heat to the ambient. Figure 28 is the heat load that the condenser has to reject during the FTP drive cycle.

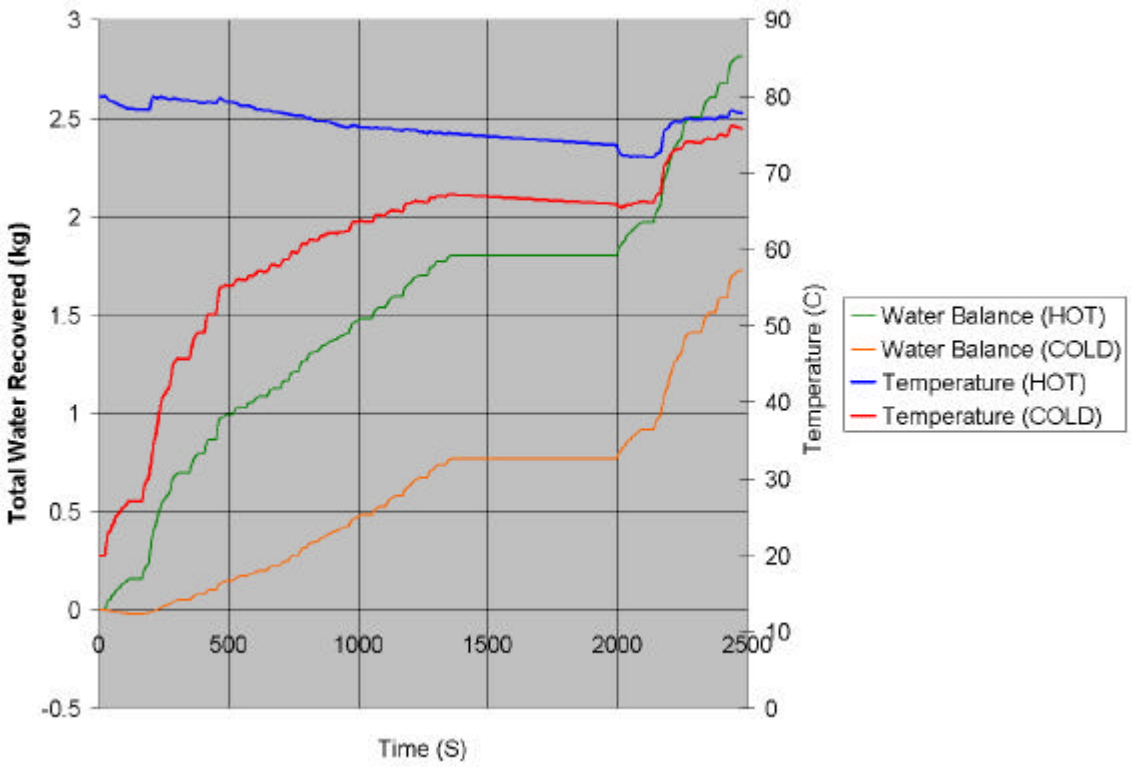

Figure 28. Condenser heat load during FTP-75 drive cycle.

Over the drive cycle, the hot cycle required a condenser that had an average heat load of 9.2 kW and the cold cycle required an average of 4.9 kW. Water balance does not rely only on the condenser's operation to maintain water balance. Certain operating conditions lend to the condensation of water inside the fuel cell stack and do not require the condenser to reclaim the water.

Without a condenser in the system, this system is incapable of maintaining the water balance. Figure 29 below shows the water balance of the system without a condenser in the system.

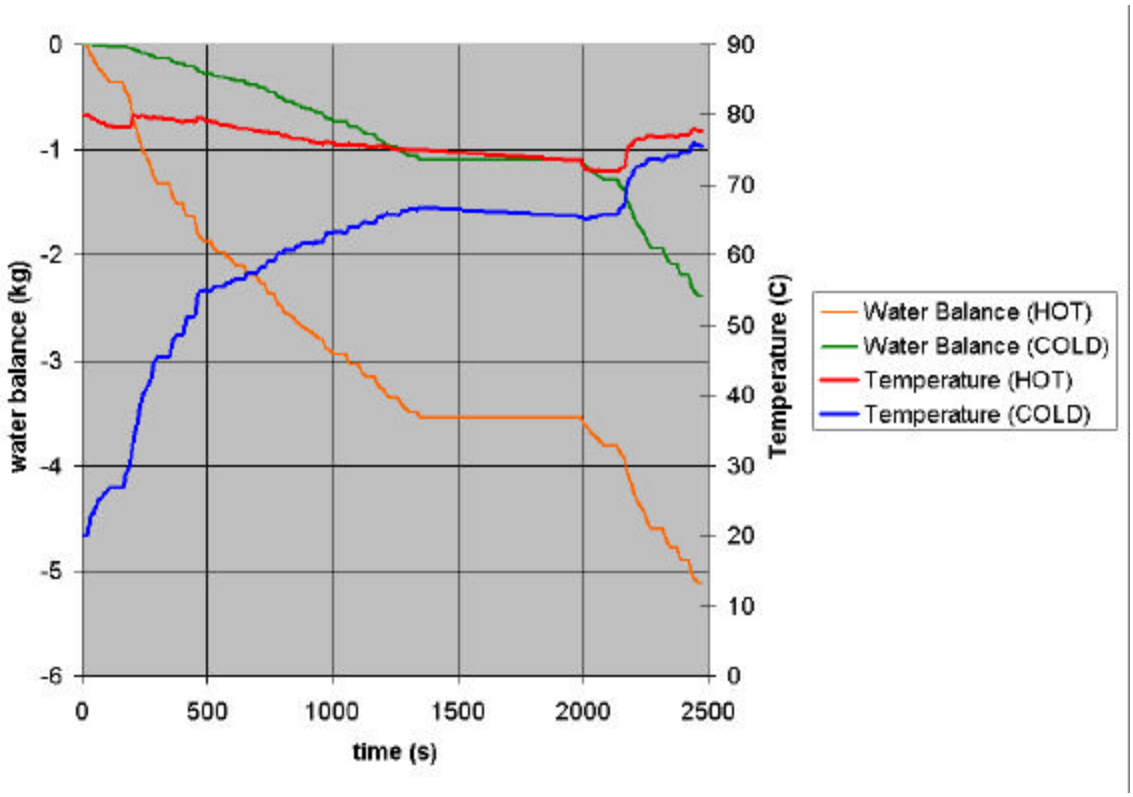

Figure 29. Water balance during FTP-75 without a condenser.

Both hot and cold-start driving cycles are unable to maintain water balance in the system. The hot system has a larger water deficit over the drive cycle because the cathode air stream is much hotter during the drive cycle, humidification requirements increase, and the air is able to carry more water that is generated inside the fuel cell stack. The cold-start system has a reduced deficit of water because of the low temperature operation. Low temperature operation is a way to help reduce the water balance issue in a fuel cell vehicle.

8.5 Standard EPA Fuel Economy Test

To gather an understanding of how this vehicle compares to that of current production vehicles, the standard EPA fuel economy test has been performed. This is the fuel economy test that yields window sticker fuel economy numbers and the published EPA fuel economy results. The test consists of two driving cycles, the FTP-75 used in

previous examples and the HWFET. The HWFET is a driving cycle represents highway driving conditions shown below in Figure 30.

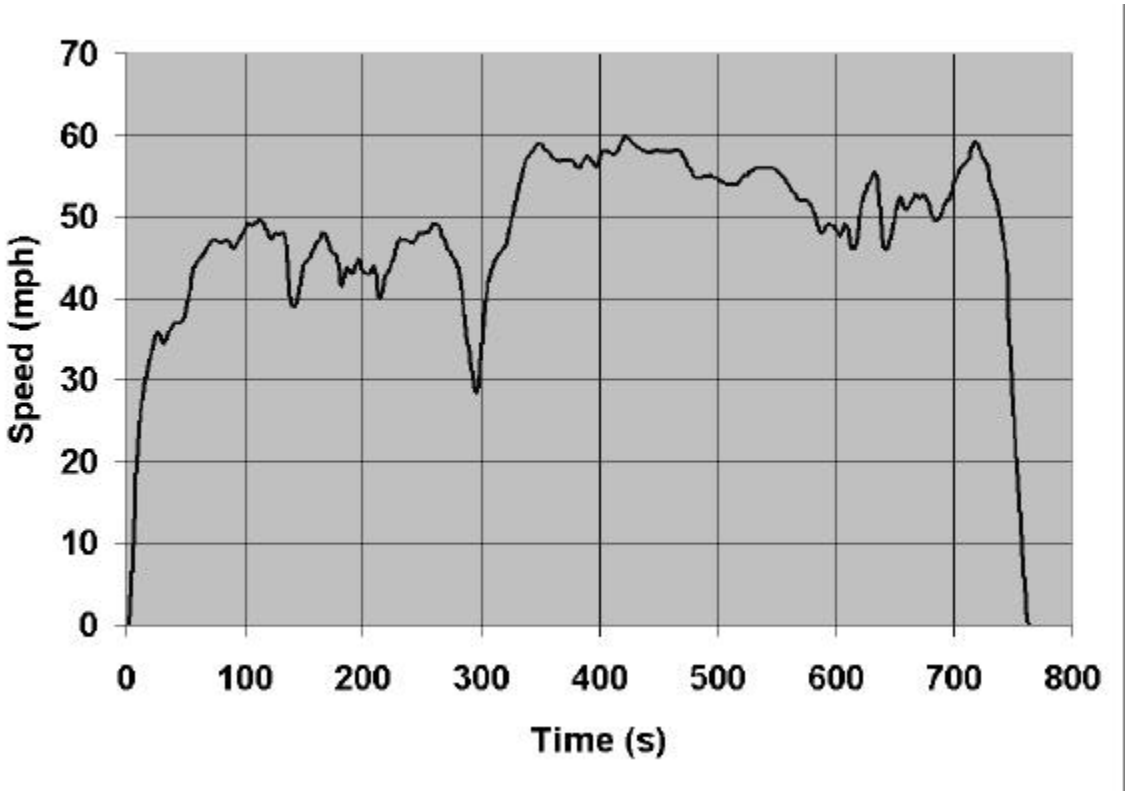

Figure 30. HWFET Driving Cycle.

The EPA test uses a cold-start FTP-75 cycle and a hot start HWFET cycle. Fuel economy of the tests are reported as either uncorrected, corrected or combined fuel economy. The uncorrected fuel economy figures are simply the raw fuel economy numbers from the FTP-75 and HWFET simulations.

Corrected or window sticker values are a percentage of the raw fuel economy results. To yield the city fuel economy number, the raw FTP-75 fuel economy is multiplied by 0.9. The highway fuel economy is the raw HWFET fuel economy multiplied by 0.78.

The combined fuel economy number, typically used for annual fuel cost calculations is a weighted percentage of city and highway fuel economy. For the combined fuel economy, the city accounts for 55% of the total and the remaining 45% goes towards the highway.

Contained in Table 19 are the results in MPGGE from the simulations to yield the fuel economy results for the fuel cell model and the stock vehicle.

Table 19. EPA fuel economy results, MPGGE.

Cycle	Raw	Corrected	Combined
Model: Fuel Cell Vehicle			
FTP-75	34.3	City = 30.9	
HWFET	39.2	Highway = 30.6	
Combined			30.9
Production Vehicle: Internal Combustion			
FTP-75	16.9	City = 15.2	
HWFET	25.2	Highway=19.7	
Combined			17.2

The results of the fuel cell vehicle are significantly better than that of the production vehicle. Using the combined vehicle results, a 77% increase in fuel economy over the production vehicle is accomplished. However, this large increase in fuel economy is not achieved solely by replacing the internal combustion engine (ICE) with a fuel cell system. If a careful analysis of a performance comparison was to be performed between the FCV and the ICE vehicle, it would show a reduction in the fuel cell vehicle performance.

8.6 Energy Impact on the US06 Driving Cycle

Standard EPA driving cycles (FTP, HWFET etc) have been used since the 1970's to evaluate the emissions and fuel economy performance of light duty vehicles. However, these driving cycles have come under some scrutiny as to their representation of real world driving conditions. Specifically the standard EPA driving cycles do not portray the increased power level of real world driving with respect to these standard cycles. So as an addendum to the standard driving cycles, the EPA has developed the US06 driving cycle seen below. This driving cycle is used to supplement the standard FTP drive cycles for tailpipe emissions. The US06 features more demanding accelerations and top speeds.

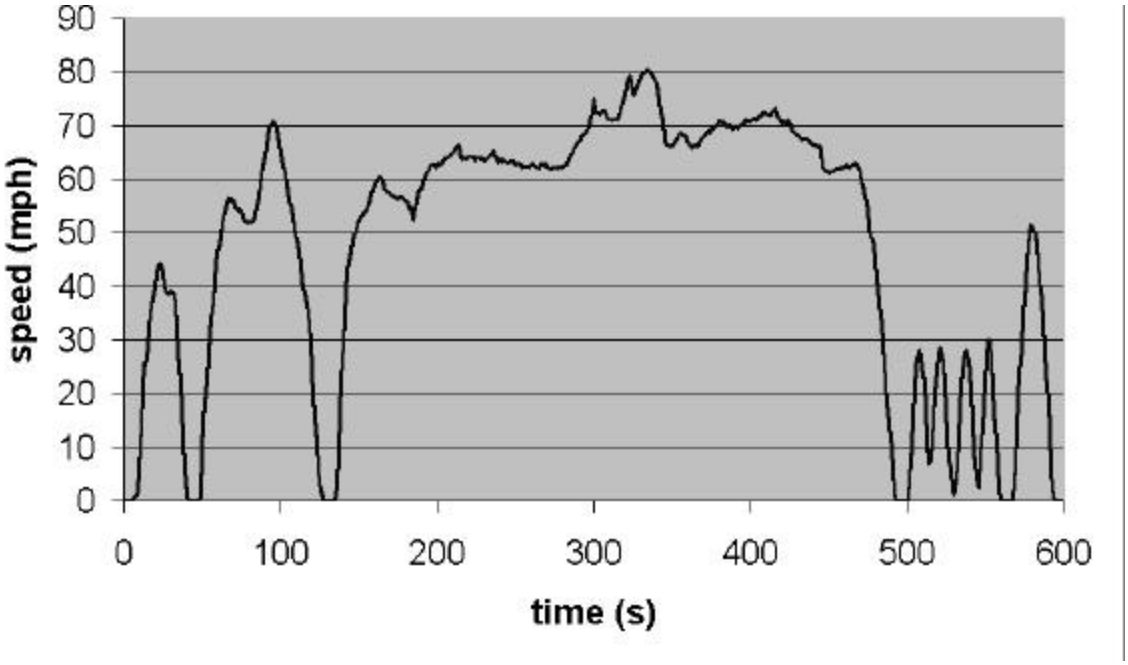

Figure 31. US06 drive cycle speed trace request.

This drive cycle has been chosen to evaluate the performance of the fuel cell vehicle model during a high power operation. Using the US06 drive cycle and the fuel cell model that has been previously used, a comparison between a hot and cold-start vehicle has been performed. As done before for the FTP drive cycle, the fuel cell system temperature for the cold-start scenario begins at a 20 C. For the hot start scenario the fuel cell system starts at 80 C. Each of the scenarios has been corrected for state of charge of the batteries, within ½%.

In Figure 32 below is the temperature profile during the US06 drive cycle. During the cold-start cycle, the fuel cell system needed 300 seconds to get to an operating temperature of 80 C.

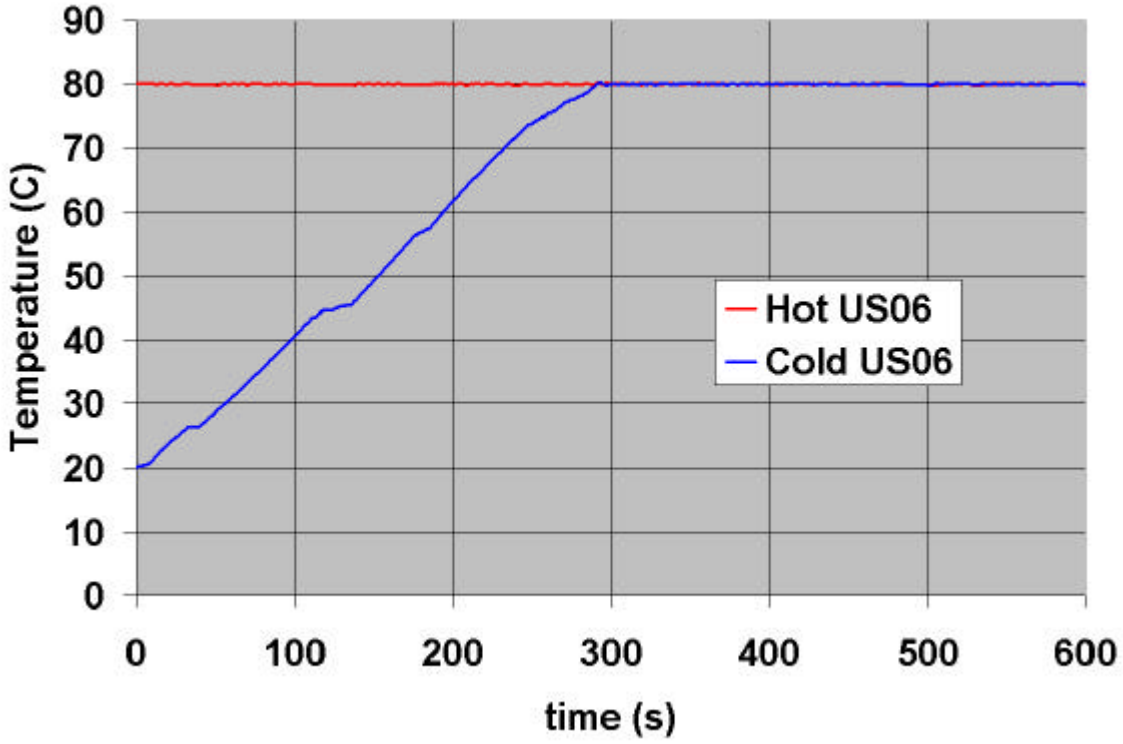

Figure 32. Temperature response during US06 Drive Cycle.

A loss analysis has been performed on the results from the drive cycle to more clearly illustrate where energy has been used. As seen in Figure 33 below, the majority of the losses occurred in the fuel cell, energy storage and wheel / axle. For both cases, the aerodynamic, auxiliary, and rolling resistance losses are the same because the same vehicle model was used for each case.

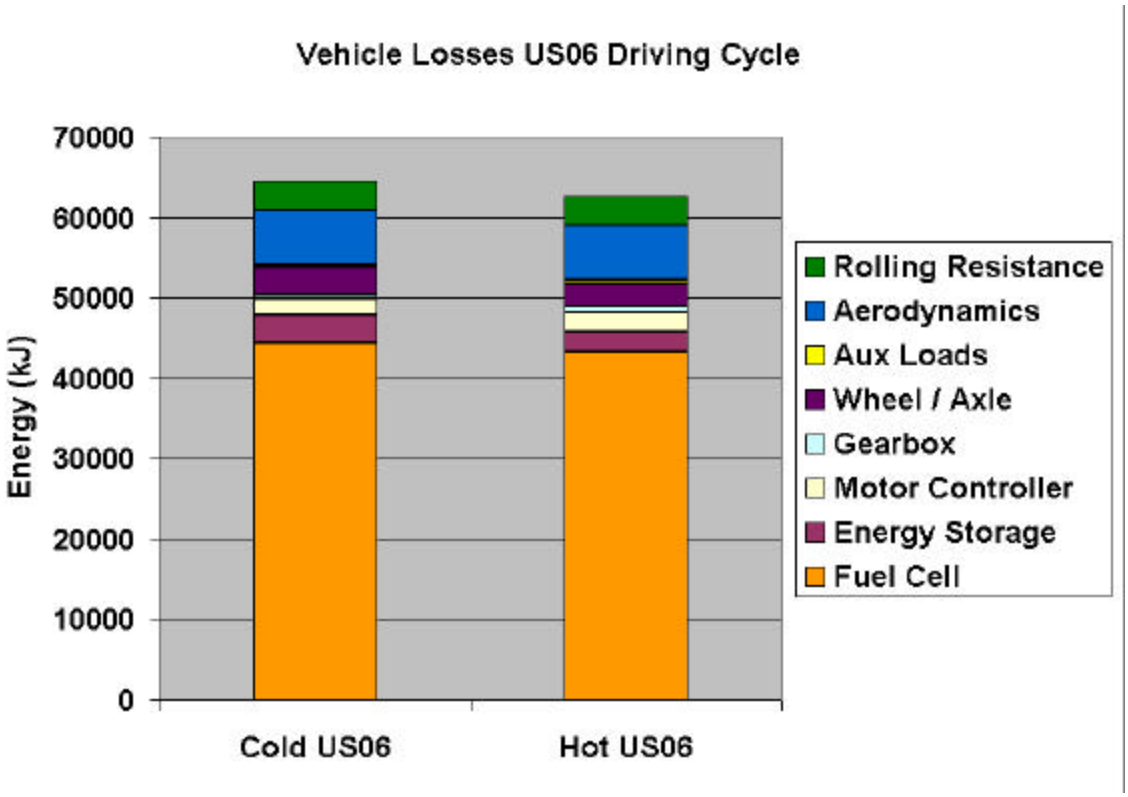

Figure 33. Vehicle losses on US06 driving cycle.

Looking more closely at the specifics of the individual component losses in Table 20 below, it is shown that the hot start scenario uses 2.87% less energy on the drive cycle. As expected, the fuel cell accounts for the majority of the losses, however the energy storage (batteries) accounts for a much higher percentage of the total change in losses than during the FTP-75. The reason for the significant increase in losses in the energy storage is because power is not available from the fuel cell during the initial thermal transient. During the cold US06 drive cycle, more energy has to be processed in and out of the batteries to meet the power requirements of the drive cycle and to correct for battery state of charge. Also to note that the modeled vehicle cannot meet the drive cycle speed trace. As a result, both simulations do not execute the same drive cycle.

Table 20. Breakdown of component losses during US06 drive cycle.

Component Losses (kJ)	Cold US06	Hot US06	Difference	% of Total Difference
Fuel Cell	44376	43248	1128	36.19 %
Energy Storage	3407	2546	861	27.62 %
Motor Controller	2007	2401	394	12.64 %
Gearbox	573	748	175	5.61 %
Wheel / Axle	3383	2887	496	15.91 %
Aux Loads	420	420	0	0.00 %
Aerodynamics	6746	6796	50	1.60 %
Rolling Resistance	3619	3632	13	0.42 %
Total	64531	62678	3117	
Percent Difference		2.87%		

This is a direct result of reduced power available to the vehicle because of cold temperature effects on the fuel cell system as described in Chapter 6.

As a result of the operating conditions and vehicle design, both vehicles could not meet the prescribed driving cycle. This brings some question to the ability to compare the loss results of the drive cycle because the vehicles did not execute the exact same drive cycle. The US06 drive cycle was specifically chosen to evaluate the performance of the vehicle, not the fuel economy. We can conclude that the data generated by the model for the US06 is useful for evaluating the performance of the vehicle and the operation of the fuel cell system.

Show below in Figure 34 is the comparison of the power supplied to the vehicle during the drive cycle.

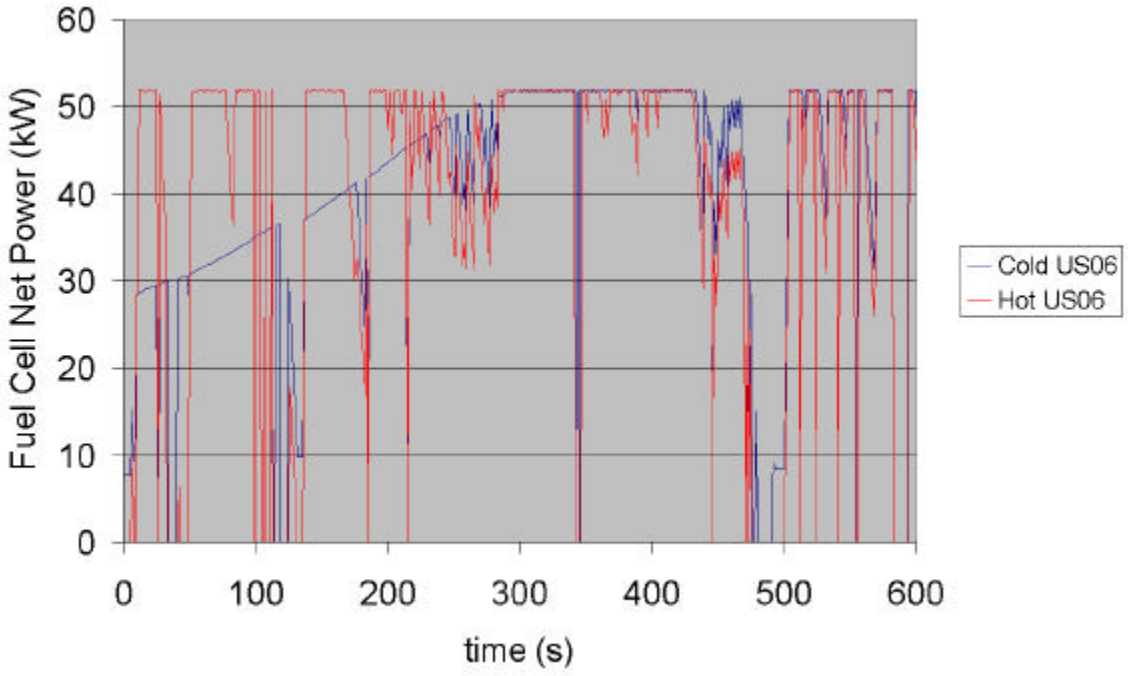

Figure 34. Comparison hot and cold starts on fuel cell power during US06.

Temperature effects are the cause for the reduction of power available for the first 300 seconds. During the drive cycle, the first 300 seconds are limited to significantly less than the full power design of the fuel cell system. During these 300 seconds, energy not available from the fuel cell system has to come from the batteries and then has to be replaced to impose the SOC corrected cycle criteria.

Battery inefficiency plays a large role in contribution towards the losses occurring during the drive cycle. This is because the energy is moved though the batteries and losses occur. This loss is the result of battery resistance to charging and discharging. A battery is more efficient charging that is it discharging.

Shown in Figure 35 is the charge and discharge resistance for a Hawker 16 Ah lead acid battery used in the vehicle model.

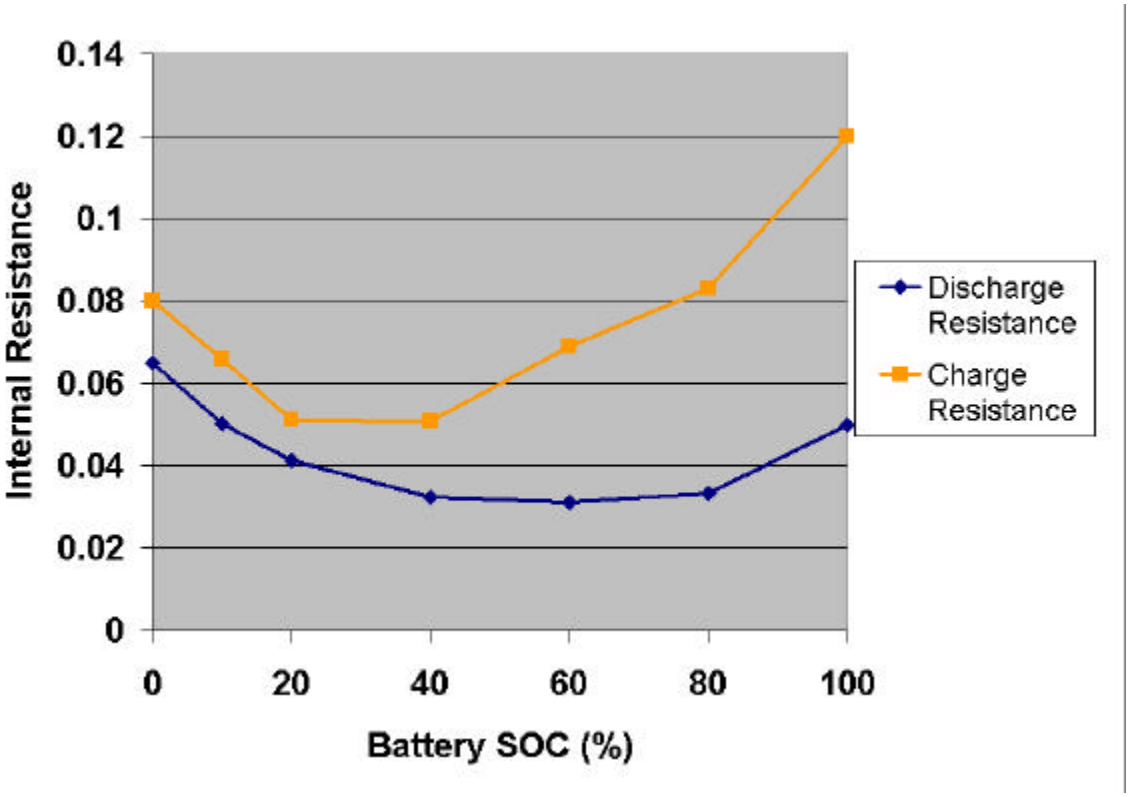

Figure 35. Charge and discharge resistance of vehicle batteries.

The charging resistance is higher than the discharge resistance. Any energy that is taken out of the battery during the drive cycle has to be replaced at an additional increased loss.

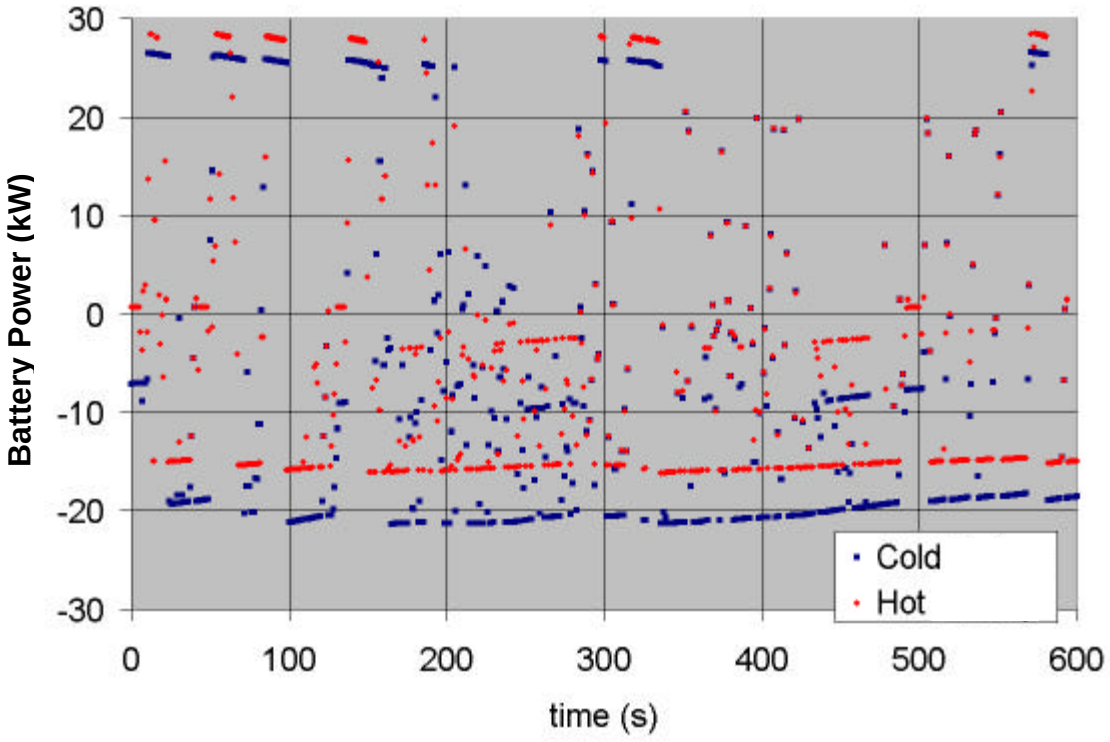

Figure 36. Battery power during US06 drives cycle.

Displayed in Figure 36 is the battery energy required during the US06 drive cycle for the hot and cold-start scenarios. The power out of the batteries (discharge) is labeled as positive in the figure and power into the batteries (charge) is labeled as negative. More power is required from the batteries during the hot cycle. This is a result of the control strategy commanding the power from the batteries and fuel cell. Even though higher power is discharged from the batteries during the hot cycle, the control strategy charges the batteries at a lower power, this significantly reduces system losses. However, battery losses are unavoidable because is it necessary to maintain overall vehicle performance through vehicle hybridization.

Taking a closer look at the fuel cell system, Table 21. Breakdown fuel cell system energy use on US06 drive cycle. The highest vehicle losses on board the vehicle are accounted for by the fuel cell system. The majority of the losses accounted are for the internal heat generation of the fuel cell stack, Stack Q Gen.

Table 21. Breakdown fuel cell system energy use on US06 drive cycle.

Component Enery Use-kJ	Hot US06	Cold US06	Difference	% Total Difference
Air Compressor	9167.3	8837.4	-329.9	18.13
Coolant Pump	525.7	564.4	38.7	2.12
Condenser Fan	121.3	135.0	13.7	0.75
Radiator Fan	21.7	13.9	-7.7	0.42
Stack Q Gen	33323.3	34752.0	1428.7	78.55
Total kJ	43159.1	44302.7	1818.7	

The power and efficiency operational points of the fuel cell are a result of the drive cycle and the vehicle control strategy. In Figure 37 below, is a comparison of the operating points for the fuel cells over the US06 drive cycle. The cold-start US06 is on the left, and the hot start US06 is on the right hand side. Since the US06 is a demanding & high power drive cycle, it is of no surprise that the majority of the operating points occur at high power levels and lower efficiencies.

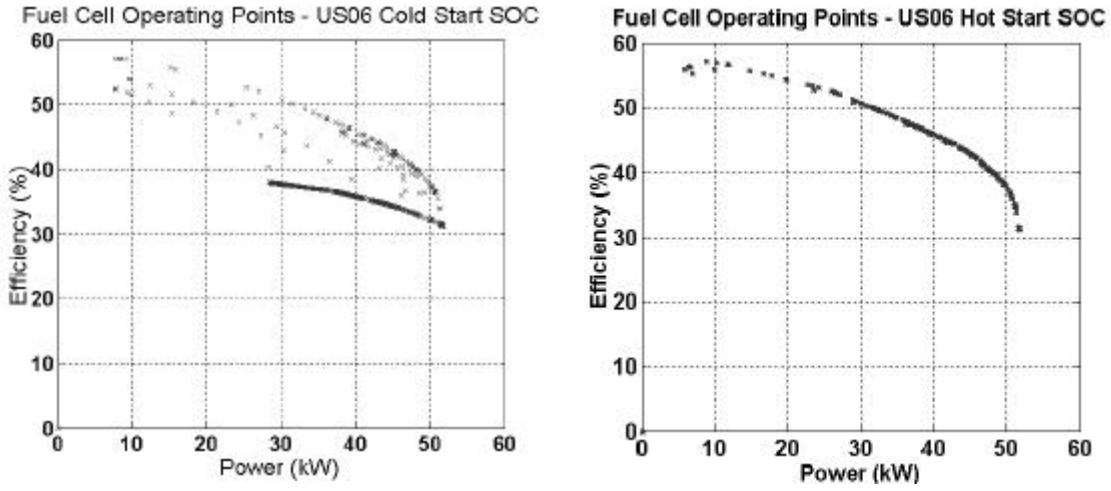

Figure 37. Fuel cell operating points vs. efficiency on US06 drive cycle.

During the cold-start scenario, many of the operating points lie along a line at the bottom of the area of point. This is a result of the cold operational temperature and the fuel cell system heating up during the drive cycle and power limitations due to cell voltage limits.

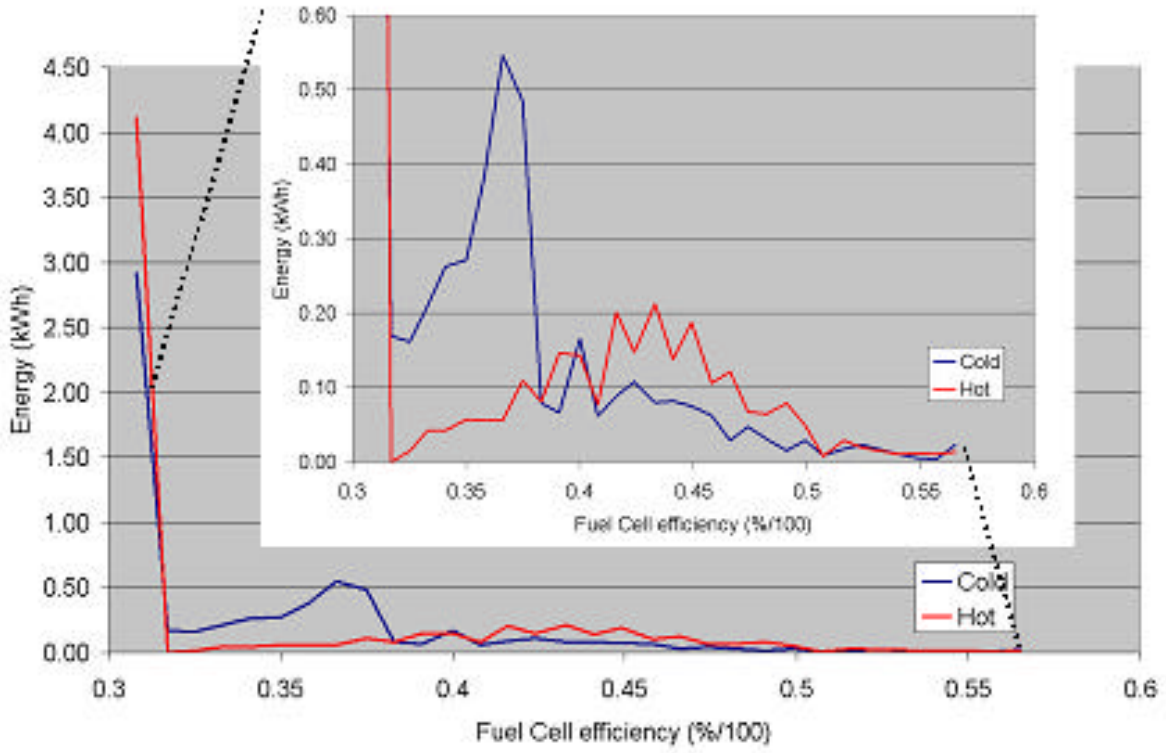

Figure 38. Histogram of energy at efficiency levels.

Figure 38 represents how much energy is generated at a specific efficiency during the hot and cold-start US06 drive cycles. A more efficient system will yield more energy generated at increased efficiency levels. In Figure 38, the hot start US06 generates more energy at higher efficiencies. At 37% efficiency the cold-start US06 begins to produce more energy at lower efficiency levels. The trends exhibited by the cold-start US06 fuel cell system concur with the decrease in fuel economy shown in Table 20.

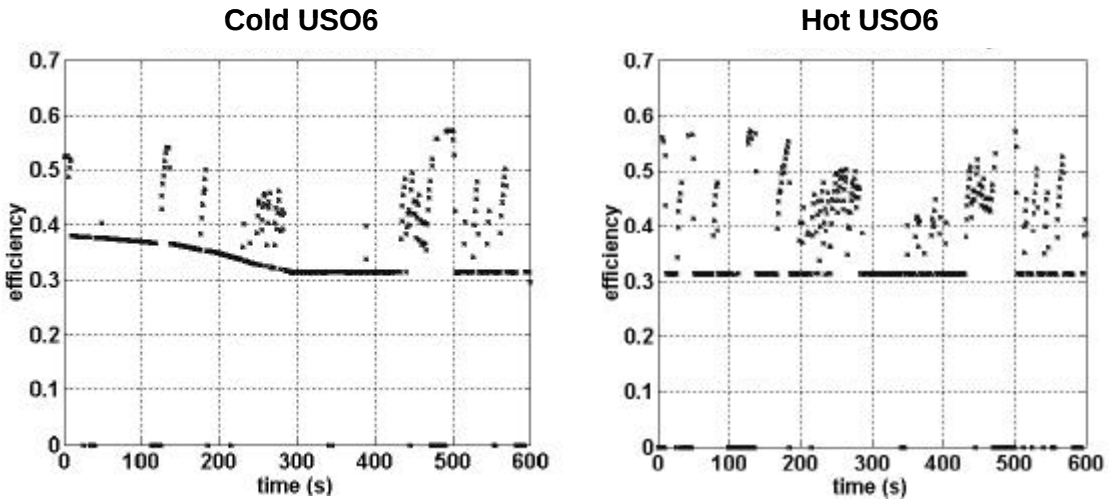

Figure 39. Hot and cold-start comparison of efficiency on the US06 cycle.

The comparison of fuel cell operating points during time is pictured in Figure 39. The fuel cell with the cold-start is on the left and the hot start is on the right.

A counter intuitive result from Figure 39 shows a decrease in system efficiency as time and temperature of the fuel cell increase. This is a direct result of the system being able to generate more power at a lower efficiency as a result of increase stack temperature. Because the system is operating at peak or near peak power, this phenomenon is prevalent and clearly illustrated, whereas during the FTP cycle this would be difficult if not impossible to perceive. This figure and drive cycle makes it possible to understand the power limiting effects of the fuel cell system on vehicle efficiency.

A trace miss comparison in Figure 40 is done to show the degree that the vehicle was unable to maintain the requested speed trace.

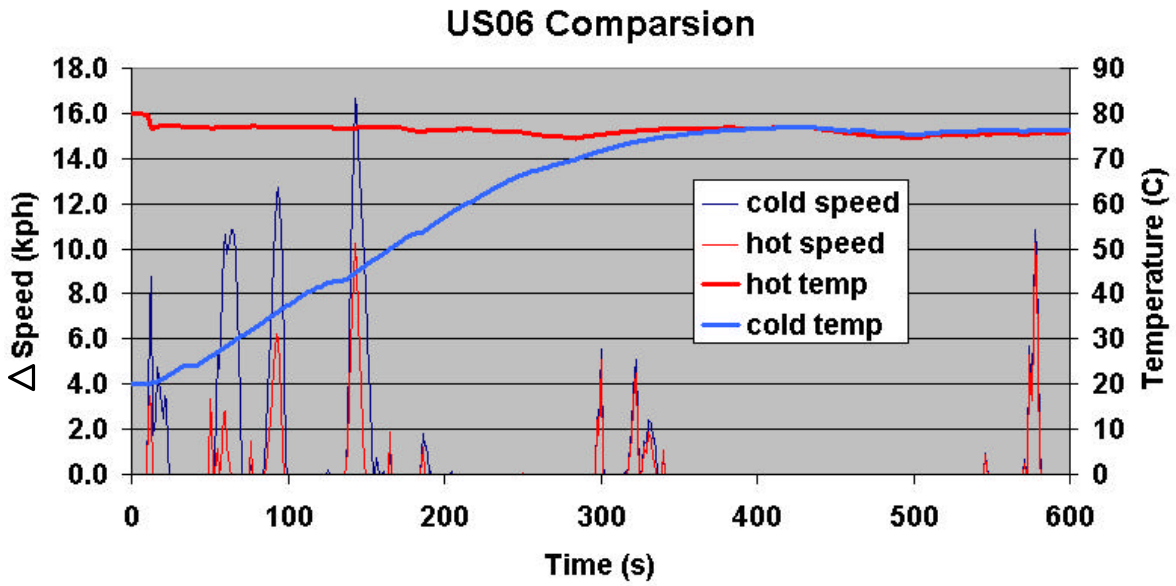

Figure 40. Trace miss comparison of US06 drive cycle.

The trace miss is the difference between the requested speed during the cycle and the actual speed achieved, taller peaks are larger differences between the requested speed and actual speed. During the 600 second cycle, the first 200 seconds are of most interest because the vehicle had the largest and most frequent trace miss. After 200 seconds both vehicles equally fell short of the request for the drive cycle. Another point to note, during the US06 drive cycle it takes the system approximately 350 seconds to arrive at the desired system operating temperature.

8.7 Impact on Performance Due to Power Limitations

Fuel cell power limiting impacts not only vehicle fuel economy, but also performance metrics such as acceleration and driveablility. To better understand the impact that temperature has on vehicle performance, a full power acceleration 0 to 97 kph (0 to 60 mph) test has been performed. The test was performed where the system was initially started at 20 C (cold) and 80 C (hot). 20 seconds into the test, the vehicle performs a

maximum power available acceleration. In Figure 41, the results show that the cold-start vehicle 0-97 kph time was 8 seconds longer than that of the hot start vehicle. Increasing the size and power available from the battery could reduce this performance difference, however extra battery capacity would go unused most of the time once the vehicle is at operating temperature.

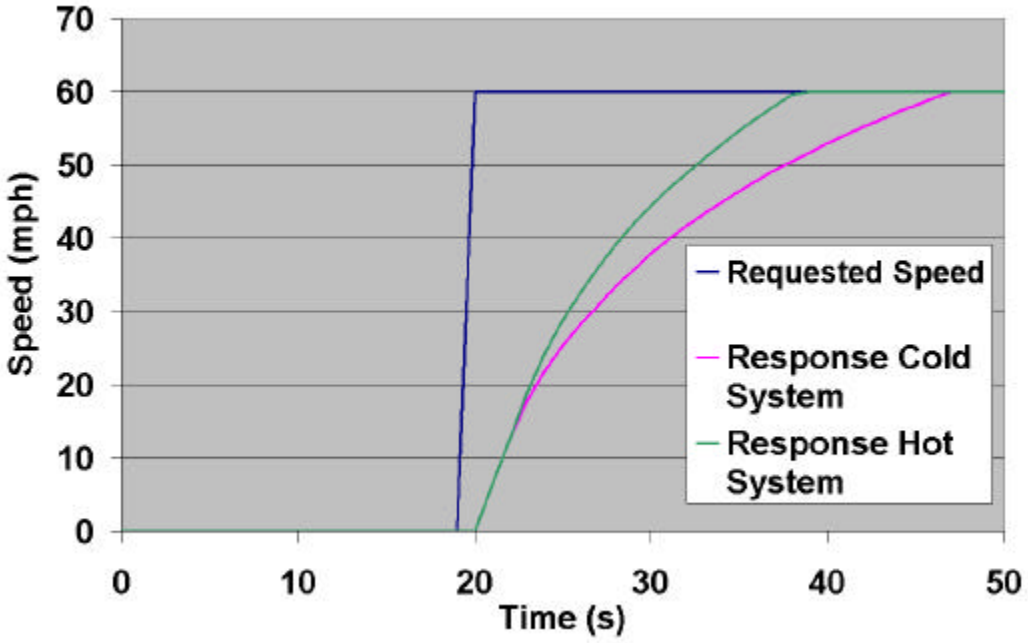

Figure 41. Hot and cold vehicle acceleration performance for a step input.

9 Conclusions and Future Work

9.1 Fuel Cell System Modeling Capabilities

The work presented has developed a net power request model for a vehicle fuel cell system. The model has the capability of quantifying the impact of low temperature operation on the efficiency and performance of a fuel cell system. A finite difference lumped capacitance model was developed that has the ability to model the initial cold-start transient. Analysis of the system involved characterizing the system during steady state operation and in a dynamic vehicle system.

The model has two main parts, the electrochemistry model, and the thermal model. The electrochemistry model is responsible for determining the operating point of the fuel cell and the parasitic power required to run the system. Addressing the issue of the cold-start transient is the responsibility of the thermal model. This model uses a finite difference lumped capacity approach to model the fuel cell stack as well as the reservoir and plumbing. The thermal model also includes a humidifier, condenser, and radiator that affect the overall performance and efficiency of the fuel cell system.

Implemented into the model is an operating control strategy that places limits on the operation of the fuel cell system that would be enforced in a practical application. The model has the ability to limit the following:

- cell voltage
- minimum and maximum power requested from the fuel cell stack
- minimum coolant pump speed
- minimum mass flow rate requested from the air compressor
- fuel cell stack operating temperature

9.2 Impact of Cold-start On Vehicle Fuel Economy and Performance

Fuel cell system design can significantly affect the cold-start performance of a fuel cell system. Through modeling, the impact of thermal mass has been quantified for warm up time to operating temperature of a fuel cell system. The overall cold-start energy use penalty is relatively small for the combination of component sizes and control strategy presented here.

Table 22. Summary of cold-start fuel economy

Cycle	FTP	US06
Hot Start	36.40	14.50
Cold-start	34.30	14.20
Difference %	5.77	2.07

EPA Test	Model Uncorrected	Production Uncorrected
City	34.30	16.9
Highway	39.20	25.2
Combined	36.51	20.64

As expected, performance reduction is seen during cold-start that affects both available power and fuel use. For this vehicle, a thermal transient of 300-800 seconds are required to reach full power. The range in time is dependant upon the drive cycle requirements and control strategy. Low drive cycle power requirements will yield a slower warm up time.

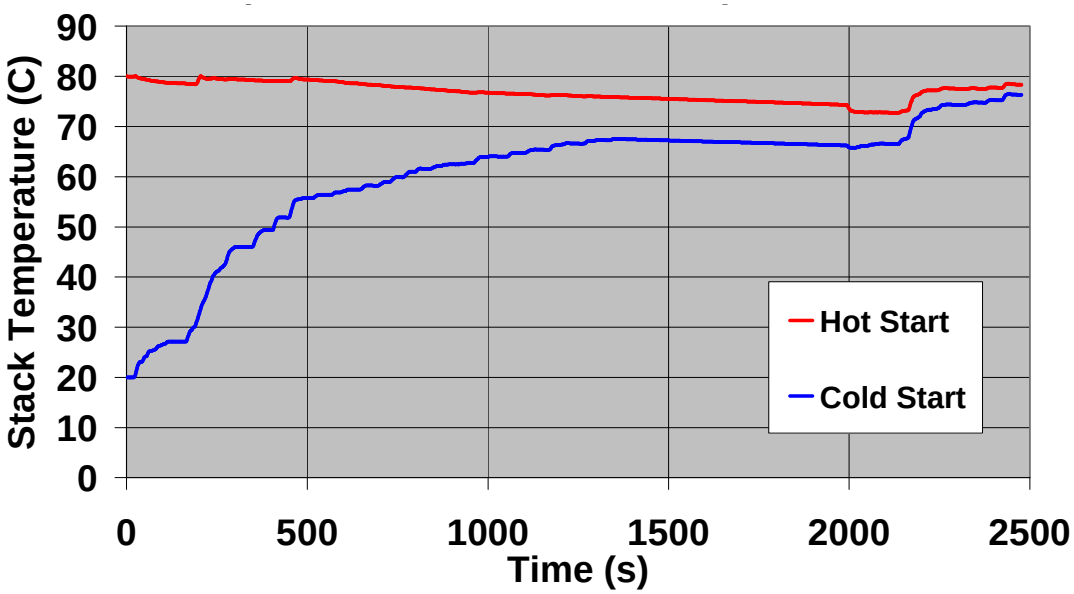

Figure 42. Comparison of Fuel Cell Temp on FTP-75.

This delay is a result of the thermal masses (fuel cell stack and coolant) which most to be heated to operating temperature.

Changing the fuel cell system design and operating control strategy could reduce the effects of cold start. One of the challenges experienced in fuel cell design are the bipolar plates and the necessary size to achieve a power useful in a vehicle considered in this work. In this model the majority of the thermal capacitance of the system is tied up in the fuel cell stack / bipolar plates. Obvious industry goals include increasing the power density such as increased membrane electrode assembly (MEA's) efficiency and performance. This would result in a decreased size of bipolar plates, subsequent reduction in thermal mass of a fuel cell system and decreased thermal transient times. Additionally high temperature materials in a fuel cell could yield an decrease in size of the balance of plant needed to run a fuel cell system such as heat exchangers, humidifiers, and condensers.

Future work to reduce cold start effects that could be done through use of this model would be to explore the operating control strategies. Use of excess power that potentially

could be generated may increase the system operating temperature more quickly. Active control of fuel cell stack operating pressure may also decrease the cold start transients.

The power available to the vehicle also suffers during the cold-start transient. For this fuel cell system it was shown that at cold-start (20 C) approximately 60% of the net power of the total designed net power is available to the vehicle.

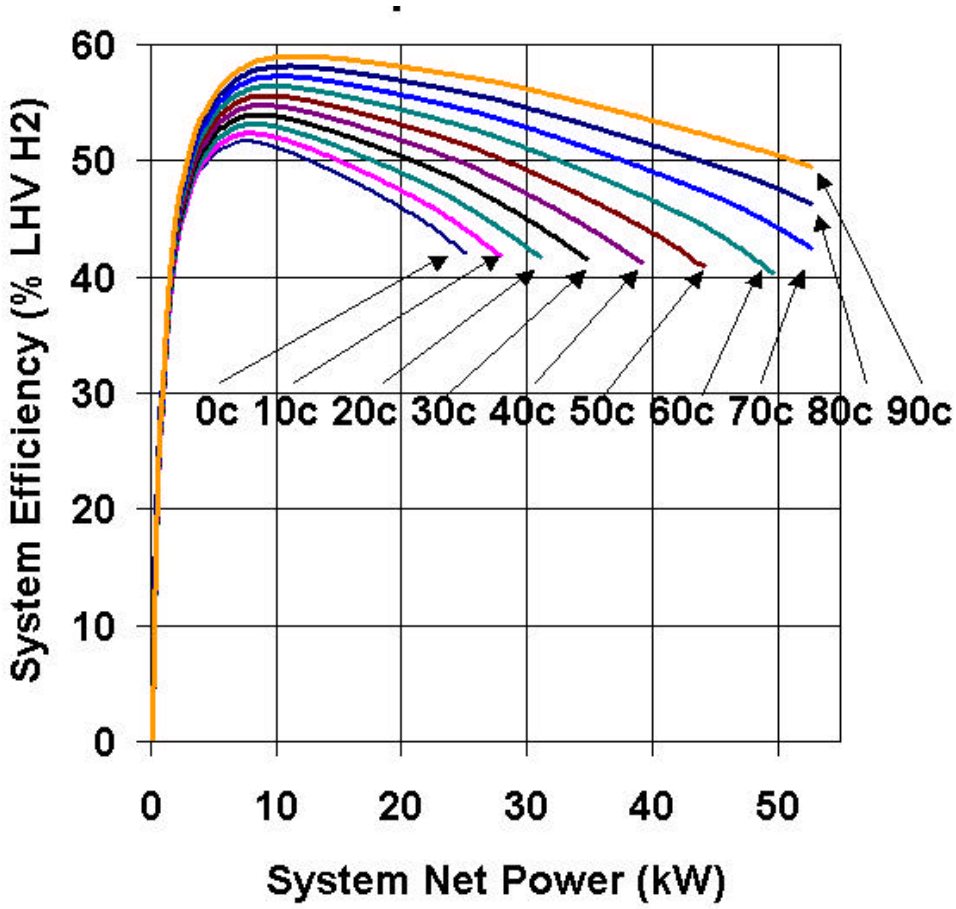

Figure 43. Efficiency vs. Power at different temperatures.

In a vehicle, a performance as well as an efficiency hit was taken as a result of the power not available at cold operating conditions. The results show that the cold-start vehicle 0-97 kph time was 8 seconds longer than that of the hot start vehicle. Increasing the size and power available from the battery could reduce this performance difference, however this extra battery capacity would go unused most of the time once the vehicle is warmed up.

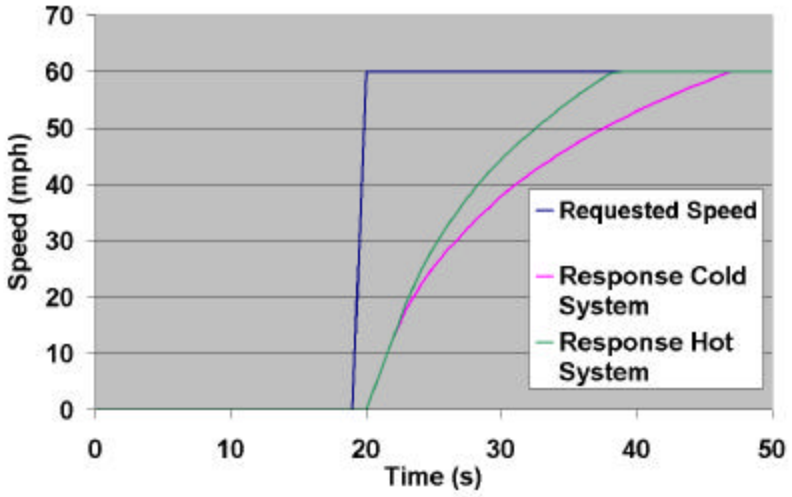

Figure 44. Hot and cold vehicle acceleration performance for a step input.

9.3 Modeling Limitations and Future Work

Presented here together are the limitations of the model and the future work that could go towards addressing these limitations. Many of these suggestions take the model from being a generalized model that effectively takes into account the major impacts of the system, to a very specific model of a actual fuel cell system design.

9.3.1 Model Runtime and Programming Issues

Development of the fuel cell model in the Simulink programming language yielded the following issues that cause problems of normal operation.

1. The polarization curve requires the use of logarithm function to achieve the characteristic performance of fuel cell system. Allowing the minimum cell voltage to be set at low voltages (i.e. 0.2 V/cell) can cause problems evaluating the logs in the polarization curve.

2. Use of the functional relationship, modeled as a regression line to change a net power request into a current density needs to pass through the zero point, see Figure 10.

3. Currently time steps are limited only to 1 second. It is possible to change this, however a few programming issues on ensuring that proper variables with time dependence in the model are evaluated to reflect the time step change. This is primarily the issue on some calculations that have been hard-coded for kj/s are equal to kW. For a time step other than 1, this kj/s = kW is not correct.

4. Operation of the system above 100 C or below 0 C will yield problems with the calculation for the saturation pressure of water vapor (psat).

5. An air flowrate for the fans of the condenser and radiator greater than zero is required.

9.3.2 Non-Programming Model Limitations

The first limitation of the model is a fixed 1 second time step. The system could be capable of using smaller time steps, however current programming limitations do not allow for time steps other that 1 second. For modeling a vehicle system like Magellan, a one second time step was more than adequate for the system. For the real Magellan, the air compression systems would more than likely be the limiting factor.

Another model limitation that would be of some interest is the air compression system. The model uses a simple lookup table that interpolates between fixed operating conditions. However, it would be desired to implement a transient air compression system model with the ability to use an expander system.

Because of a limited data, the coolant pump model suffered from a single operating line. Better data that would take into account pressure and mass flow could be easily

implemented into the program. Additionally a better understanding and more comprehensive data about the coolant pressure drops in the system would be required.

Most of the experience with fuel cells deals with operational temperatures above freezing. Since a target for fuel cells is transportation use, fuel cells would be used in a freezing environment. However, this offers additional challenges both practical and analytical.

This model is limited to PEM fuel cell systems. Future work may include using other types (SOFC, DMFC etc) of fuel cell systems that could be used for power generation. Reviewed previously as a piece of literature is a dynamic electrochemistry model developed by Ceraolo, et al. (2001). His model described the chemical kinetics that occurs inside the fuel cell. It would be advantageous to implement this if a transient fuel cell model is desired. Finally, the model developed here should be further validated through application to other designs and comparison to laboratory data.

References

Adams, James A., Woong-chul Yang, Keith A. Oglesby and Kurt D. Osborne, “The Development of Ford’s P2000 Fuel Cell Vehicle,” SAE Paper 2000-01-1061, March 6-9 2000

ADVISOR, Wipke, Keith, “CTTS Vehicle System Analysis Homepage,” http://www.ctts.nrel.gov/analysis

Atwood, Paul. Gurski, Stephen D. Nelson, Douglas J. Wipke, Keith B. and Markel, Tony (2002), "Degree of Hybridization Modeling of a Hydrogen Fuel Cell PNGV-Class Vehicle," Proceedings of the 2002 Future Car Congress, June 3-5, Arlington, VA, SAE paper 2002-01-1945, 10 pgs.

Barbir, Frano. Balasubramanian, Bhaskar. Neutzler, Jay. “Trade-off Design Analysis of Operating Pressure and Temperature in PEM Fuel Cell Systems,” ASME AES-Vol. 39, 1999

Boettner Daisie D., Gino Paganelli, Yann G. Guezennec, Giorgio Rizzoni, Michael J. Moran, “Proton Exchange Membrane Fuel Cell System Model for Automotive Vehicle Simulation and Control,” IMEC2001 / AES-23666 Proceedings of 2001 ASME Congress and Expositions Nov 11-16 2001

Candusso, Denis, Elisabeth Rulliere, Seddik Bacha, “Modeling of a Fuel Cell Hybrid Power Source for a Small Electric Vehicle,” 18th Electric Vehicle Symposium 2001
Ceraolo, R. Giglioli, C. Miulli, A. Pozio, “A Dynamic Model of Proton Exchange Membrane Fuel Cell” 18th Electric Vehicle Symposium 2001

Doss, Ezzat Danial., Rajesh Ahluwalia, Romesh Kumar, “Hydrogen-Fueled Polymer Electrolyte Fuel Cell Systems for Transportation,” Chemical Technology Divison, Argonne National Lab, ANL-98/16 August 1998

Fronk, Matthew H., David L. Wetter, David A. Masten, Andrew Bosco, "PEM Fuel Cell System Solutions for Transportation," SAE Paper 2000-01-0373, in SAE SP-1505, Fuel Cell Power for Transportation 2000, pp. 103-108.

Fuchs, M. Barbir, F. Husar A. Neutzler, J. Nelson, D. J. Ogburn, M. J. and Bryan, P. (2001), " Performance of an Automotive Fuel Cell Stack," SAE Transactions, Journal of Engines pp. 1-5. (also in Proceedings of the 2000 Future Car Congress, April 2-6, Arlington, VA, SAE paper 2000-01-1529).

Gurski, Stephen D. Nelson, Douglas J. (2002), "Design and Integration Challenges for a Fuel Cell Hybrid Electric Sport Utility Vehicle," accepted for the Proceedings of the 2002 SAE Congress, SAE Paper 2002-01-0095, in SP-1691, 16 pages.

Gurski, Stephen D. Evans, Dallas. Knox, Daniel. Conover, Mark. Harris, Anthony. Lohse-Busch, Henning. Kraft, S. Nelson, Douglas J. (2002), "Design and Development of the 2001Virginia Tech FutureTruck: A Fuel Cell Hybrid Electric Vehicle," Proceedings of the 2001 FutureTruck Challenge, June 4-13, 2001, Milford, MI, SAE SP-1701, 18 pages.

Ijaz, Mujeeb Ismael, "Methanol Fuel Cvell Vehicle Demonstration Mazda Premacy FC-EV, Power by TH!NK," 18th Electric Vehicle Symposium 2001

Incopera Frank P., DeWitt, David P. Fundamentals of Heat and Mass Transfer, Fourth Edition, John Wiley & Sons Inc., 1996

Kroger, D.G., "Radiator Characterization and Optimization," #840380, Vol. 93 SAE Transactions, 1984 pp. 2.984-2.990

Kulp, Galen. Gurski, Stephen D. and Nelson, Douglas J. (2002), "PEM Fuel Cell Air Management Efficiency at Part Load", Proceedings of the 2002 Future Car Congress, June 3-5, Arlington, VA, SAE paper 2002-01-1912, 14 pgs.

Larminie, James., Andrew Dicks, Fuel Cell Systems Explained, John Wiley & Sons. LTD, 2000

Nelson, Dr. Douglas J.,Virginia Polytechnic Institute and State University,Mechanical Engineering Department,Blacksburg, Virginia 24061-0238, (540) 231-4324 Doug.Nelson@vt.edu

Ngy-Srun A.P, Dr. Ing. "Influence of Front End of Vehicle, Fan and Fan Shroud on the Cooling System of Fuel Cell Electric Vehicle," 18th Electric Vehicle Symposium 2001

Ogburn, M. W. Luttrell, B. King, S. Postle, R. Fahrenkrog,D. J. Nelson (1999), "Fuel Cell SystemEfficiency in the Virginia Tech 1999 Hybrid Electric FutureCar," Proceedings of the 1999 Environmental and Advanced Technology Vehicles Conference & Exposition, June 13-16, 1999, Ypsilanti, MI, published by SAE/ESD on CD-Rom, 13 pages.

Shapiro, Howard N., Michael J. Moran, Fundamentals of Engineering Thermodynamics, John Wiley & Sons, Inc., 1995

Yamanashi, Fuminori, Isaya Matsuo, "Development of Nissan's Direct Hydrogen Fuel Cell Vehicle," 18th Electric Vehicle Symposium 2001

Appendix A

These are the block diagrams used in the Simulink model.

Below is the hierarchical layout of the model. The names listed on each of the following pages coincide with the names in the hierarchical list below.

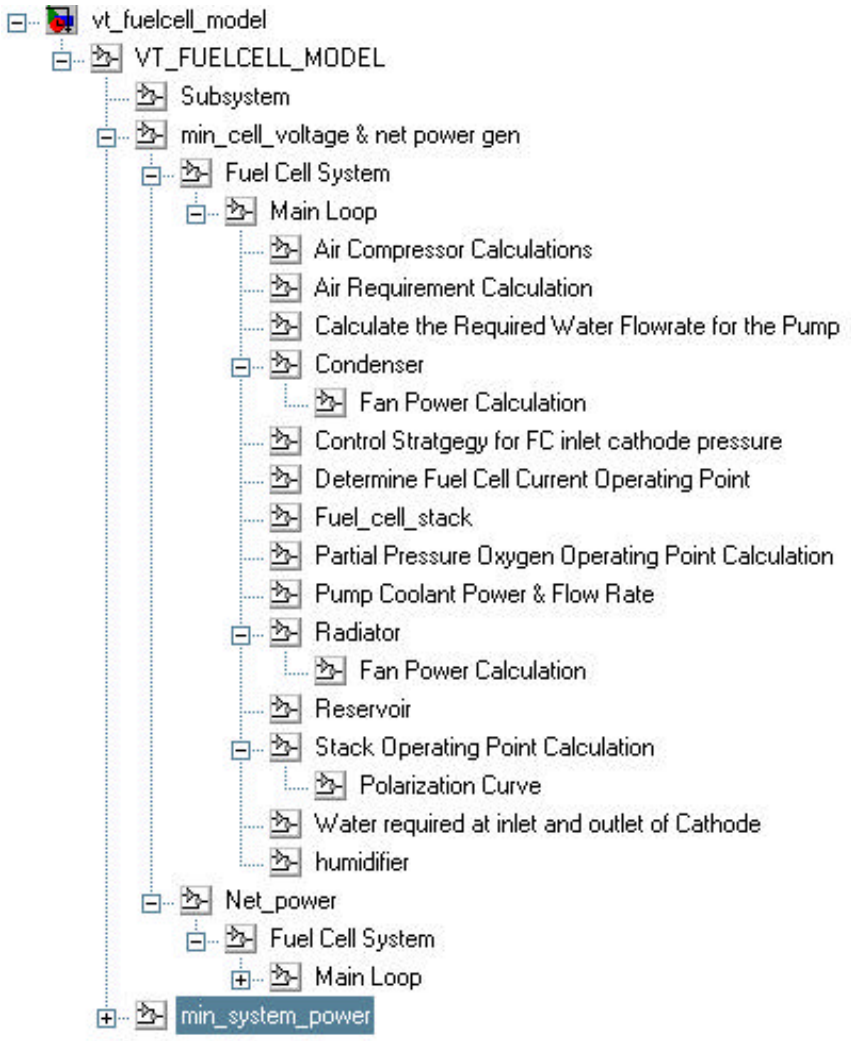

VT Fuel Cell Model

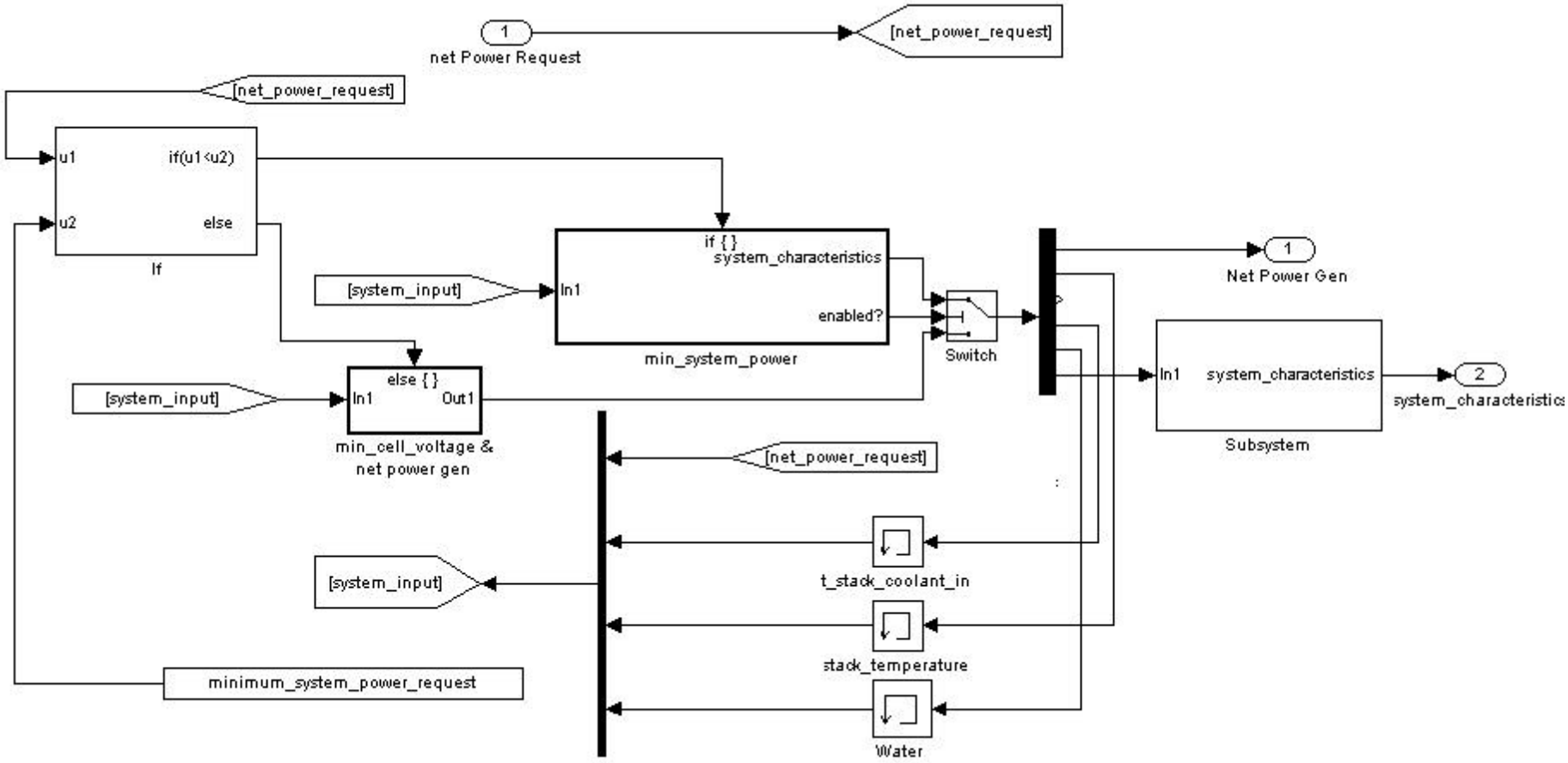

Point where system chooses a goal, based on the request. Also funnels the information to the next time step for the thermal model.

Min Cell Voltage and Net Power Gen

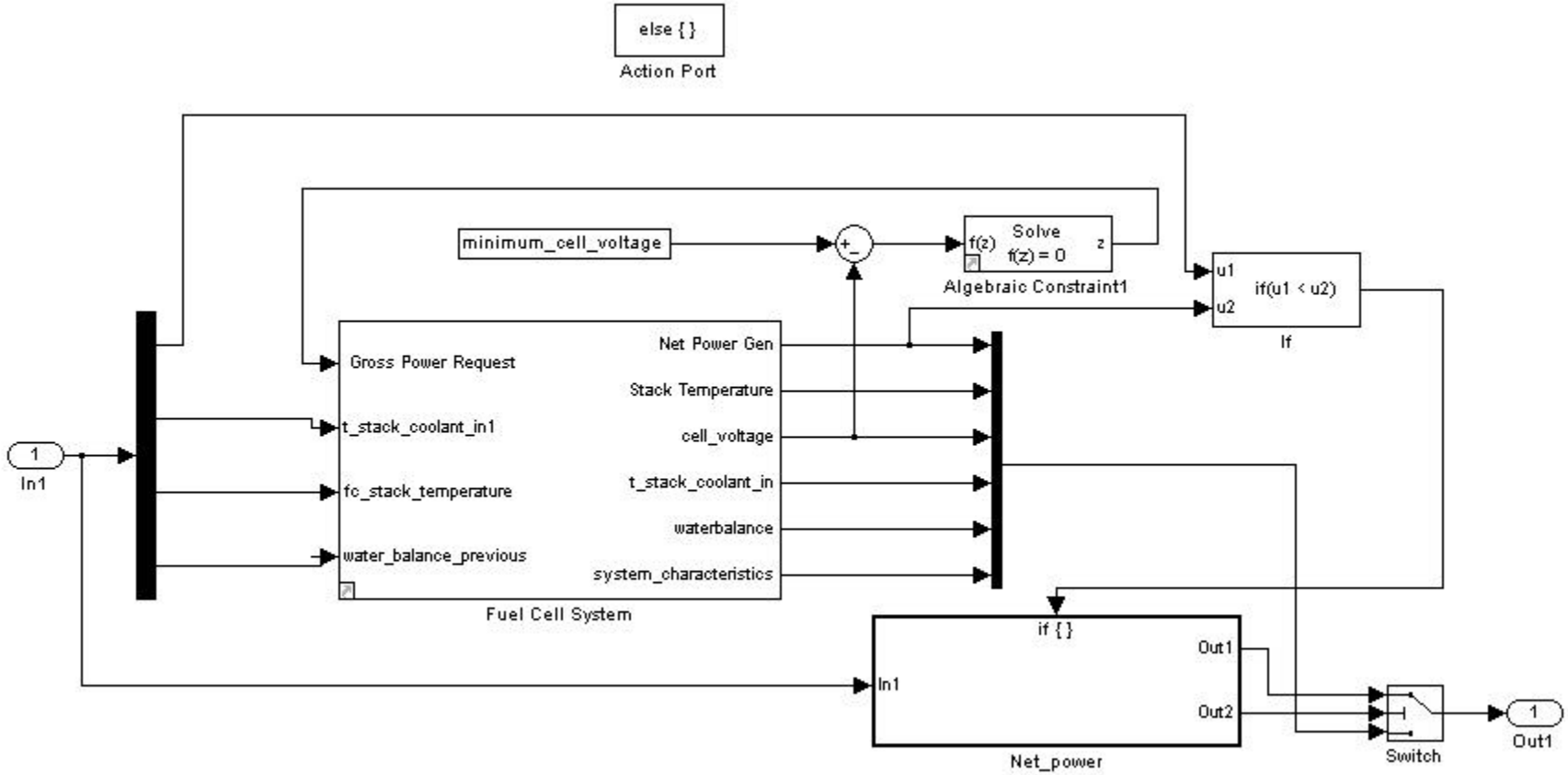

Location at the point where the model determines if a minimum cell voltage has to be enforced or the system will try and converge to a net power request

Fuel Cell System. Page 1 / 7

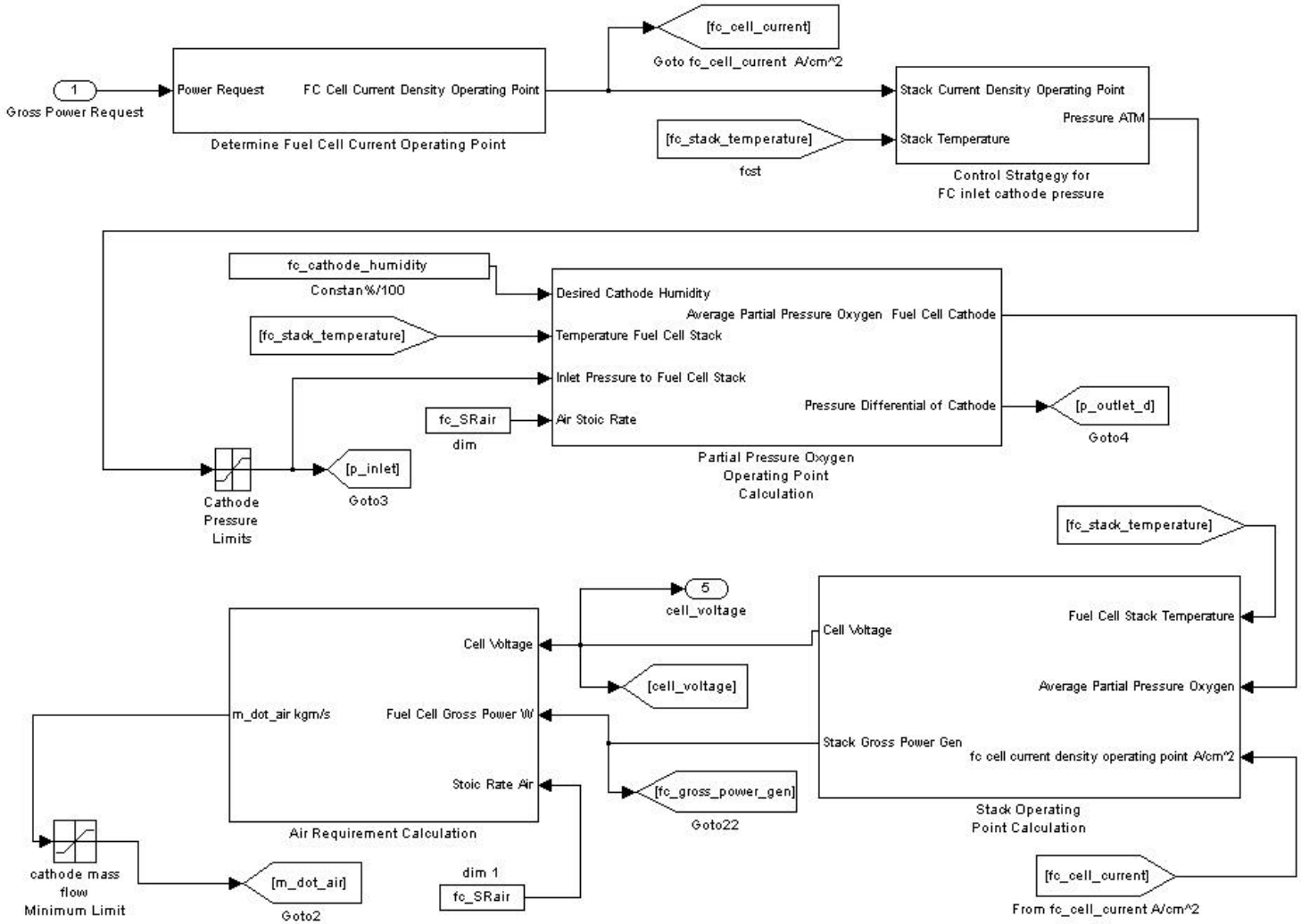

Electrochemistry model / part of the main fuel cell model.
Here the fuel cell operating point is determined

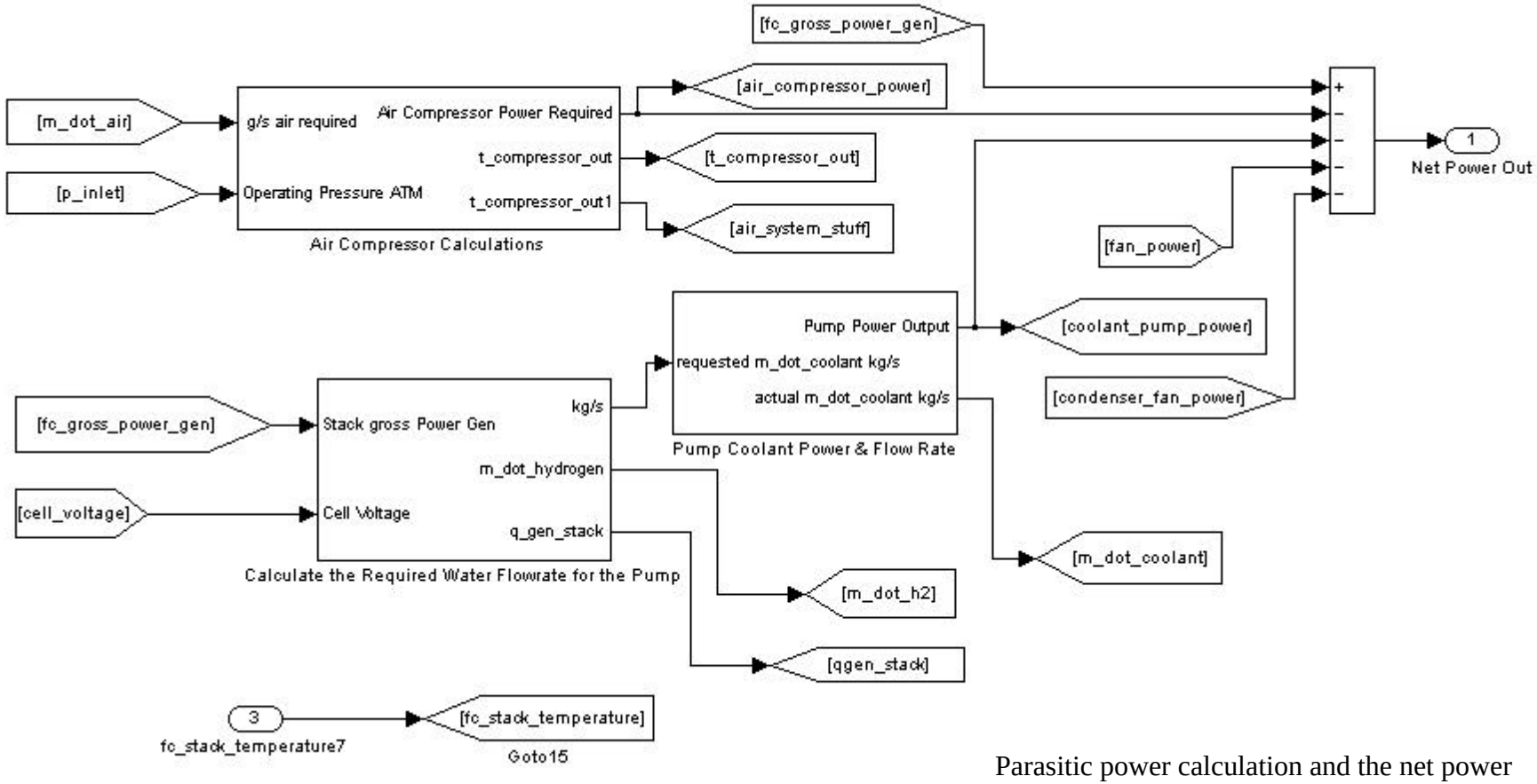

Parasitic power calculation and the net power point calculation

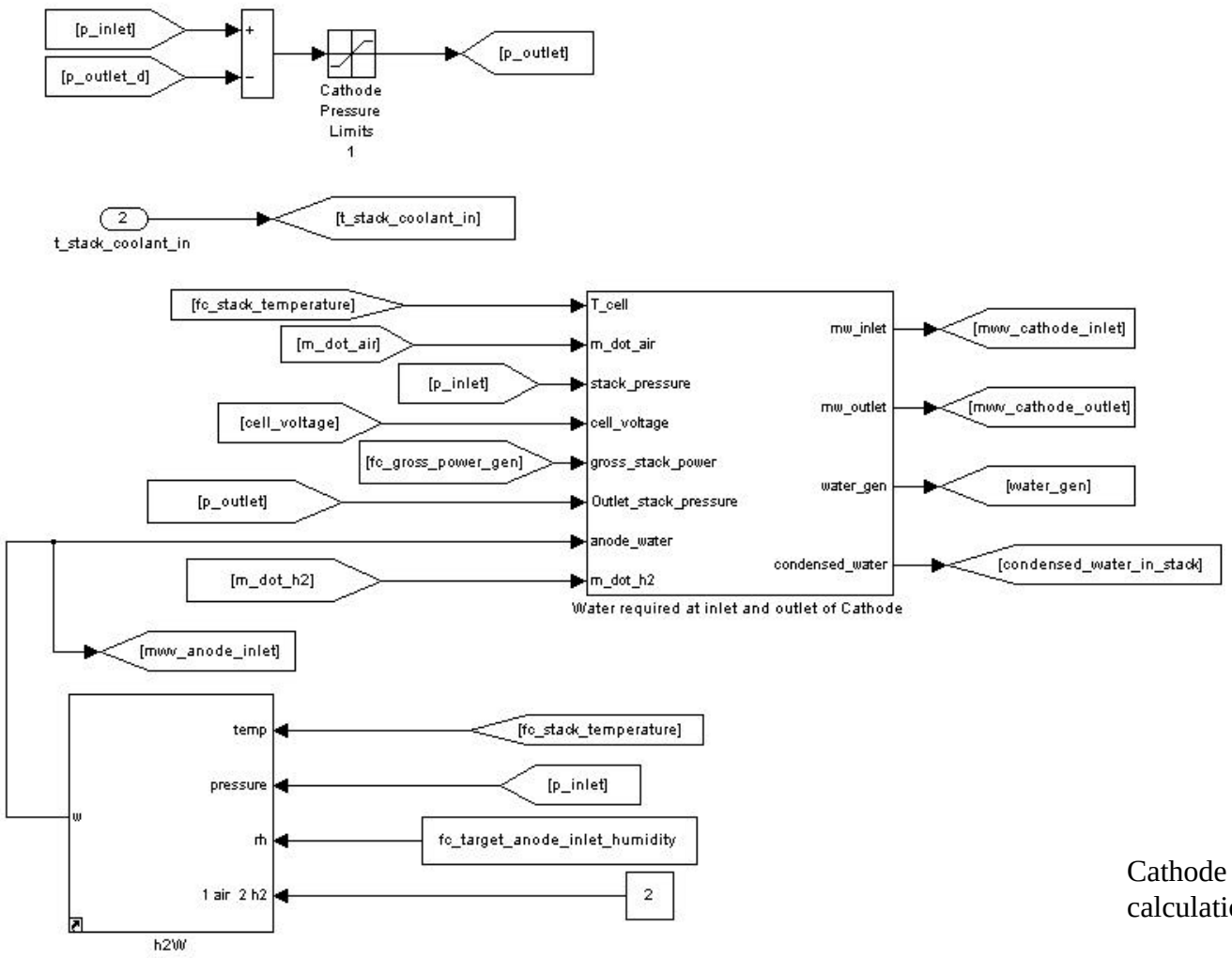

Cathode inlet operating conditions calculations

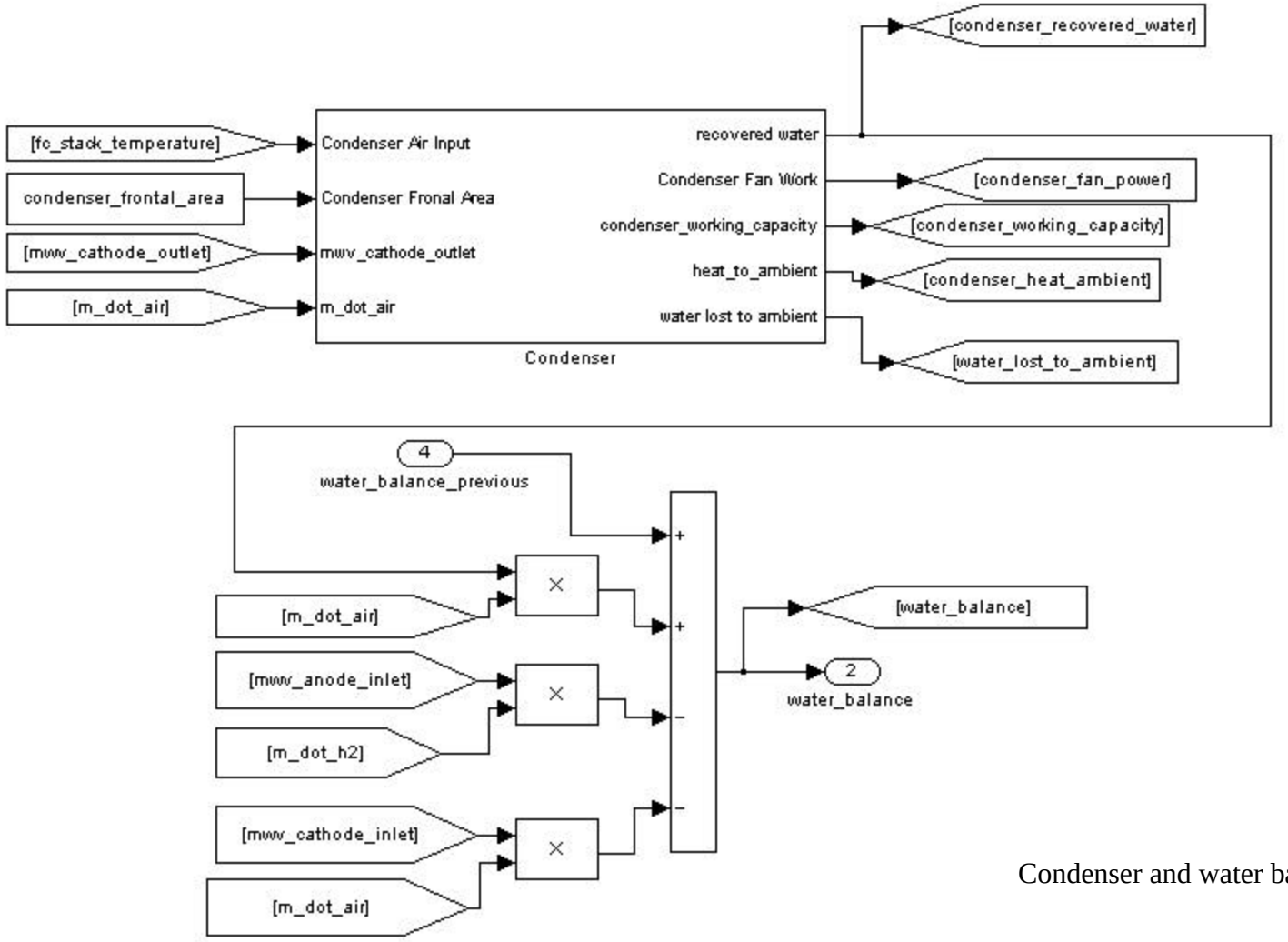

Condenser and water balance calculations

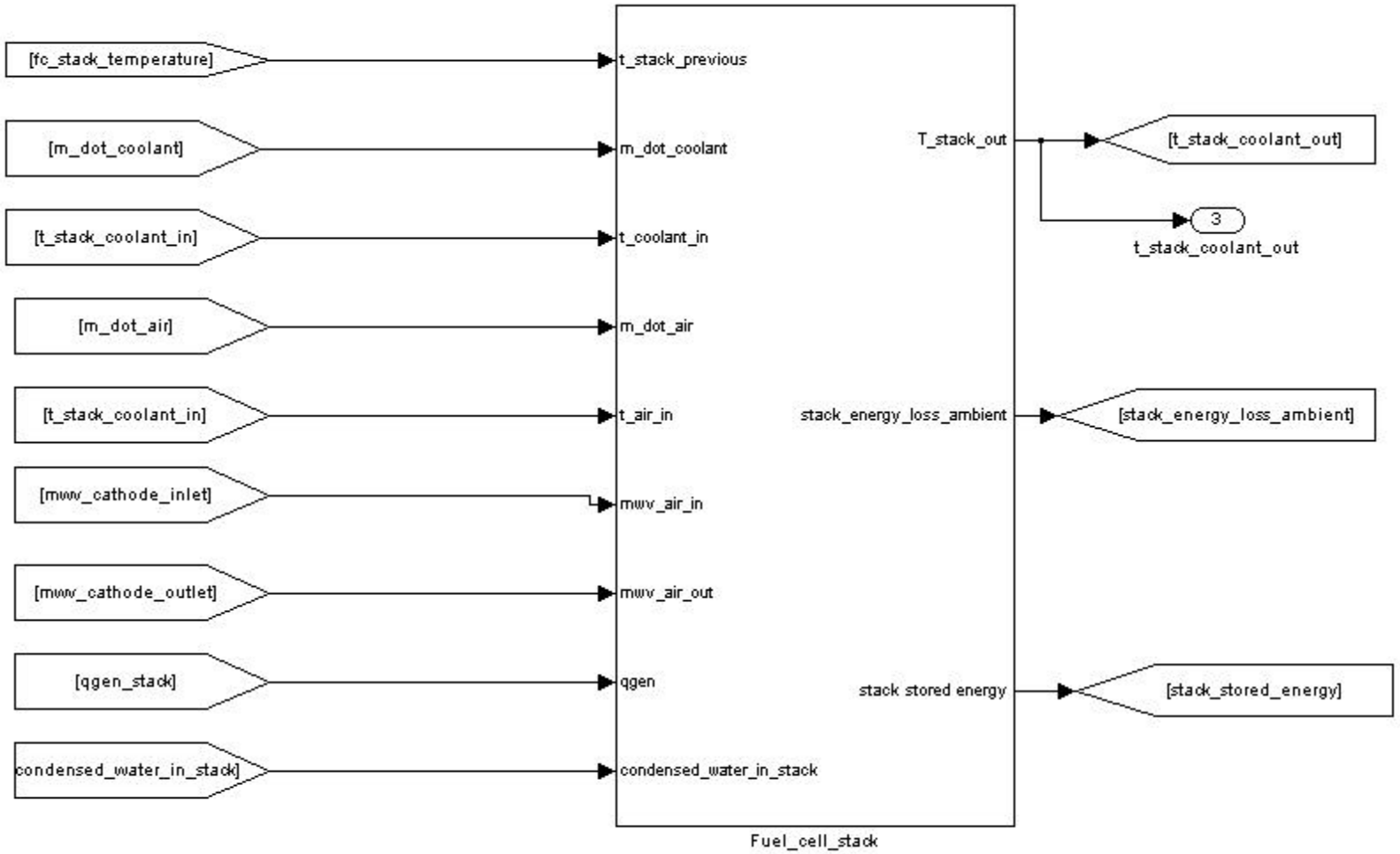

Fuel cell stack block diagram

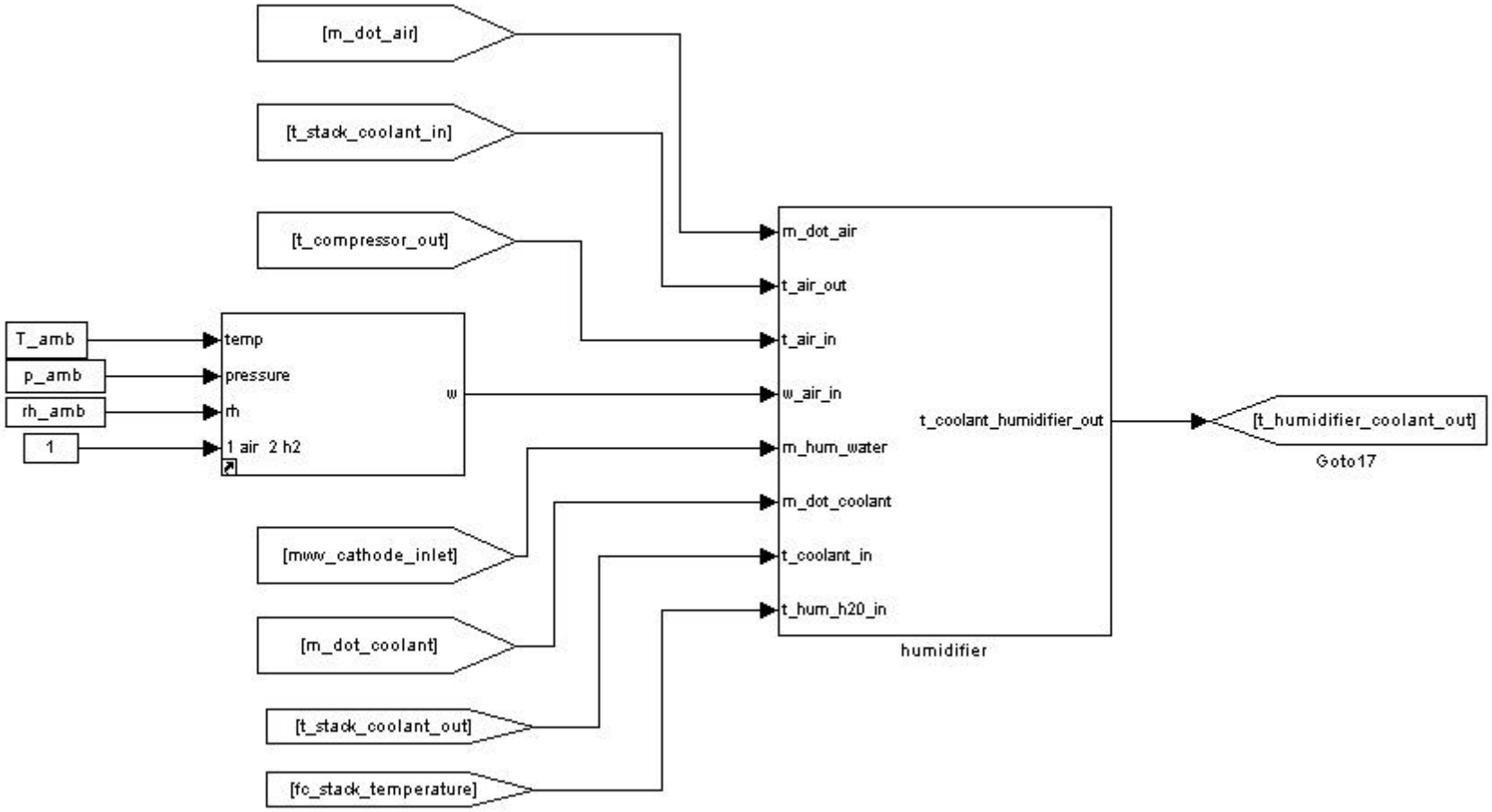

Humidifier
Block
Diagram

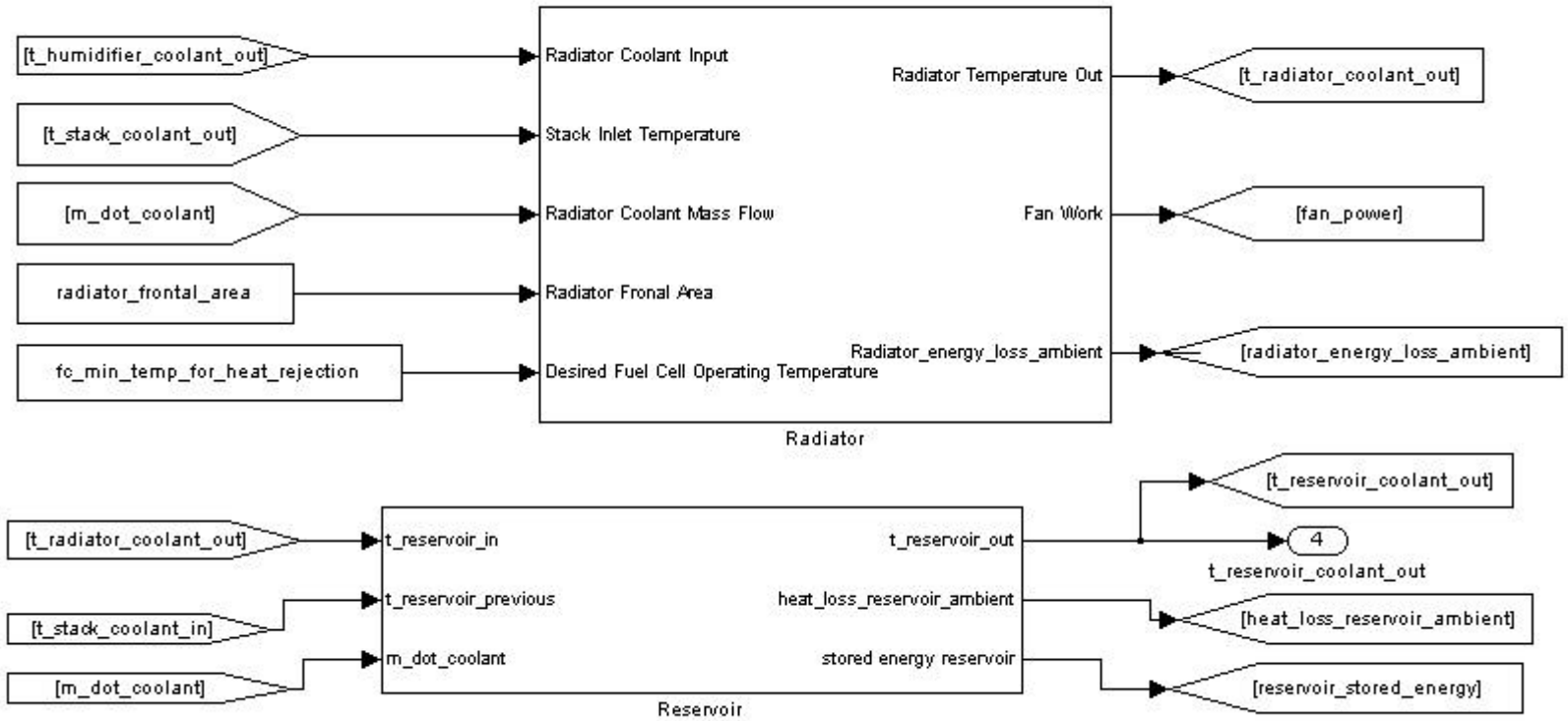

Reservoir and radiator block diagrams

Main Loop – Air Compressor Calculations

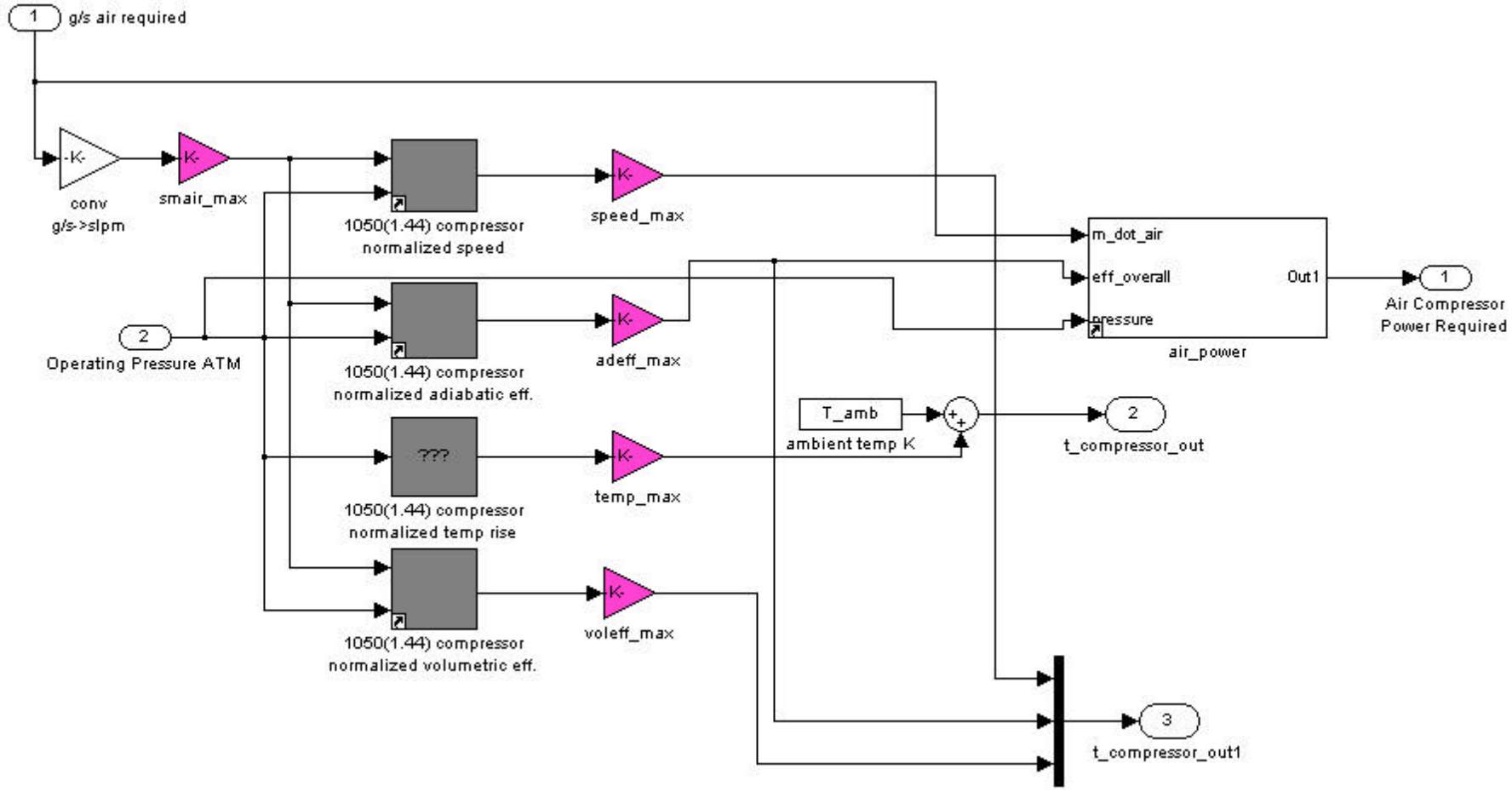

Air compressor operating point diagram. This has the lookup tables and interpolation routines to determe the adiabatic efficiency, temperature rise and volumetric eff. As well as the block to determine the air power required

Main Loop – Air Requirement Calculation

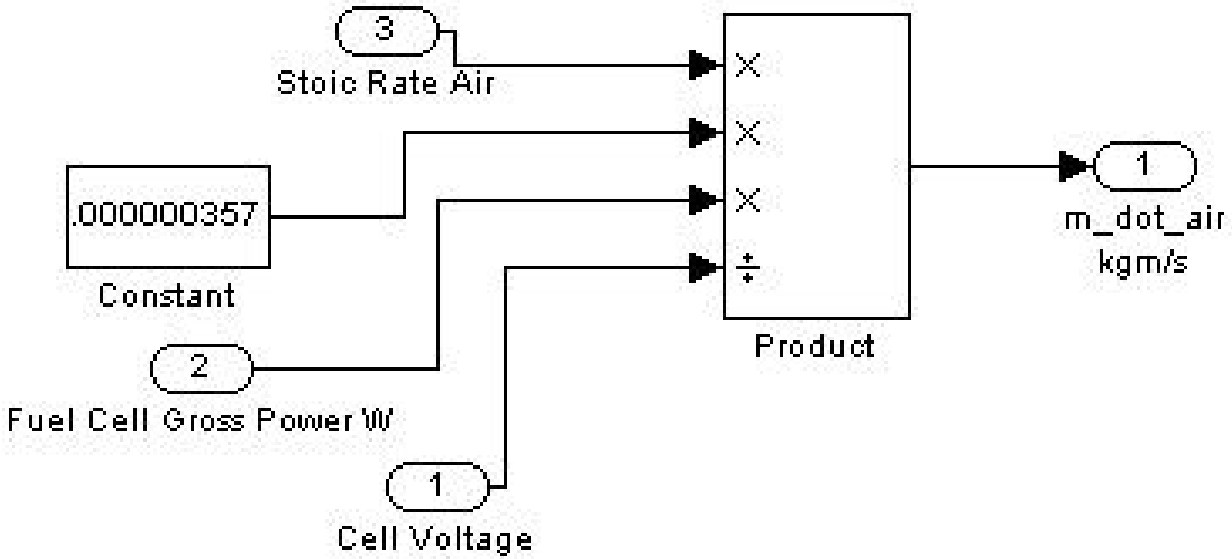

Calculation to determine the mass flow rate of air required at the current operating point.

Main Loop –Calculate The Required Water Flowrate for the Pump

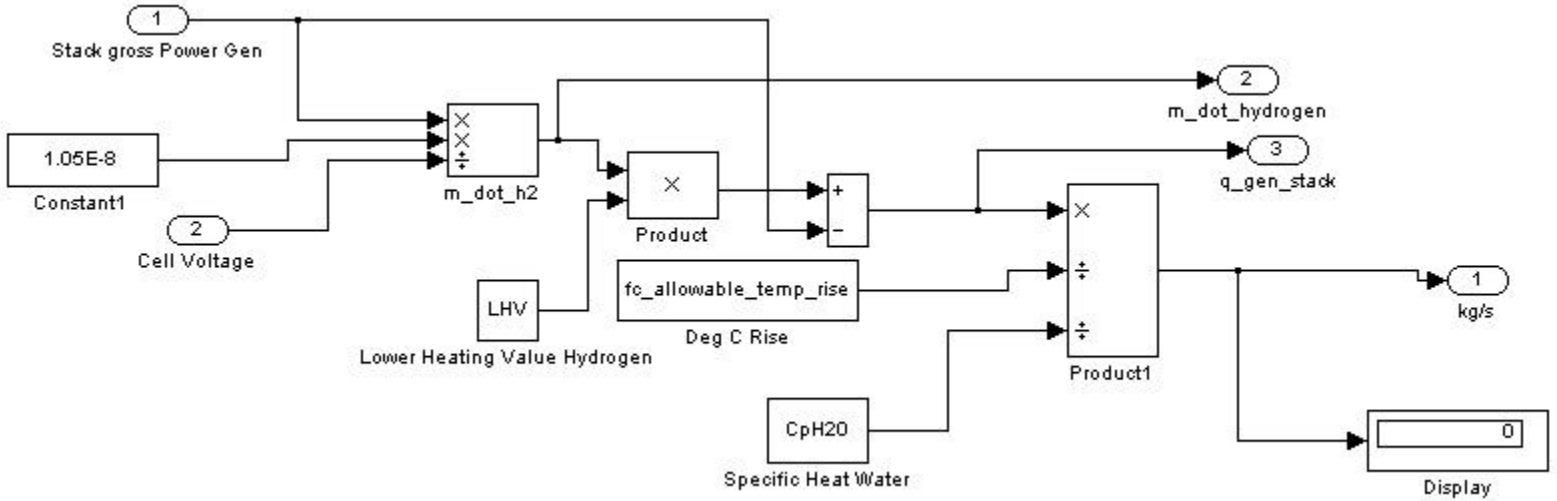

Calculation to fix the flowrate to achive the maximum temperature rise across the stack

Main Loop –Condenser

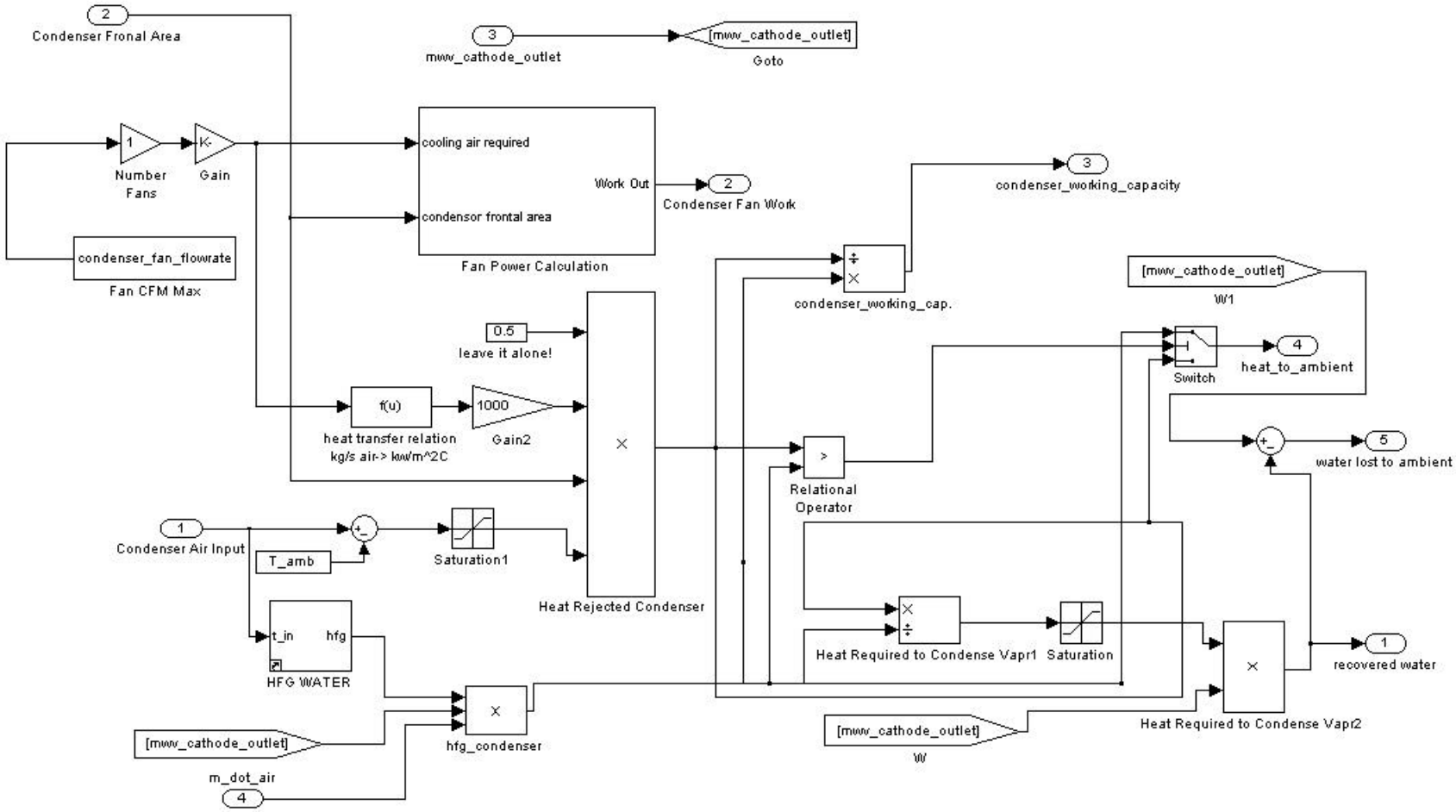

Condenser performance model that predicts how much water could be extracted from the cathode air stream

Main Loop –Condenser-Fan Power Calculation

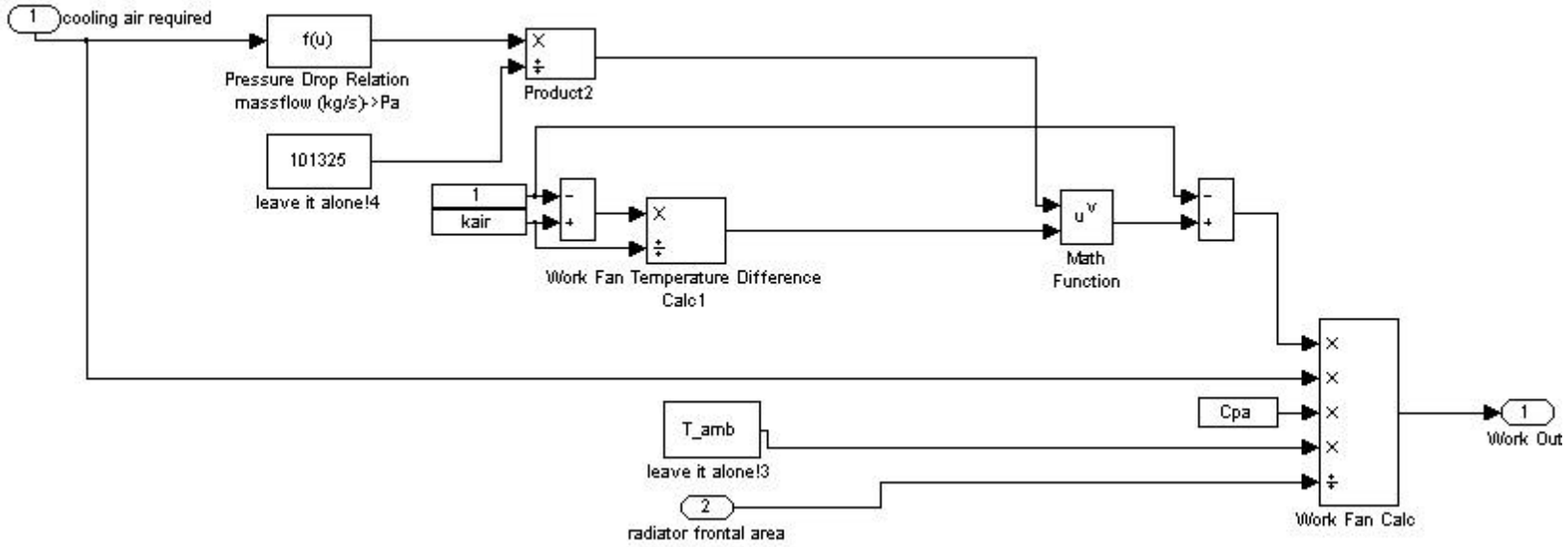

Condenser fan power calculation used for the parasitic power calculation

Main Loop –Control Strategy for FC Inlet cathode Pressure

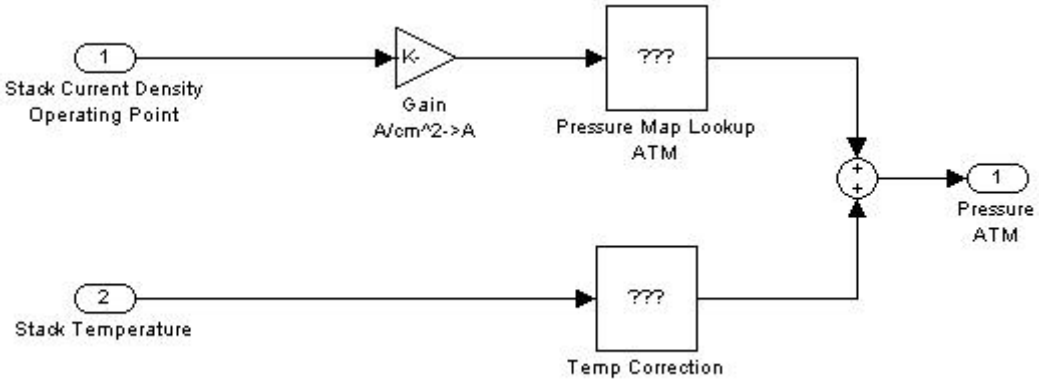

Function that changes the stack current density and stack temperature to an operating pressure for the stack.

Main Loop –Determine Fuel Cell Current Operating Point

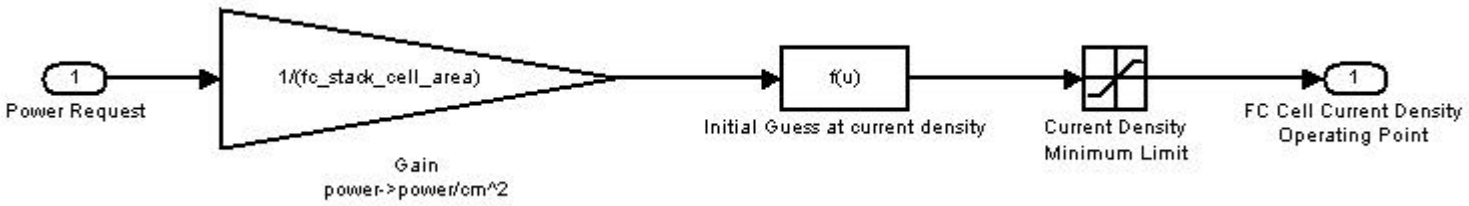

Main Loop – Fuel Cell Stack

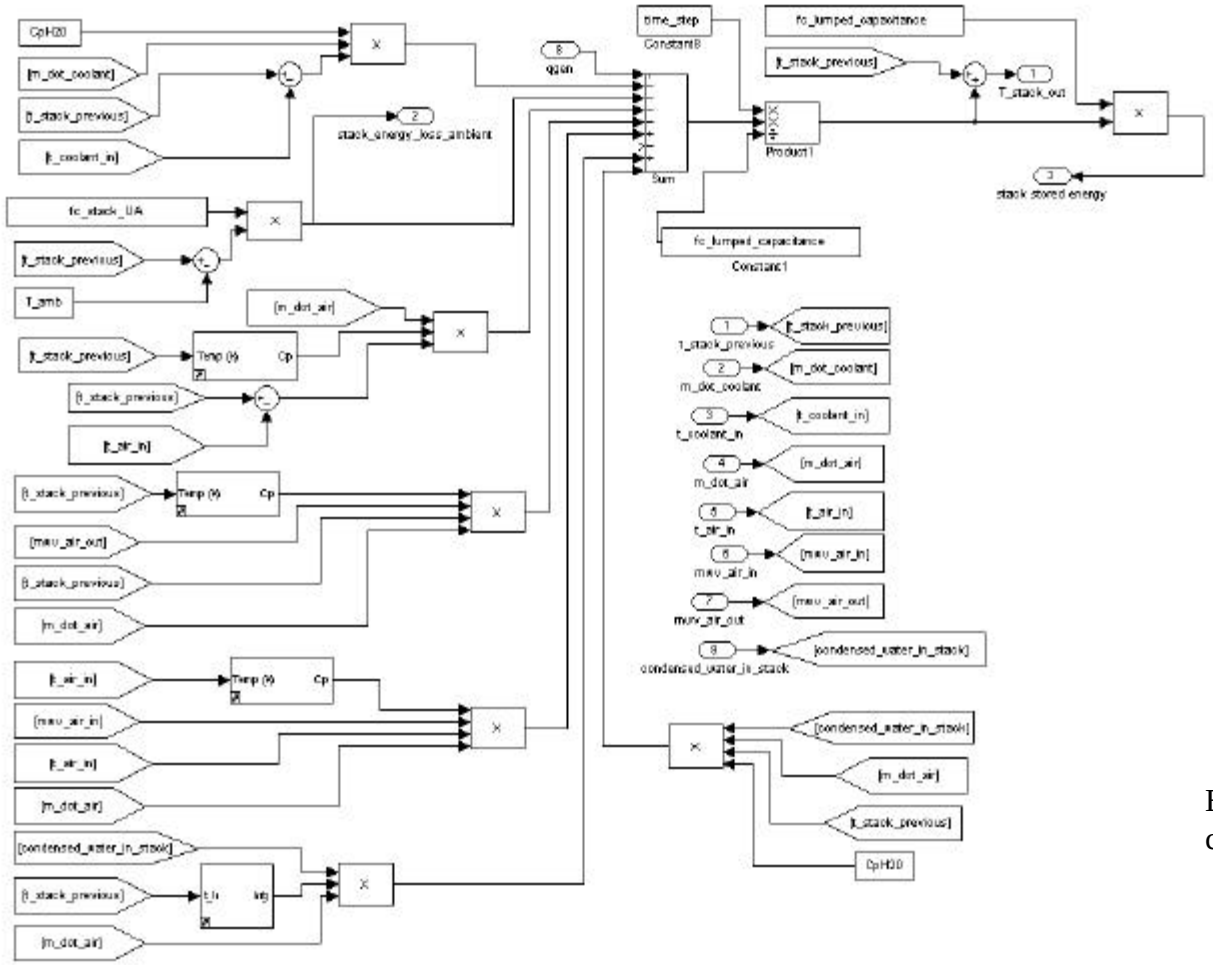

Energy and Mass balance internal to the fuel cell stack

Main Loop –Partial Pressure Oxygen Operating Point Calculation

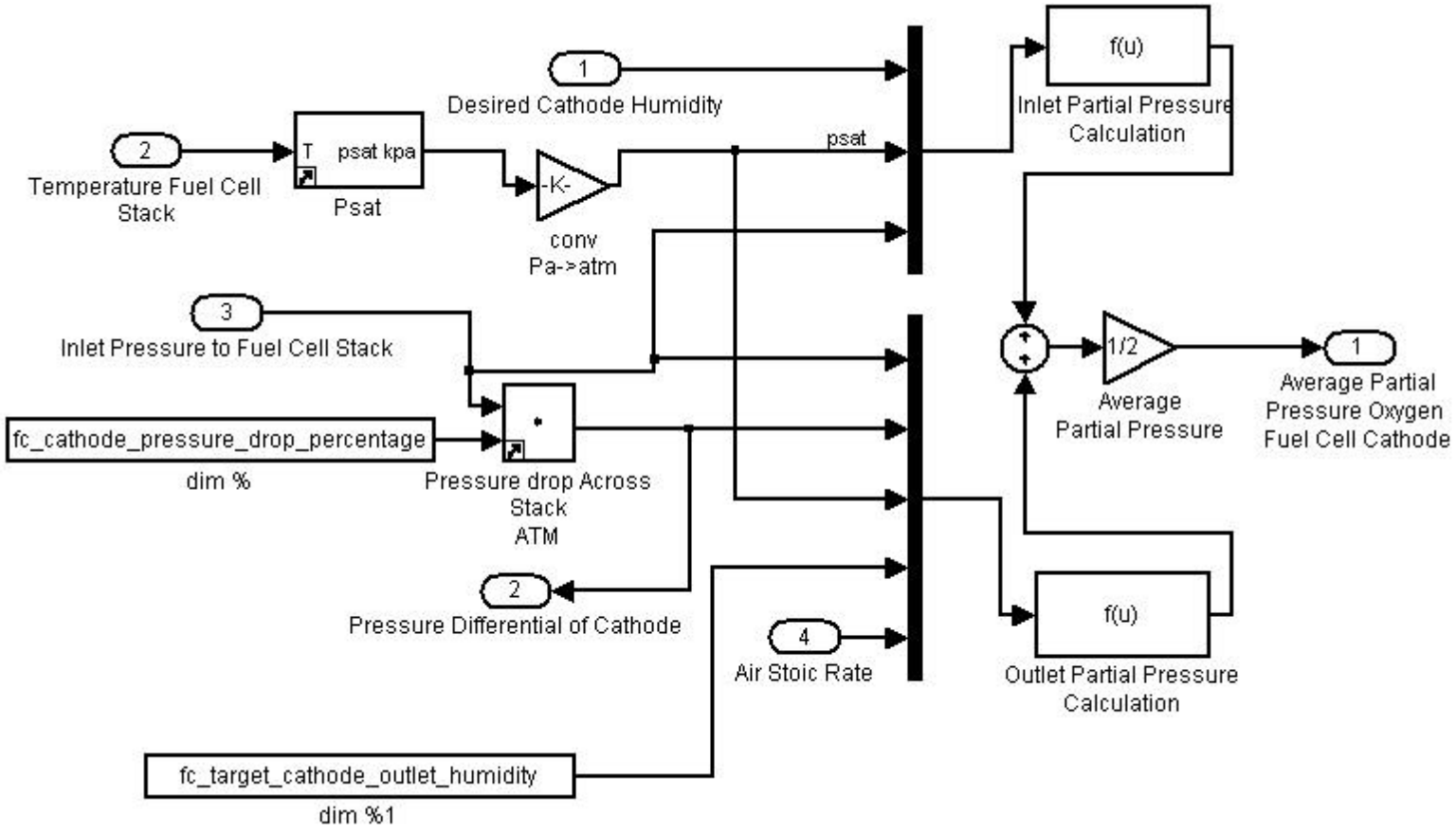

Main Loop –Radiator

Radiator performance model and thermostat to determine the temperature drop across the radiator

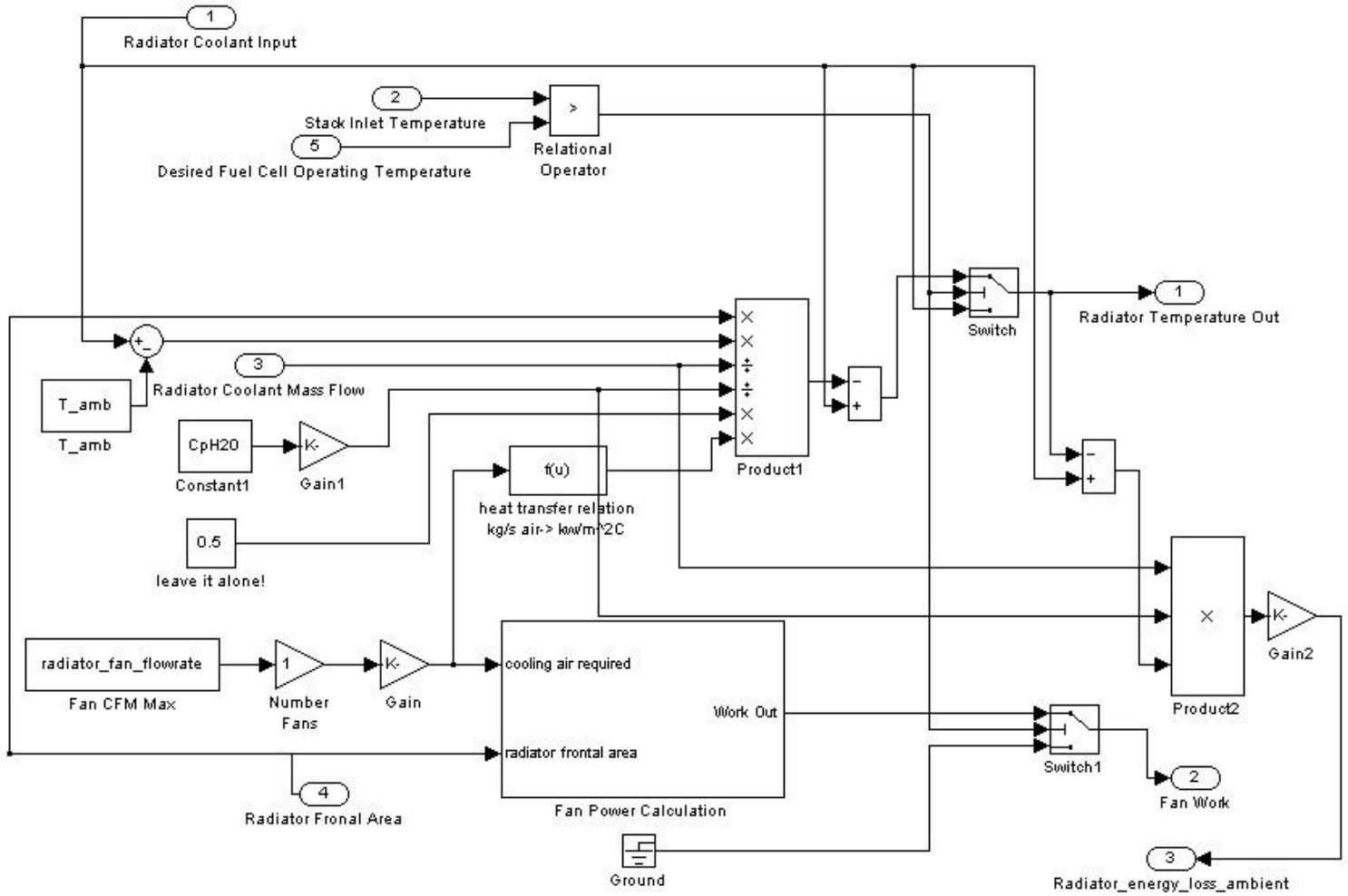

Main Loop – Radiator-Fan Power Calculation

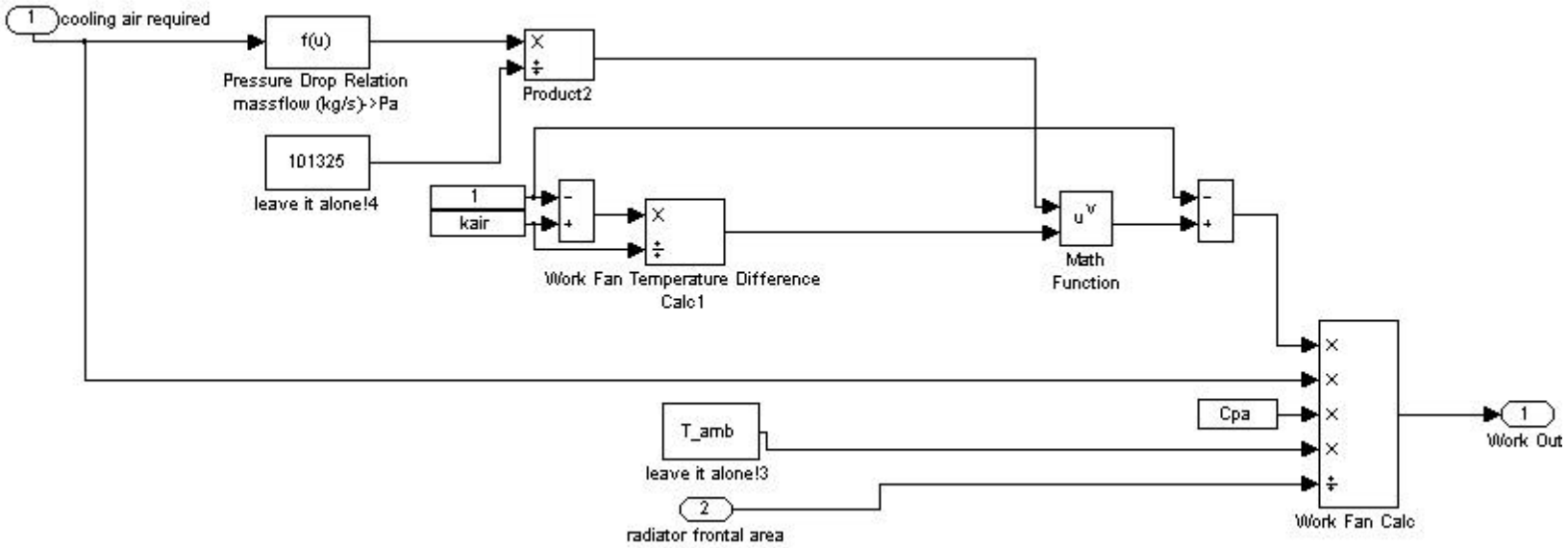

Main Loop – Reservoir

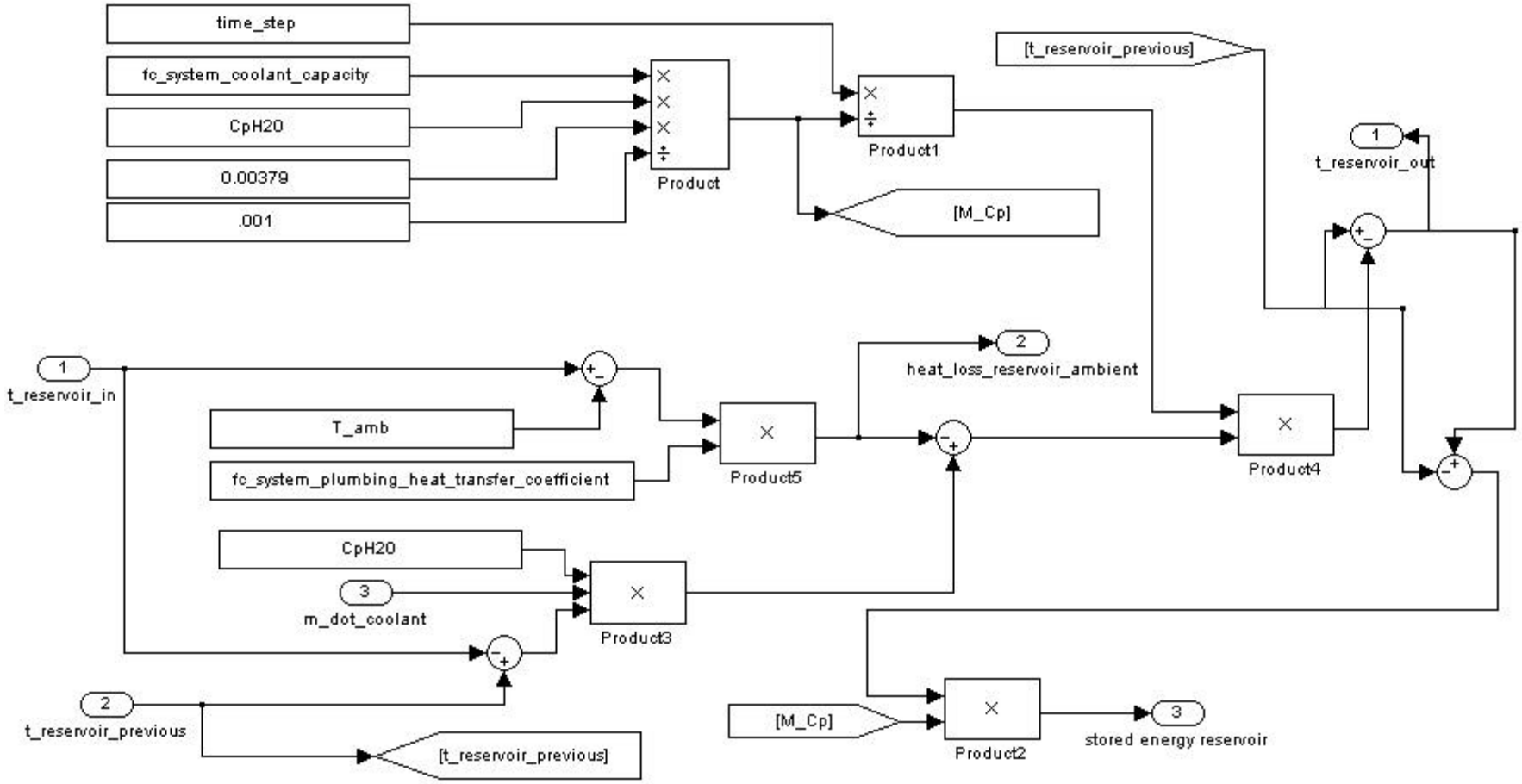

Energy and mass balance in the reservoir model

Main Loop –Stack Operating Point Calculation

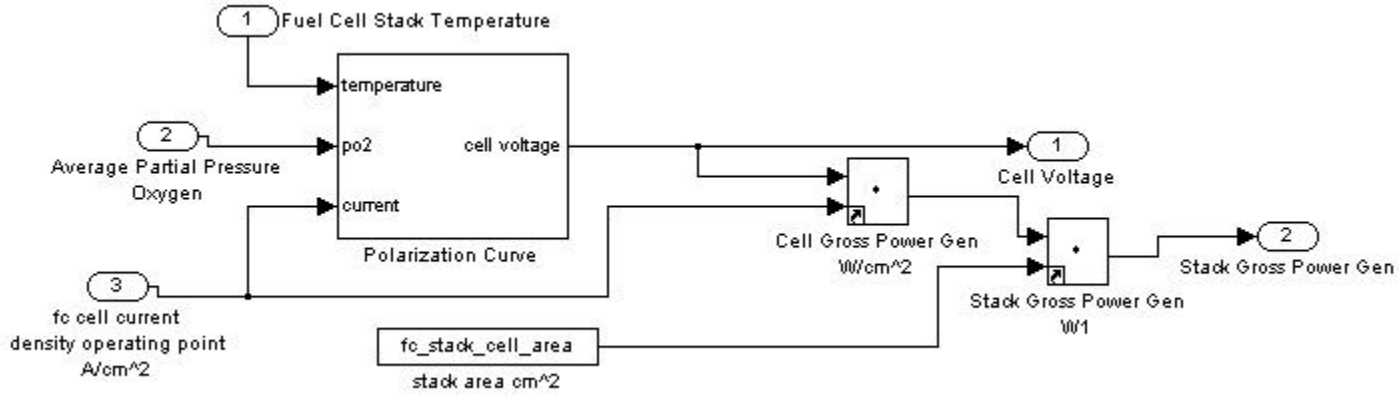

Polarization curve and stack operating point calculation

Main Loop –-Stack Operating Point Calculation-Polarization Curve

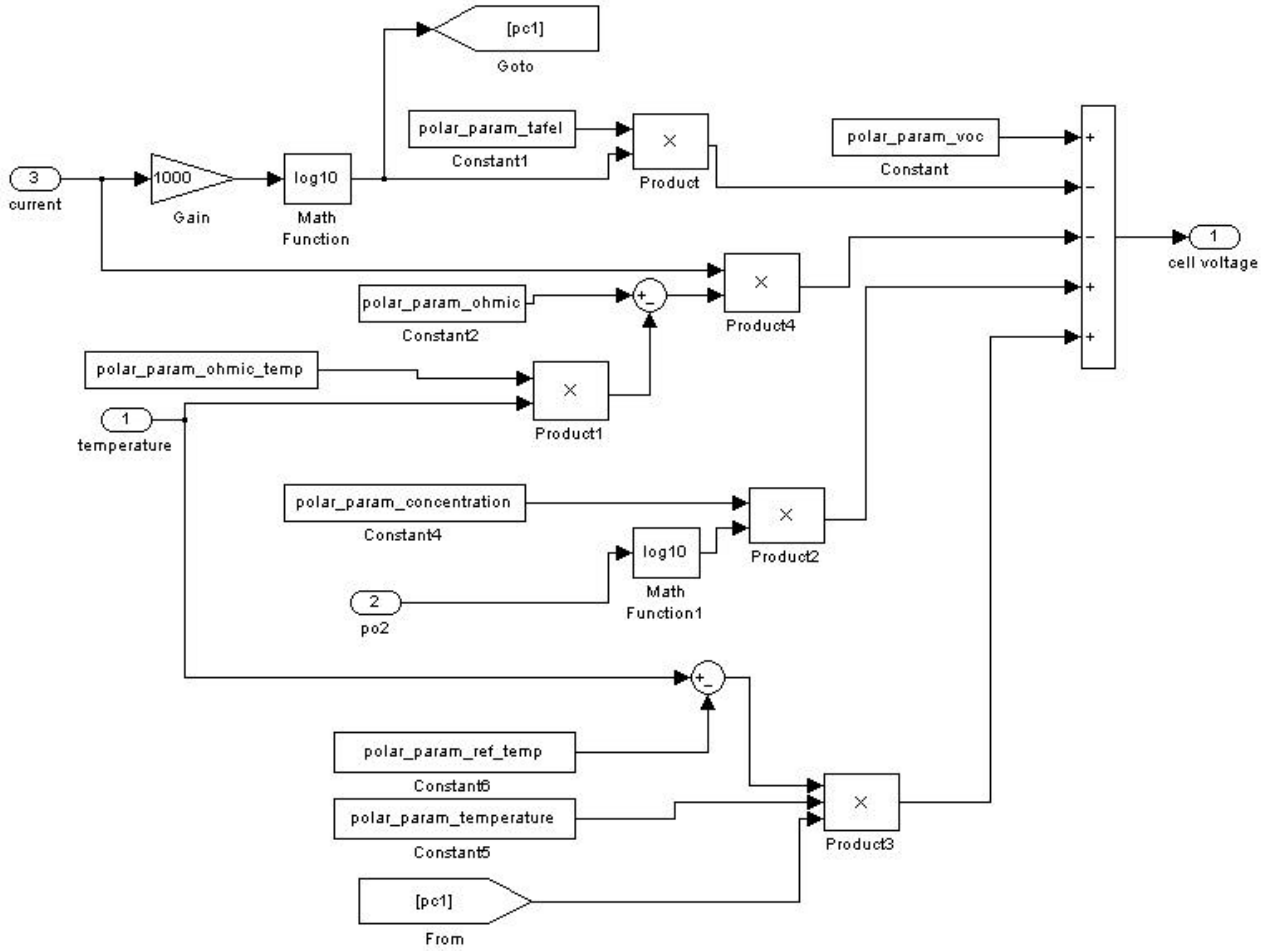

Main Loop – Water Required at Inlet and Outlet of Cathode

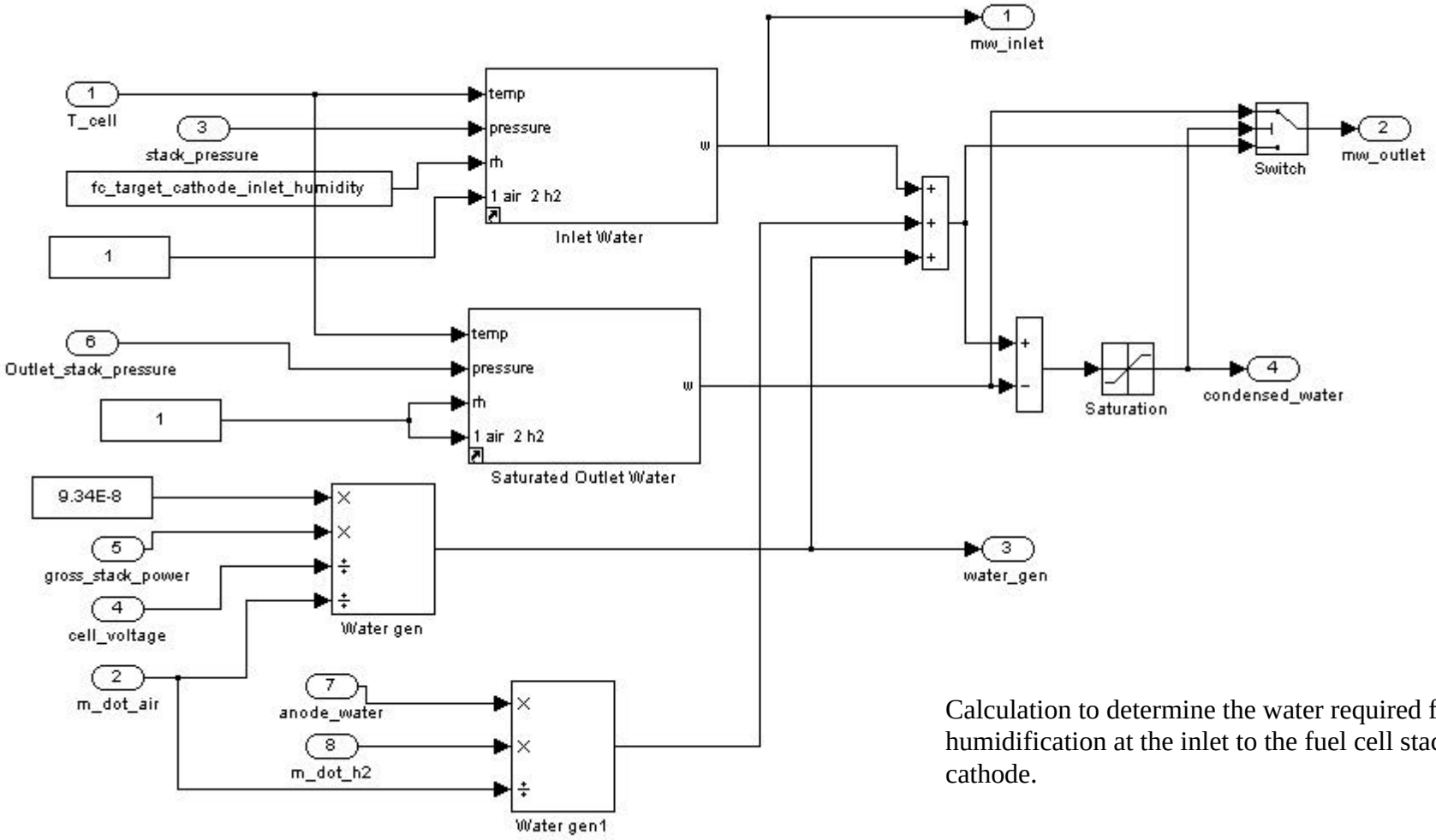

Calculation to determine the water required for humidification at the inlet to the fuel cell stack cathode.

Main Loop –Humidifer

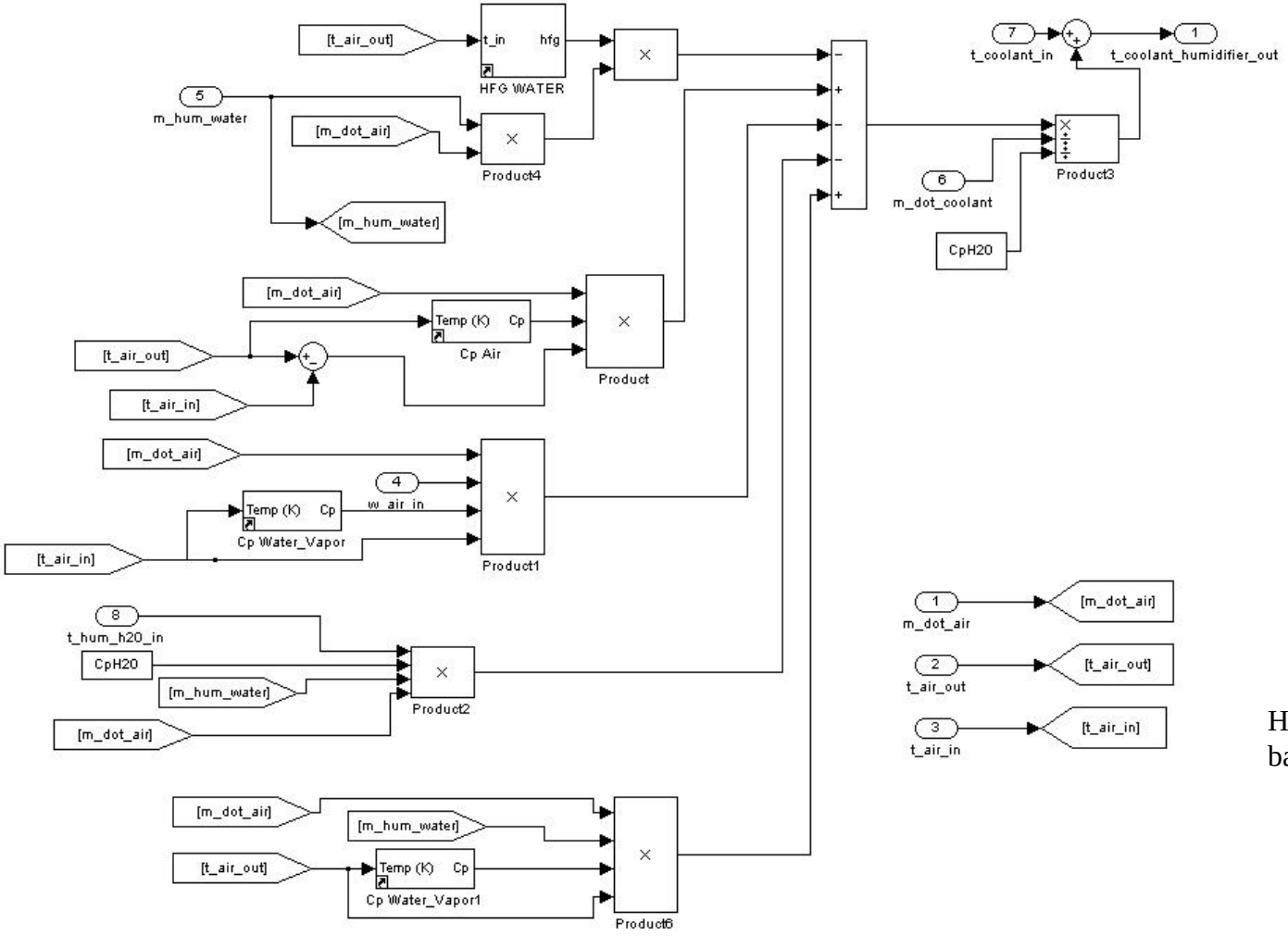

Humidifier energy and mass balance calculation

Specific Heat Air Calculation

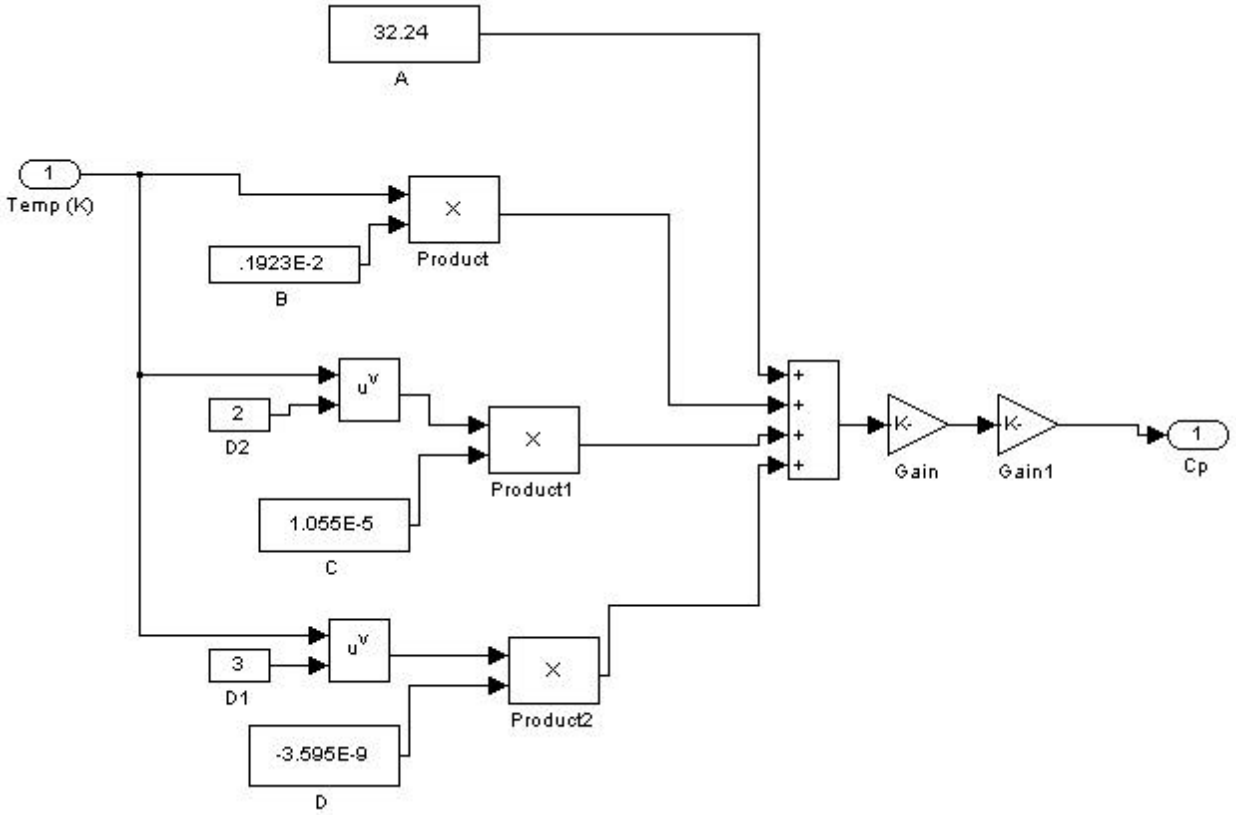

Equation fit for the specific heat of air calculation

Relative Humidity to Humidity Ratio – H2W

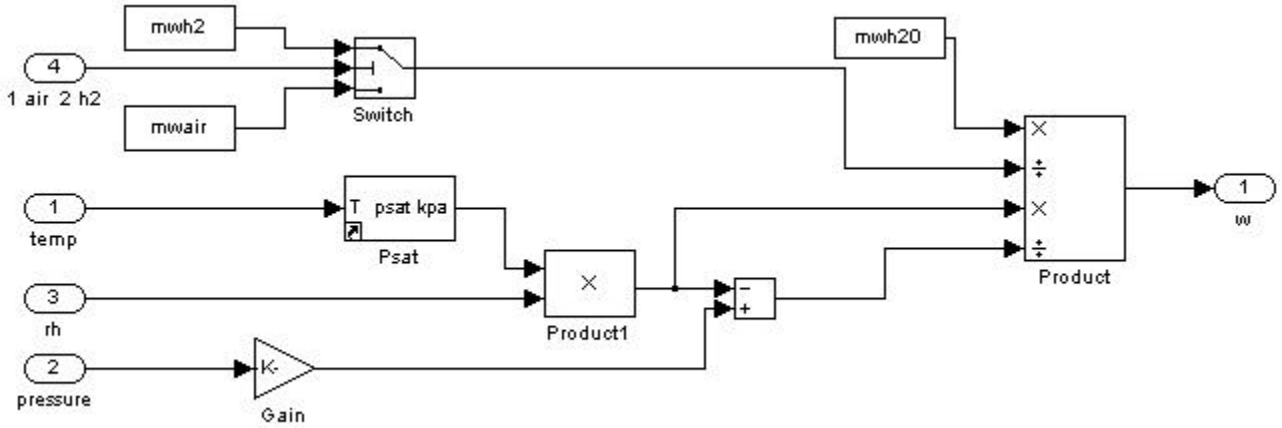

Function to change the relative humidity to a humidity ratio

Heat of Vaporization- HFG

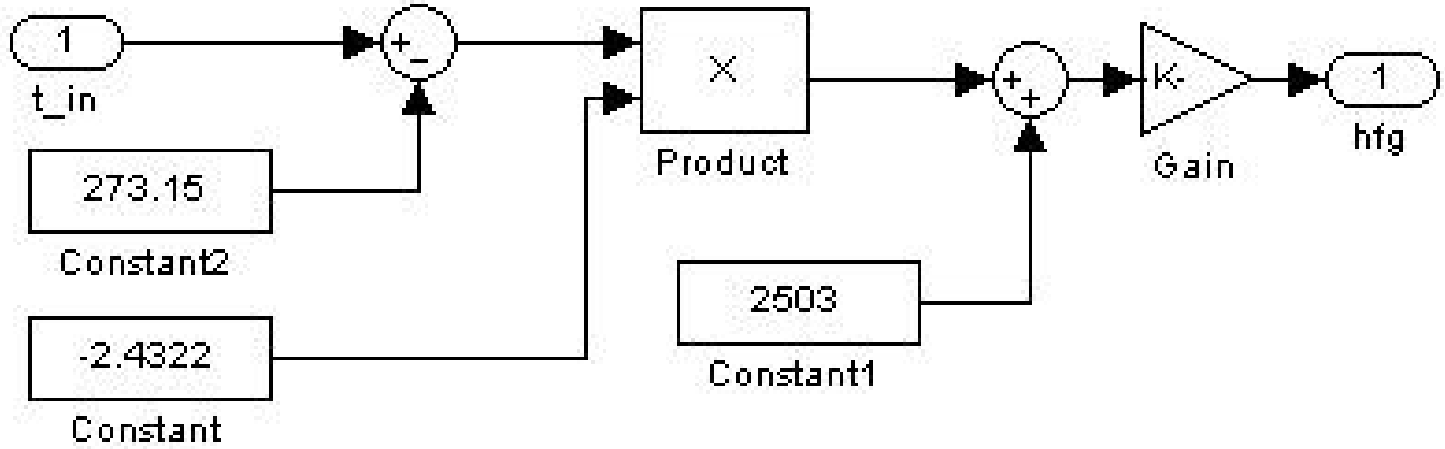

HFG curve fit. Data from Shapiro, et al.

Saturation Pressure of Water Vapor PSAT

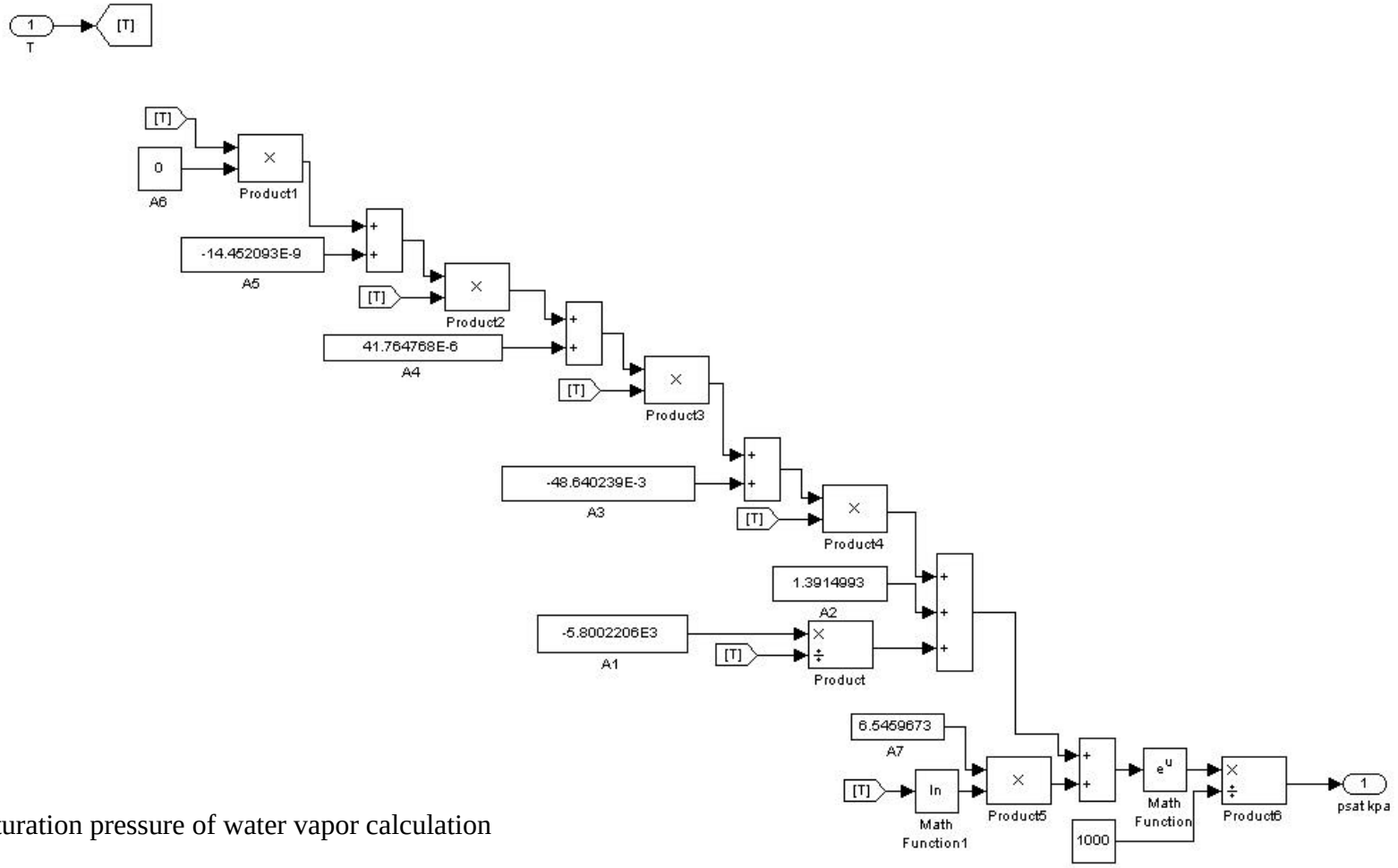

Saturation pressure of water vapor calculation

Main Model-Air Power

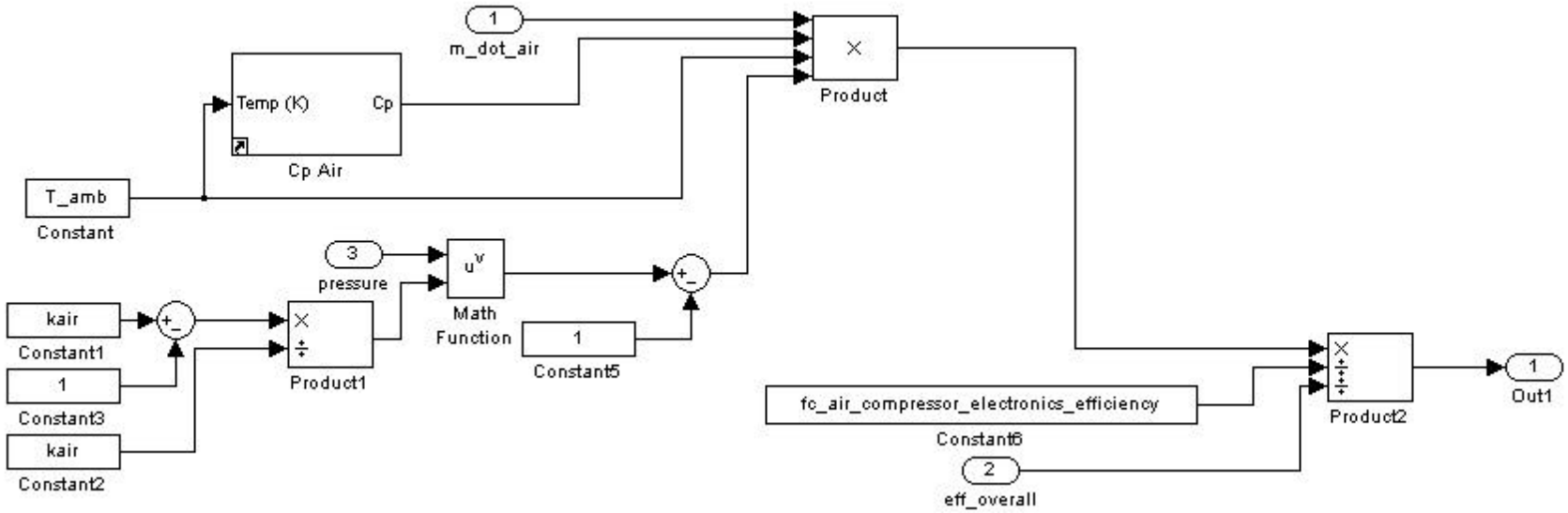

Air power calculation for the air compressor

Appendix B

This is the input file :system_char_lib.m
Needed for input to run the fuel cell system model

```
% FUEL CELL STACK CHARACTERISTICS
fc_lumped_capacitance = 120000;  % m*Cp_graphite     j/k  lumped
capacitance of fuel cell stacks
fc_stack_UA = 6;  %Overall heat transfer convected to ambient;  J/K
fc_cell_area = 678;
fc_cathode_pressure_drop_percentage = .15;
num_cells = 210;
fc_stack_cell_area = 678*num_cells;
polar_param_voc = 1.03;
polar_param_tafel = 0.06;
polar_param_ohmic = 1.12;
polar_param_ohmic_temp = 2.49E-3;
polar_param_concentration = 0.10;
polar_param_ref_temp = 333;
polar_param_temperature = 0.00041;
minimum_cell_voltage = 0.60;


% FUEL CELL SYSTEM OPERATING CONDITIONS
fc_SRair = 2.5;

fc_minimum_current_density = .005;
fc_m_dot_air_min = .001;
fc_target_cathode_outlet_humidity = 1;   % Relative humidity that you
would like to have at the outlet of the cathode of the fuel cell stack.
fc_target_anode_inlet_humidity = .8;      % Relavite humidity that you
want at the inlet to the anode of the fuel cell stack
fc_min_temp_for_heat_rejection = 273.15+80;  % Temperature at which you
want to reject heat above.  Meaning, no heat will be rejected below
this temp.  Keeps the system hot
fc_cathode_pressure_drop_percentage = .15;  % Pressure difference,
based on stack pressure in %percent that exsists across the stack on
the cathode air stream.
fc_cell_minimum_voltage = 0.6;  % Cell voltage that you do not want to
operate below
fc_minimum_current_density = .002;  % minimum current density you want
to run the stack at.
fc_allowable_temp_rise =5;
fc_max_cathode_inlet_pressure = inf;
fc_min_cathode_inlet_pressure = 1.01;
fc_pressure_i_map_in = [0:500];
fc_pressure_i_map_out = linspace(1,1.8,501);
fc_temp_cor_map_in = [200:400];
fc_temp_cor_map_out = linspace(0,0,201);
minimum_system_power_request = 5000;
fc_target_cathode_inlet_humidity = .6;
fc_cathode_humidity = fc_target_cathode_inlet_humidity;

%AIR COMPRESSOR CHARACTERISTICS
AA =
[0,.6,1,1.4,1.7,1.9,2.05,2.2,2.35,2.5,2.6;1,1.35,1.8,2.1,2.3,2.5,2.65,2
```

```
.8,2.9,3,3.05;1.8,2.15,2.4,2.65,2.8,2.95,3.1,3.25,3.4,3.55,3.65;2.6,2.8
,3.05,3.25,3.4,3.55,3.7,3.85,4,4.15,4.25;3.3,3.45,3.7,3.9,4,4.2,4.35,4.
45,4.6,4.75,4.85;3.95,4.1,4.3,4.5,4.6,4.75,4.9,5.05,5.2,5.35,5.45;4.55,
4.7,4.9,5.05,5.2,5.3,5.45,5.6,5.75,5.85,5.95;5.2,5.3,5.45,5.6,5.7,5.85,
6,6.15,6.3,6.5,6.65;5.75,5.85,6,6.2,6.3,6.5,6.65,6.8,7,7.15,7.3;6.35,6.
5,6.65,6.8,6.95,7.15,7.3,7.5,7.7,7.85,8.05;7,7.15,7.3,7.5,7.65,7.85,8.0
5,8.2,8.45,8.6,8.9]; %speed matrix for modified opcon -- last modified
7/31/00
BB =
[.115,.121,.135,.149,.157,.162,.167,.169;.172,.187,.204,.216,0.224,.232
,.242,.254;.229,.254,.271,.281,.293,.3,.310,.319;.288,.314,.334,.346,.3
59,.359,.367,.377;.348,.372,.396,.41,.419,.416,.425,.436;.409,.432,.459
,.471,.481,.478,.487,.497;.477,.494,.523,.533,.544,.539,.548,.558;.543,
.556,.584,.595,.607,.599,.608,.618;.596,.618,.642,.654,.667,.658,.668,.
679;.649,.681,.701,.715,.725,.721,.730,.742;.706,.741,.762,.777,.785,.7
83,.792,.806;.764,.803,.823,.839,.847,.843,.849,.872;.831,.872,.883,.89
9,.908,.902,.905,.939;.911,.942,.951,.958,.967,.971,.972,1.007;.989,1.0
12,1.019,1.016,1.026,1.051,1.049,1.076;1.067,1.081,1.087,1.074,1.085,1.
131,1.125,1.144]; %speed matrix for Opcon 1050 -- last modified 2/16/01
CC =
[.535,.715,.711,.566,.424,.321,.243,.161;.546,.769,.809,.741,.663,.618,
.6,.571;.558,.824,.894,.859,.816,.779,.751,.703;.555,.849,.944,.913,.87
7,.839,.807,.758;.526,.867,.968,.95,.920,.881,.851,.801;.497,.87,.983,.
971,.954,.909,.883,.836;.472,.860,.993,.986,.963,.936,.909,.863;.447,.8
44,.993,.996,.963,.945,.918,.876;.425,.814,.988,.997,.963,.954,.927,.88
7;.403,.78,.975,.986,.963,.946,.925,.887;.382,.729,.957,.971,.963,.936,
.923,.886;.361,.679,.926,.957,.955,.926,.919,.871;.337,.644,.885,.937,.
933,.917,.916,.857;.306,.608,.853,.909,.905,.904,.906,.858;.283,.569,.8
21,.881,.877,.886,.891,.859;.262,.531,.789,.854,.849,.868,.875,.86];
%adiabatic efficiency matrix for Opcon 1050 -- last modified 2/17/01
DD =
[.688,.617,.526,.47,.437,.416,.397,.386;.756,.682,.617,.58,.558,.541,.5
21,.498;.823,.747,.698,.672,.647,.632,.612,.592;.877,.798,.756,.73,.705
,.69,.672,.653;.905,.846,.8,.772,.754,.738,.721,.701;.931,.878,.828,.80
6,.791,.771,.756,.74;.944,.896,.849,.832,.815,.802,.788,.773;.957,.911,
.869,.852,0.835,.824,0.81,.797;.968,.921,.888,.871,.855,.845,.833,.819;
.978,.931,.905,.887,.874,.858,.846,.832;.987,.94,.915,.897,.888,.869,.8
6,.845;.995,.948,.925,.907,.898,.881,.874,.851;.993,.945,.933,.917,.908
,.892,.889,.857;.975,.942,.933,.926,.918,.894,.893,.86;.962,.94,.933,.9
36,.927,.884,.887,.863;.951,.938,.933,.946,.937,.875,.88,.867];
%volumetric efficiency matrix for Opcon 1050 -- last modified 2/17/01
compressor_pressure_map = [1.1 1.3 1.6 1.8 2 2.2 2.4 2.7];
compressor_mass_flow_map = [.0625 .125 .1875 .25 .3125 .375 .4375 .5
.5625 .625 .6875 .75 .8125 .875 .9375 1];
compressor_temperature_rise_map = [.084 .237 .4375 .56 .6686 .77 .866
1];

adeff_max = 0.675;                          % maximum expected adiabatic
efficiency
voleff_max = 0.975;                 % maximum expected volumetric
efficiency
temp_max = 96.15;                   % maximum delta expected outlet
temperature of compressor (K)
speed_max = 16;                     % maximum speed of compressor
(RPM/1000)
smair_max = 132.4*60;
```

```
compressor_speed_min = 2000;
fc_air_compressor_electronics_efficiency = 0.88;


%THERMAL SYSTEM CHARACTERISTICS
fc_system_coolant_capacity = 5;  % Capacity of cooling system in US
Gallons
fc_system_plumbing_heat_transfer_coefficient = 16.66;%  W-K
Overall Heat Xfer coef from coolant to ambient, 16.66 Measured VA Tech
radiator_frontal_area = 1;  %m^2
radiator_fan_flowrate = 1700;
condenser_fan_flowrate =1700;
condenser_frontal_area = .77;
coolant_pump_max_flowrate = 87.5;
coolant_pump_min_flowrate = 5;
coolant_pump_min_power = 0;
coolant_pump_max_power = 1.95;

%AMBIENT CONDITIONS
T_amb = 300;
p_amb = 101.325;
rh_amb = .75;
dt = 1;   % Time Step in seconds that the current model operates on

%CONSTANTS

LHV = 1.1968E8; %j/kg
mwh20 = 18.016;      % Molecular weight of water  kg/kmol
mwair = 28.97;       % Molecular weight of air kg/kmol
mwh2 = 2.0016;       % Molecular weight of hydrogen

Cpa = 1007;         % Specific Heat of Air  j/kg-k
Cpwv = 1860;        % Specific heat of water vapor j/kg-k
CpH20 = 4178;       % Specific heat of water j/(kg-k)

kair = 1.4;         % Specific heat ratio for air
density_air = 1.19;  % assumed density of dry air entering compressor
(kg/m^3)

time_step = 1;
fc_system_init_temp = 273.15+20;
fc_min_temp_for_heat_rejection = 273.15+80;
'LOADED
****************************SGSGS**********************************'
```

Table 23. Fuel Cell Stack Attributes

Attribute	Value	Units	Description
fc_lumped_capacitance	120000	j / K	The lumped heat capacitance of the fuel cell stacks. The value was developed assuming that the majority of the fuel cell stack with thermal interaction consists of graphite.
fc_stack_UA	6	j / K	Overall heat transfer coefficient associated with natural convection from the fuel cell stack. The value has been determined by using the Nussult number associated with vertical plates and the geometry associated with the fuel cell
fc_cell_area	678	cm^2	Overall active area associated with 1 cell in the fuel cell stack.
fc_cathode_pressure_drop_percentage	0.15	dim	The percentage pressure drop of the total pressure between the cathode inlet and outlet.
num_cells	210	dim	Number of cells electrically wired in series in the fuel cell stack

Table 24. Polarization Equation

Attribute	Value	Units	Description
polar_param_voc	1.03		Open circuit voltage for the polarization equation cell voltage
polar_param_tafel	0.06		
polar_param_ohmic	1.12		
polar_param_temp	2.49E-03		
polar_param_concentration	0.1		
polar_param_ref_temp	333	K	
polar_param_temperature	0.00041		

Table 25. Thermal system characteristics

Attribute	Value	Units	Description
fc_system_coolant_capacity	5	gal	
fc_system_plumbing_heat_transfer_coefficient	16.66	W-K	Overall heat transfer coefficient from coolant to ambient measured at Virginia Tech
radiator_frontal_area	1	m^2	Frontal area of radiator required
radiator_fan_flowrate	1700	CFM	Electric fan flow rate required
condenser_fan_flowrate	500	CFM	Electric fan flow rate required
condenser_frontal_area	0.77	m^2	Frontal area of condenser required
coolant_pump_max_flowrate	87.5	GPM	Maximum pump flow rate available
coolant_pump_min_flowrate	5	GPM	Minimum pump flow rate allowed
coolant_pump_min_power	0	HP	Minimum power for pump flow rate
coolant_pump_max_power	1.95	HP	Maximum pump power required

Table 26. Fuel Cell Operating Conditions

Attribute	Value	Units	Description
minimum_cell_voltage	0.6	V	Minimum cell voltage that the system will not operate below
fc_SRair	2.5	dim	Excess air mass flow rate compared to the stoichiometric required for power generation
fc_minimum_current_density	0.005	A/cm^2	Minimum amount of current the fuel cell will operate at. Because of LOG terms in the polarization equation the system at low current densities will yield very high and incorrect open circuit voltages
fc_cathode_humidity	0.6	%/100	Relative humidity the system will achieve at the inlet to the cathode
fc_m_dot_air_min	0.001	kg /s	Minimum mass flow rate that the air compressor will supply
fc_target_anode_inlet_humidity	0.8	%/100	Relative humidity the system will achieve at the anode (hydrogen) inlet
fc_min_temp_for_heat_rejection	353.15	K	Desired operating tempature at which the system can reject heat through the radiator to the ambient
fc_allowable_temp_rise	5	K or C	maximum amount of temperature rise that the fuel cell can tolerate
fc_max_cathode_inlet_pressure	infinity	ATM	Maximum pressure allowed at the cathode inlet
fc_min_cathode_inlet_pressure	1.01	ATM	Minimum pressure possible at the cathode inlet. (Make sure that a vaccume conditions are not possible)

Table 27. Fuel Cell Stack Control Strategy

Attribute	**Value**	**Units**	**Description**
fc_pressure_I_map_in	see above	current (A)	Input range related to current that the fuel cell could operate.
fc_pressure_I_map_out	see above	ATM	Control Strategy of fuel cell current vs. operating pressure
fc_temp_cor_map_in	see above	K	Possible fuel cell operating temperatures
fc_temp_cor_map_out	see above	ATM	Correction factor associated with temperature
minimum_system_power_requrest	5000	W	Minimujm power that the fuel cell system will produce. If the power is below the minimum, the system produces 0 gross power

Table 28. Ambient Conditions

Attribute	**Value**	**Units**	**Description**
T_amb	300	K	Ambient Temperature
p_amb	101.325	kPa	Ambient Pressure
rh_amb	0.75	%/100	Ambient Relative Humidity
fc_system_init_temp	278.15	K	Initial Starting temperature of the Fuel cell system

Table 29. Fluid Property Constants

Attribute	**Value**	**Units**	**Description**
LHV	1.20E+08	J/kG	Lower heating value for hydrogen
mwh20	18.016	kg/kmol	Molecular weight of water kg/kmol
mwair	28.97	kg/kmol	Molecular weight of air kg/kmol
mwh2	2.0016	kg/kmol	Molecular weight of hydrogen
CpH20	4178	j/kg-k	Specific heat of water
kair = 1.4	1.4	dim	Specific heat ratio for air
density_air	1.19	kg/m^3	assumed density of dry air entering compressor (kg/m^3)

Vita

My name is Stephen Gurski. My past education experience has been at Virginia Tech, where I received my bachelors in Mechanical engineering in 2000. During my undergraduate years at Virginia Tech, I was involved in a student-engineering project called the Hybrid Electric Vehicle Team. I spent three years on the team working on fuel cell vehicles.

I continued on with my education at Virginia Tech as apart of the masters program in mechanical engineering. At this point, I continued my work in fuel cell vehicles as team leader for the Hybrid Electric Vehicle Team. I have been an author and co-author for many papers on the subject of fuel cell vehicles that are available through the Society of Automotive Engineers (SAE).

This paper was to fulfill the thesis requirement for my Masters of Science degree in Mechanical Engineering.

I will continue my fuel cell and advanced vehicle work as a project manager for a student engineering competition at Argonne National Lab in Chicago, Illinois.